# SEDIMENTARY RESPONSES TO ANTHROPOGENIC ALTERATIONS WITHIN THE NAKDONG AND YEONGSAN ESTUARIES, SOUTH KOREA

A Dissertation

by

JOSHUA RAYMOND WILLIAMS

Submitted to the Office of Graduate and Professional Studies of
Texas A&M University
in partial fulfillment of the requirements for the degree of

DOCTOR OF PHILOSOPHY

| | |
|---|---|
| Chair of Committee, | Timothy Dellapenna |
| Committee Members, | Guan-hong Lee |
| | Patrick Louchouarn |
| | Niall Slowey |
| | William Sager |
| Head of Department, | Debbie Thomas |

December 2014

Major Subject: Oceanography

## ABSTRACT

Over the last half-century, the Nakdong and Yeongsan Estuaries of the Republic of Korea (S. Korea) have experienced a wide range of engineered coastal modifications including construction of seawalls, extensive land reclamation, and installation of estuarine dams. Combined, these alterations have considerably modulated the timing and intensity of river discharge, appreciably reduced the tidal prism, prevented natural tidal exchange, modified the shoreline profile, and altered the transport of sediment and organic matter within the coastal zone. Additionally, chronologic reconstructions suggest that rapid industrialization of the region has resulted in a pronounced increase in anthropogenic mercury. In order to assess the sedimentary impacts of these modifications, cores were investigated using $^{210}$Pb, $^{7}$Be, and $^{137}$Cs radioisotope geochronology, laser diffraction particle size analyses, $\delta^{13}$C and $\delta^{15}$N isotope ratio mass spectrometry, total mercury concentration, and X-radiography. Bathymetric, CHIRP seismic, and side-scan sonar data were also utilized to evaluate the spatial distribution of sediments and determine average Holocene sediment accumulation rates. Overall, observations record a shift in depositional environments as a response to an extensive array of anthropogenic alterations. Ultimately, land reclamation and dam construction have severely altered the fate and transport of sediment within these estuarine systems. As a consequence, sedimentation rates have increased dramatically and depositional events occur episodically corresponding to high discharge dam releases. Also, the timing of mercury enrichment within the sedimentary record corresponds to increases in regional historic emissions, suggesting the utility of mercury as a geochronologic tool to corroborate traditional radioisotopic methods.

ACKNOWLEDGEMENTS

I would like to thank my committee chair, Dr. Timothy Dellapenna, and my committee members, Dr. Guan-hong Lee, Dr. Patrick Louchouarn, Dr. Niall Slowey, and Dr. William Sager, for their guidance and support throughout the course of this research.

I am grateful to the Ministry of Oceans and Fisheries of Korea who supported this research, under the research program entitled 'Development of Integrated Estuarine Management System'. I also received additional support from the joint National Science Foundation/National Research Foundation EAPSI program (NSF 10591). I would also like to acknowledge the Korea Hydrographic and Oceanographic Administration (KHOA) for generously providing bathymetric data. I am thankful for support in laboratory and technical work provided by all members of the Coastal Geology Laboratory and Coastal and Estuarine Morphodynamics Laboratory.

Finally, I would like to thank my mother and father for their many years of encouragement and financial support, and to my wife to be for her patience and love. Without the support of these people, achieving this goal would not have been possible.

NOMENCLATURE

| | | |
|---|---|---|
| $^{7}Be$ | Radioactive Beryllium | |
| $^{13}C$ | Stable Carbon isotope | |
| $^{137}Cs$ | Radioactive Cesium Isotope | |
| $^{15}N$ | Stable Nitrogen Isotope | |
| $^{210}Pb$ | Radioactive Lead Isotope | |
| $^{210}Pb_{sup}$ | Supported $^{210}Pb$ Activity | dpm $g^{-1}$ |
| $^{210}Pb_{total}$ | Total $^{210}Pb$ Activity | dpm $g^{-1}$ |
| $^{210}Pb_{xs}$ | Excess $^{210}Pb$ Activity | dpm $g^{-1}$ |
| $^{209}Po$ | Radioactive Polonium Isotope | |
| $^{210}Po$ | Radioactive Polonium Isotope | |
| $A_0$ | Initial Activity | dpm $g^{-1}$ |
| Ag | Silver | |
| $A_z$ | Activity at Depth | dpm $g^{-1}$ |
| CHIRP | Compressed High Intensity Radar Pulse | |
| CRM | Certified Reference Materials | |
| ENE | East-Northeast Direction | |
| EPA | Environmental Protection Agency | |
| HCl | Hydrochloric Acid | |
| HF | Hydrofluoric Acid | |
| Hg | Mercury | |
| $HNO_3$ | Nitric Acid | |
| HPGe | High Purity Germanium | |
| $N_2$ | Atmospheric Nitrogen | |
| n | Number of samples | |
| NW | Northwest Direction | |
| $\rho_s$ | Density of sediment (2.65) | g $cm^{-3}$ |

| | | |
|---|---|---|
| $\rho_w$ | Density of the pore water | g $cm^{-3}$ |
| $R^2$ | Coefficient of Determination | |
| RSD | Relative Standard Deviation | % |
| $S_{Avg}$ | Average Sediment Accumulation Rate | cm $yr^{-1}$ |
| $S_{Bath}$ | Bathymetric Accumulation Rate | cm $yr^{-1}$ |
| SE | Southeast Direction | |
| SW | Southwest Direction | |
| $t_{1/2}$ | Half life | |
| T-Hg | Total Dry Mercury | ng $g^{-1}$ |
| TOC | Total Organic Carbon | % |
| USGS | United States Geological Survey | |
| z | Corrected depth | cm |
| α | Alpha Radiation | |
| δ | Standard Reporting Delta Notation | |
| Δ | Relative Change in Variable | |
| λ | Decay constant of $^{210}Pb$ (0.031). | $year^{-1}$ |
| σ | Standard Deviation | |

TABLE OF CONTENTS

Page

LIST OF FIGURES

LIST OF TABLES

# CHAPTER I
# INTRODUCTION AND SYNOPSES

## 1.1 Introduction

The document herein describes research conducted on the Nakdong and Yeongsan Estuaries of the Republic of Korea (S. Korea), investigating the sedimentary impacts of anthropogenic alterations to these systems. This work is significant considering the extensive and rapid coastal modifications within S. Korea within the last century. Considering rivers with greater than 200, 500, and 1000 $km^2$ drainage basin areas, corresponding estuaries have been determined as closed by a form of anthropogenic structure in 37%, 56%, and 71% locations, respectively (Table 1.1) (Lee et al. 2011). Few studies have investigated the ramifications of the substantial changes occurring in these systems within the last century. This work strives to increase knowledge by evaluating the natural responses to these modifications.

The analyses and conclusions from these data sought to reconstruct the geomorphological changes that have occurred within the last century due to engineered modifications. This was achieved through the examination of core data to establish sedimentation rates and geochronological control, and subsequently evaluating the changes in grain size distribution, organic matter source, mercury concentration, sedimentary structure, and bulk isotopic concentration within this temporal framework. Additionally, bathymetric change analysis, CHIRP seismic, and side-scan sonar data were utilized to evaluate the spatial distribution of sediments and determine average Holocene sediment accumulation rates. The extent of the methods used varies between the estuaries, with more geochemical and geophysical work done within the Yeongsan Estuary.

| River Name | Watershed Area ($Km^2$) | Length (Km) | Openness |
|---|---|---|---|
| Hangang | 35770 | 494 | Open estuary |
| Imjingang | 8897 | 244 | |
| Yeseonggang | 3916 | NA | |
| Sacheon(cheon) | 351 | 30 | |
| Gogneungcheon | 261 | 46 | |
| Nakdonggang | 23394 | 510 | Closed estuary |
| Seonakdongang | 285 | 26 | |
| Geumgang | 9912 | 398 | Closed estuary |
| Seomjingang | 4960 | 224 | Open estuary |
| Yeongsangang | 3468 | 137 | Closed estuary |
| Anseongcheon | 1656 | 60 | Closed estuary |
| Sapgyocheon | 1650 | 59 | |
| Mangyeunggang | 1504 | 81 | Closed estuary |
| Dongjingang | 1124 | 51 | |
| Wangpicheon | 514 | 61 | Open estuary |
| Tamjingang | 509 | 55 | Open estuary |
| Yangyangnamdaecheon | 474 | 55 | Open estuary |
| Samcheogosipcheon | 394 | 56 | Open estuary |
| Yeongdeogosipcheon | 375 | 55 | Open estuary |
| Suncheondongcheon | 367 | 36 | Open estuary |
| Gagogcheon | 265 | 42 | Open estuary |
| Gangneungnamdaecheon | 259 | 33 | Open estuary |
| Watancheon | 245 | 25 | Closed estuary |
| Ungcheoncheon | 235 | 39 | Closed estuary |
| Jujincheon | 229 | 29 | Open estuary |
| Hoeyagang | 218 | 42 | Open estuary |

Table 1.1 Summary of estuaries in S. Korea designated by watershed size, river length, and state of openness.

The analysis of these results in the context of the extensive coastal engineering that has occurred, has improved our understanding of the effects that land reclamation and dam construction have had on sediment dynamics and facies distribution within estuaries. Furthermore, examining current conditions and considering the extensive coastal development within these estuaries led to the modification of traditional facies

models to include anthropogenic features for estuaries. Holistically, the primary objective of this study has been to describe and define the mechanisms for changes in depositional parameters as a natural response to anthropogenic alterations within the Nakdong and Yeongsan Estuaries. The following sections provide an overview for each of the following chapters, respectively. Each chapter within this document has been included with the intention to act as an independent manuscript.

## 1.2 Synopses of Chapters

### *1.2.1 Nakdong Estuary - Geomorphological Shifts*

The Nakdong Estuary, located within the coastal zone of Busan, South Korea, has been subjected to a series of engineered alterations typical of many eastern Asian estuaries. The construction of two estuarine dams (1934 and 1983) and numerous seawalls associated with land reclamation projects have altered the timing and flux of sediment, and resulted in three contrasting discharge energy regimes. Additionally, the impoundments have appreciably reduced the tidal prism by at least 50%. Consequently, vast geomorphologic changes have occurred including the development of five new barrier islands. In order to assess the impacts of these modifications, 19 vibracores were obtained throughout the estuary. The dispersal and accumulation of sediment was evaluated utilizing $^{210}$Pb and $^{137}$Cs radioisotope geochronology of 6 cores. Average sediment accumulation rates range from 2.19 cm yr$^{-1}$ adjacent to the first constructed dam to as high as 6.55 cm yr$^{-1}$ in the middle region of the estuary. These high rates are further supported by comparison of bathymetric survey data from 1985 to 2009. Laser diffraction grain size analyses and X-radiographs revealed distinctive changes associated with dam construction, and correlation of events between cores conveys the episodic sedimentation corresponding to floodgate releases. Ultimately, anthropogenic alterations have resulted in a shift from a tide-dominated to a wave-dominated estuary. The increase in sediment trapping efficiency that has ensued resulting from extensive coastal construction provides the basis for reevaluating traditional facies models for estuaries. A

conceptual model is developed here to characterize the alterations in sediment depositional patterns according to relative discharge energy of the adjacent floodgate.

*1.2.2 Yeongsan Estuary - Sedimentological Changes*

Over the last half-century, coastal zones within the Republic of Korea (S. Korea) have experienced a wide range of engineered coastal modifications including construction of seawalls, extensive land reclamation, and installation of estuarine dams. The Yeongsan Estuary has experienced all of these modifications and provides an ideal case study on how sedimentation changes within a macrotidal estuary in response to these alterations. Combined, these alterations have considerably modulated the timing and intensity of river discharge, prevented natural tidal exchange, modified the shoreline profile, and altered the transport of sediment and organic matter within the coastal zone. These impacts have been investigated using 30 gravity cores analyzed for $^{210}$Pb radioisotope geochronology, laser diffraction particle size analyses, $\delta^{13}$C and $\delta^{15}$N isotope ratio mass spectrometry, and X-radiography. Average sediment accumulation rates range from $0.9 \pm 0.6$ cm yr$^{-1}$ to $10.0 \pm 2.9$ cm yr$^{-1}$, with the highest rates proximal to the downstream side of the dam, and some areas determined to be either actively eroding or recently dredged. These results are supported by comparison of multiple bathymetric surveys, and CHIRP seismic data suggest an order of magnitude increase from average Holocene sediment accumulation rates. Side scan sonagrams collected adjacent to the dam reveal distinctive scouring, transitioning to areas accumulating fine-grained sediments. Shifts in the organic matter source inputs are apparent in pre/post-dam sediments and reflect the occluding of tidal influence above the dam, resulting in increasingly terrestrial dominated signatures. Additionally, a time series of cores collected during periods of limited and high discharge analyzed for $^{7}$Be, indicates sediment deposition occurs episodically corresponding to high discharge dam releases. Our observations record a shift in depositional environments as a response to an extensive array of anthropogenic alterations. Ultimately, land reclamation and dam construction have severely altered the fate and transport of sediment within the estuarine

system. As a consequence, sedimentation rates have increased dramatically and depositional events are primarily controlled by discharges from the estuarine dam.

*1.2.3 Yeongsan Estuary – Historical Input of Anthropogenic Hg*

The rapid economic growth of the Republic of Korea (S. Korea) within the last half-century has resulted in a pronounced increase in anthropogenic Hg emission from coal combustion, oil refining, cement production, and waste incineration. The impacts of increasing atmospheric sources have been investigated with a historical reconstruction of Hg input from 30 sediment cores collected from the Yeongsan Estuary. Within the last several decades, this region has undergone severe anthropogenic alteration, including the construction of an estuarine dam forming the Yeongsan Lake, and installation of numerous seawalls that eliminated vast tidal flats and restricted estuarine circulation. Total mercury concentrations (T-Hg) from pre-industrial sediments (i.e. background values) are significantly lower than those measured in sediments deposited after 1980, with an average increase from $8.59 \pm 2.66$ ($n = 274$) to $23.19 \pm 9.57$ ng $g^{-1}$ ($n = 273$), respectively. Surface sample T-Hg analyses shows that concentrations are highest above the dam, with a decreasing gradient offshore. The synchronous enrichment of T-Hg within the sedimentary record and increased historical emissions suggests that regional sources dominate the input to the Yeongsan Estuary. This indicates that with sufficient regional historic emission data, T-Hg may be utilized as a geochronologic tool to corroborate traditional radioisotopic methods.

# CHAPTER II

# SHIFTS IN DEPOSITIONAL ENVIRONMENTS AS A NATURAL RESPONSE TO ANTHROPOGENIC ALTERATIONS: NAKDONG ESTUARY, SOUTH KOREA*

## 2.1 Introduction

Historically throughout much of the world, estuaries have been hubs for human settlement. This is due to their protection from and access to the open sea, high rates of biological productivity providing sustenance, and being the confluence point of rivers allowing access to inland navigation. Today, this remains evident with many of the largest shipping ports, industrial, and metropolitan centers being located adjacent to estuaries. However, in combination with vast drainage basin characteristic changes, this has ultimately resulted in extensive alteration of natural systems.

On the Korean Peninsula and throughout much of East Asia, traditional agricultural practices include terraced upland agricultural fields and rice farming, which utilize local water resources through irrigation and drainage canals (Crawford and Lee 2003). Additionally, coastal construction of estuarine dams to impede saltwater intrusion, and extensive seawalls in land reclamation and river divergence projects have considerably modified the shoreline within the last century (Yoon et al. 2007). Together, this has resulted in significant engineering of the drainage system in most watersheds, altering both net transport of sediment and freshwater from these systems and modulating the timing of the discharge (Yoon and Woo 2000, Choi et al. 2005). As a result, the sediment dynamics and ecosystems within the estuaries into which these rivers flow have been significantly altered.

Several studies have demonstrated the impacts on estuarine sedimentation after the emplacement of dams and/or reservoirs near the coast. The impoundment of the Senegal River on the West coast of Africa has increased the influence of marine forcing factors



*Reprinted with permission from "Shifts in Depositional Environments as a Natural Response to Anthropogenic Alterations: Nakdong Estuary, South Korea" by Williams, J. R., Dellapenna, T. M. and Lee, G., 2013, *Marine Geology*, 343, 47-61, Copyright (2013) by Elsevier B.V.

(i.e. wave reworking) in the outer estuary, resulting in vast and rapid morphological changes of sand bars. Subsequent to the construction of the dam, the mouth of the estuary narrowed and several mouth bars accumulated (Barusseau et al. 1998). The reduction of water discharge and sediment supply within the Yalu Estuary, located on the border of N. Korea and China, due to dam and reservoir construction within the last century was investigated with hydrodynamic calculations, heavy mineral and grain size analyses, and comparison of historical records. A decrease in the bedload transport flux and an increase in the amount of sediment transported landward due to extensive decreases in discharge, coupled with recent dredging activities has significantly altered the estuarine geomorphology, including migration of barrier islands (Gao et al. 2012). After the construction of a dam in the Keum Estuary on the West coast of S. Korea, the sedimentation rate increased by a factor of 1.9, and an increase in accumulation of fine-grained sediments occurred due to a stronger flood dominated tide and a decrease in overall current velocity (Kim et al. 2006). Coastal engineering projects and dam construction within the Haringvliet Estuary in the Netherlands also resulted in a decreased tidal prism, an increase in the relative influence of waves on morphology, and an increased sediment volume within the estuary (Tönis et al. 2002).

The Nakdong Estuary is a prevalent example of an anthropogenically engineered estuary. Within the last century, two large estuarine dams have been emplaced preventing natural flow conditions and the intrusion of saltwater. The Noksan Dam was the first constructed in 1934, and eliminated the flow from the West Nakdong River (Figure 2.1). The Nakdong Estuarine Dam was built between 1983-1987 and has since highly regulated the discharge from the East and West Eulsuk Channels. Consequently, the saltwater wedge that once reached approximately 40 km upstream is now occluded at the dam, considerably reducing the tidal prism (Ryu and Chang 1979). Additionally, within the Nakdong Estuary and the proximate Jinhae Bay, several seawalls have been constructed with the development of several industrial centers within the last half-century. These shoreline and discharge modifications have resulted in exceptionally rapid geomorphologic changes including the development of a series of barrier islands.

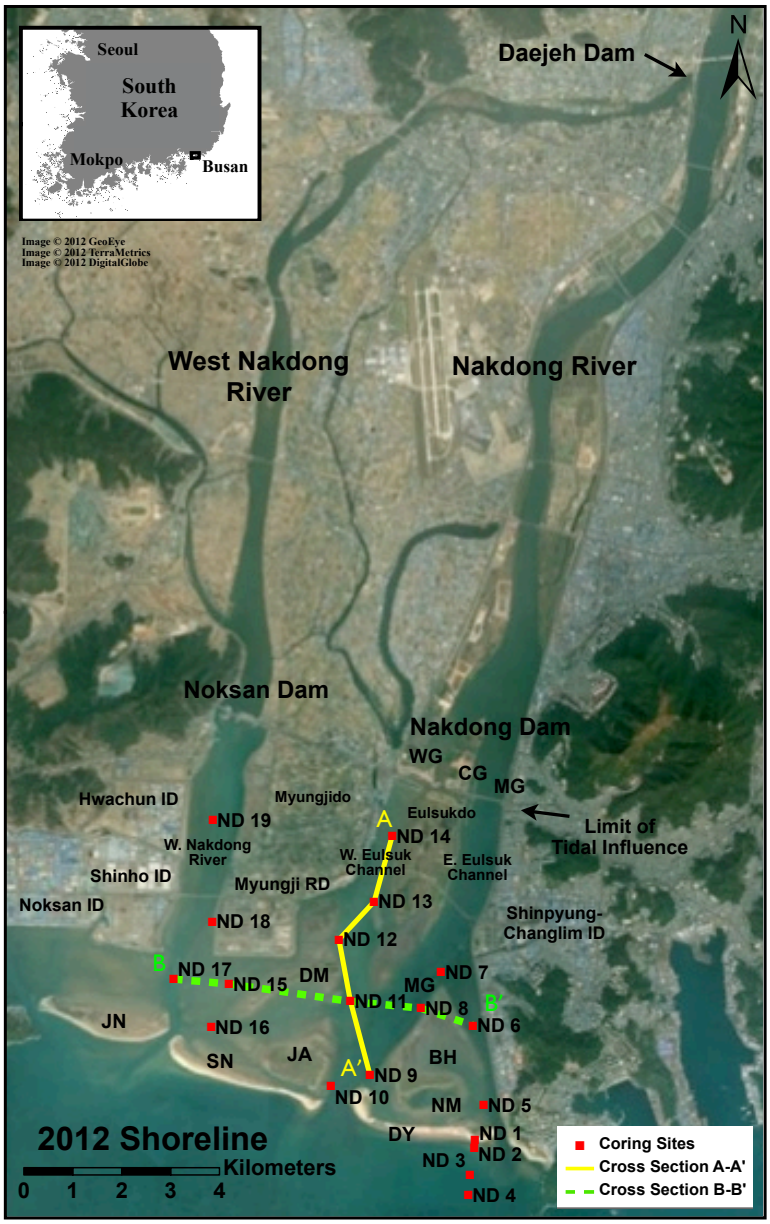


Figure 2.1 Detailed study area map showing location of the Nakdong Estuary within South Korea and all core sampling locations and cross sections shown in Figures 2.8 and 2.9. Noksan, Nakdong, and Daejeh Dam locations, channel names, barrier islands, and industrial (ID) and residential districts (RD) are indicated (WG=Western Floodgate, CG=Control Floodgate, MG=Main Floodgate, JN=Jinudo, DM=Daemadeung, JA=Jangjado, BH=Bakhabdeung, SN=Sinjado, DY=Doyodeung, NM=Namutsitdeung, and MG=Maenggeummeorideung).

The geomorphologic evolution of the barrier islands within the Nakdong Estuary has also been accompanied by changes in the grain size distribution of surficial sediments. Studies conducted prior to and after the construction of the Nakdong dam were compiled and compared and indicated a reduction of up to 40% in sand composition within the central estuary (Kim and Lee 1980, Lee 1993, Kim and Ha 2001). However, although few samples were taken landward of the barrier islands within the estuary, it has been shown that significant variations in grain size (up to 52.9% change in sand content) can occur seasonally, making comparisons between samples collected during different seasons in previous studies dubious (Yoon and Lee 2008). Seasonal variability is also supported by grain size trend analyses studies conducted along the barrier islands (Kim and Rhew 2007, Khim et al. 2009). The effect of different wave climates on grain size distribution and topographical expression has also been observed and modeled for Jinudo (Yoo et al. 2011). These results show that the forcing factors of wind direction, wave energy, discharge, and sediment flux control the sediment transportation dynamics of the estuary, barrier islands, and subaqueous delta.

While other studies have focused on the spatiotemporal evolution of the barrier islands (Kim et al. 2007, Yoon et al. 2007), the ecological impact (Jeong et al. 2007), or modeled remediation techniques to reduce dredging efforts above the dam (Ji 2006), a paucity of data exists concerning the accumulation rates and recent sedimentary record within the Nakdong Estuary. Core analyses-based studies have been limited by spatial resolution and have primarily focused on millennial time scales (Oh 1994, Eun et al. 1998). Optically stimulated luminescence has been utilized to acquire a recent accumulation rate, but with limited resolution (Kim 2009).

Schubel and Carter (1984) defined the trapping (filtering) efficiency of an estuary as the fraction of total sediment that is introduced to the system that is retained within, supplied either through river or marine derived sources. The difference between sediments being advected seaward from the estuary and transported landward through tidal and meteorological forcing results in a net flux at the estuary mouth. Measuring the

parameters that control these sediment dynamics can be used in determining the trapping efficiency and in making comparisons between estuaries (Bokuniewicz 1995). Quantification of the sediment trapping efficiency has been modeled through physical oceanographic criterion such as nontidal residual circulation (estuarine circulation pattern, river discharge, density gradients), tidal mixing strength, and geometry (Biggs and Howell 1984, Schubel and Carter 1984). These models result in an estimated percentage of sediment trapped, indicating net import or export, which can be related to hydrographic classification (Schubel and Carter 1984). Additionally, these physical parameters control the distribution of depositional environments, which have resulted in general models for facies distribution within natural estuaries (Dalrymple et al. 1992). However, changes in sediment trapping efficiency of systems due to impoundments has not been evaluated for many estuaries. Despite this, dramatic changes in geomorphology, high accumulation rates, and changes in grain size distribution have all been attributed to alterations of estuaries indicating rapid changes in trapping efficiency (Barusseau et al. 1998, Tönis et al. 2002, Kim et al. 2006, Gao et al. 2012).

Therefore, it is the objective of this study to determine the impacts on sediment trapping efficiency of anthropogenic engineering of the Nakdong Estuary. Ultimately, the alterations of the Nakdong Estuary forced a reclassification from a tide-dominated to wave-dominated system. This change has occurred at a significant rate corresponding with the redistribution of depositional environments. By examining the sediment redistribution within this transition, this estuary provides an excellent study in which to evaluate how systems adapt based on changing relative energy inputs of waves, tidal currents, and river discharge. Since this transformation occurred rapidly within the last century, it allows observation of how a system responds naturally to anthropogenic forces. The shift in depositional environments observed in the Nakdong estuary due to human interventions also acts as an analog to natural systems transitioning due to environmental changes such as increased/decreased wave climate or fluvial discharge.

Through the determination of average sediment accumulation rates by $^{210}Pb$ and $^{137}Cs$ geochronology and grain size analyses of cores, this study examines the stratigraphy and identifies areas of highest sediment accumulation. By analyzing these results in the context of the extensive coastal engineering that has occurred, it is hoped that there is an improved understanding of the effects of land reclamation and dam construction on the sediment dynamics and facies distribution within estuaries.

**2.2 Study Area**

The Nakdong Estuary is located in the southeastern portion of South Korea, adjoining the city of Busan with an approximate population of 4 million people (Figure 2.1). The Nakdong River is the second largest in the country with a drainage basin area of around 26,000 $km^2$ and a length of nearly 520 km (Jeong et al. 2007, Hwang et al. 2010). The length of the estuary from the dams to the seaward extent of the barrier islands is approximately 7 km, and extends from a width of 5.5 km at the dams to 9.5 km across the barrier islands. There are 3 main channels (herein referred to as the West Nakdong River, West Eulsuk Channel, and East Eulsuk Channel) that separate the two main islands of Myungjido and Eulsukdo (Figure 2.1). Currently, there are eight sand shoals or barrier islands that are located seaward of the main islands (Jinudo, Daemadeung, Jangjado, Bakhabdeung, Sinjado, Doyodeung, Namutsitdeung, and Maenggeummeorideung) that have formed primarily within the last century (Figure 2.1).

Climatic conditions of the Korean peninsula are strongly controlled by monsoonal seasonality. Strong north to northwesterly winds and minimal precipitation are characteristic of winter months, while relatively weak south to southeasterly winds and heavy precipitation are typical for summer months (June-Sept.) with typhoons commonly resulting in high rainfall events. Specifically at the Nakdong Estuarine Dam, nearly all of the water released annually occurs between July-Aug., with minimal discharge occurring the remainder of the year (Figure 2.2), with discharge volume being highly variable and dependent on annual precipitation (Figure 2.3). Unlike many other estuaries on the Korean coast, relatively few islands are located offshore of the Nakdong

Estuary to attenuate waves generated in the Korean Straight. However, strong northwesterly monsoonal winds are not a significant factor (compared to the west coast of Korea) due to the location of the Nakdong Estuary on the southeastern side of the peninsula. Significant wave height and direction data indicate that for the majority of the year (Aug.-Mar.) swell direction is from the ENE, while during the summer months the wave propagation is from the SW, with wave heights predominantly less than 2 m year round (Yoon and Lee 2008). The Nakdong Estuary is classified as microtidal with a 1.5 m tidal range occurring on a semi-diurnal tidal cycle in which the predominant flood direction is to the NW and ebb flow to the SE. Using the classification system of Davis and Hayes (1984), the Nakdong estuary has recently been characterized as wave-dominated based on a mean wave height of 1.06m and a mean tidal range of 1.07m (Yoon and Lee 2008).

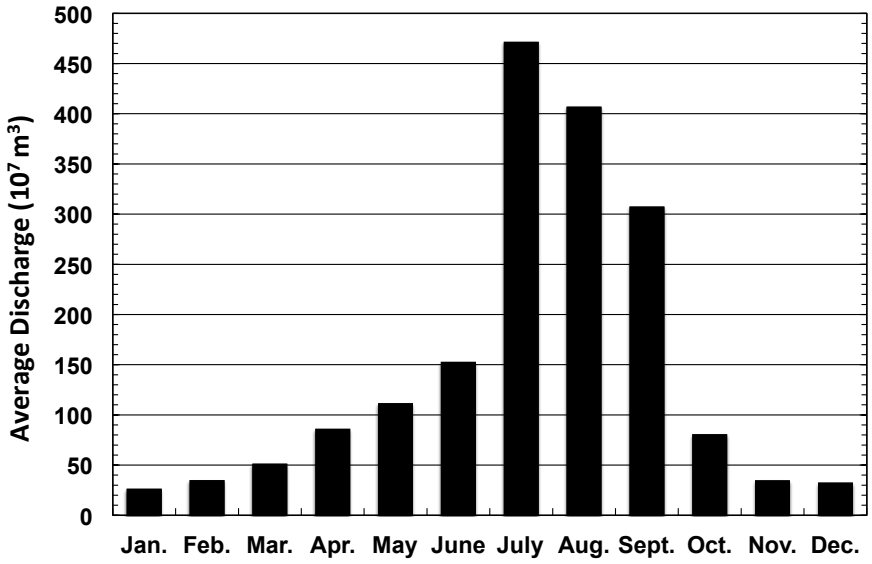


Figure 2.2 Average monthly discharge (includes all 3 floodgates) from the Nakdong Estuarine Dam for the period of Jan. 1990 - Aug. 2010. Note that discharge scale units are $10^7$ $m^3$.

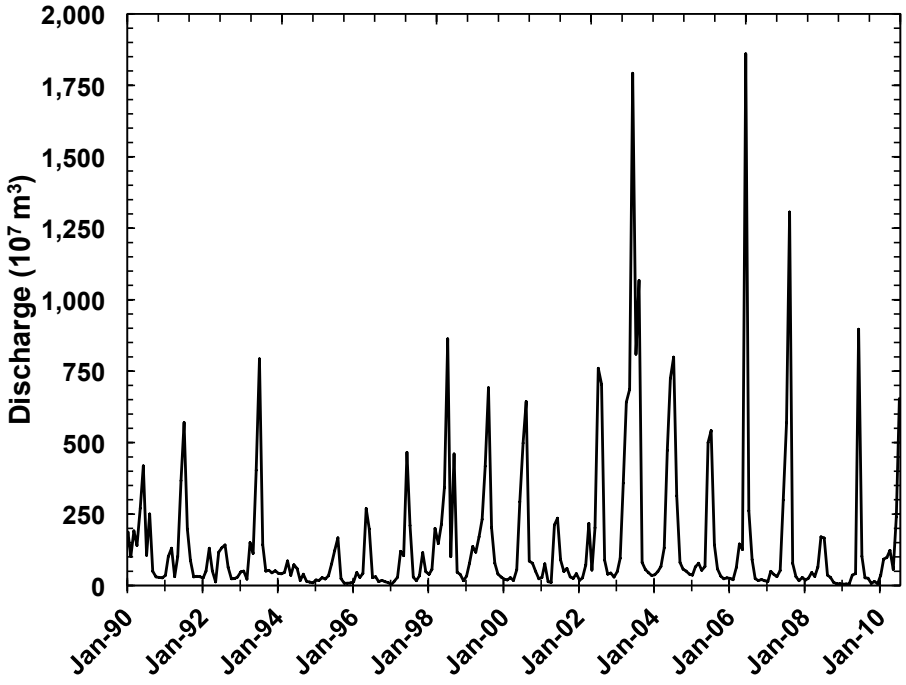


Figure 2.3 Time series of total monthly discharge (includes all 3 floodgates) from the Nakdong Estuarine Dam from Jan. 1990 - Aug. 2010. Note that discharge scale units are $10^7$ $m^3$.

Major shoreline changes have occurred within the last century due to the construction of seawalls for land reclamation projects and the confinement of the Nakdong River channels (Figure 2.4). Prior to the commencement of coastal engineering, the shoreline was considerably different from the current configuration (Figure 2.4a). The West Nakdong River dams were the first to be established in 1934. This project consisted of two locations of construction, which placed floodgates at the divergent point of the West Nakdong River from the Nakdong River at the Daejeh Dam (upstream approximately 18 km), and the point where the river enters the estuary at the Noksan Dam (Figure 2.1). At the same time, a seawall was constructed on the western portion of the downstream side of the Noksan Dam, spanning approximately 0.75 km

(Figure 2.4b). The Noksan and Daejeh Dams have remained inactive since construction. In the mid to late 1960‘s, the major industrial districts of Hwachun and Shinho were developed following land reclamation projects bordering the West Nakdong River (Figure 2.4c). This project extended the shoreline seaward nearly 2 km, eliminating the intertidal zone between the mainland and Shinhodo, and emplaced approximately 4 km of seawalls. Additionally, major industrial development began for the land bordering the East Eulsuk Channel with the initiation of the Shinnying-Changlim district (Figure 2.4c). The Nakdong Estuarine Dam was constructed between 1983-1987, consisting of two sections that extend across Eulsukdo (Figure 2.4d). The portion of the dam in the East Eulsuk Channel consists of the Main and Control Floodgates, while the West Eulsuk Channel contains the Western Floodgate (Figure 2.1). These dams have been engineered with a radially opening floodgate design which, when opened, release water from the bottom of the water column. The vast majority of discharge from the Nakdong Dam occurs in the East Eulsuk Channel from the Main Floodgate. The construction plan of the dam also included a seawall along the eastern side of Eulsukdo, beginning at the dam and running approximately 2 km in length. Concurrent with the Nakdong Dam construction project, the Shinnying-Changlim industrial district underwent further development and a major seawall (over 4 km) was emplaced along the channel (Figure 2.4d). Shortly following the completion of these projects, reclamation began in 1990 for the Myungji residential and Noksan industrial districts. The Myungji construction solidified the seaward edge of the island with approximately 3 km of seawalls, while the Noksan construction rapidly shifted the shore over 1 km to expand the Shinho industrial port westward (Figure 2.4d). Ultimately, these dams have divided the Nakdong Estuary into three distinct discharge energy regimes, with the East Eulsuk Channel receiving high discharge, the West Eulsuk Channel receiving occasional discharge, and the West Nakdong River receiving no discharge.

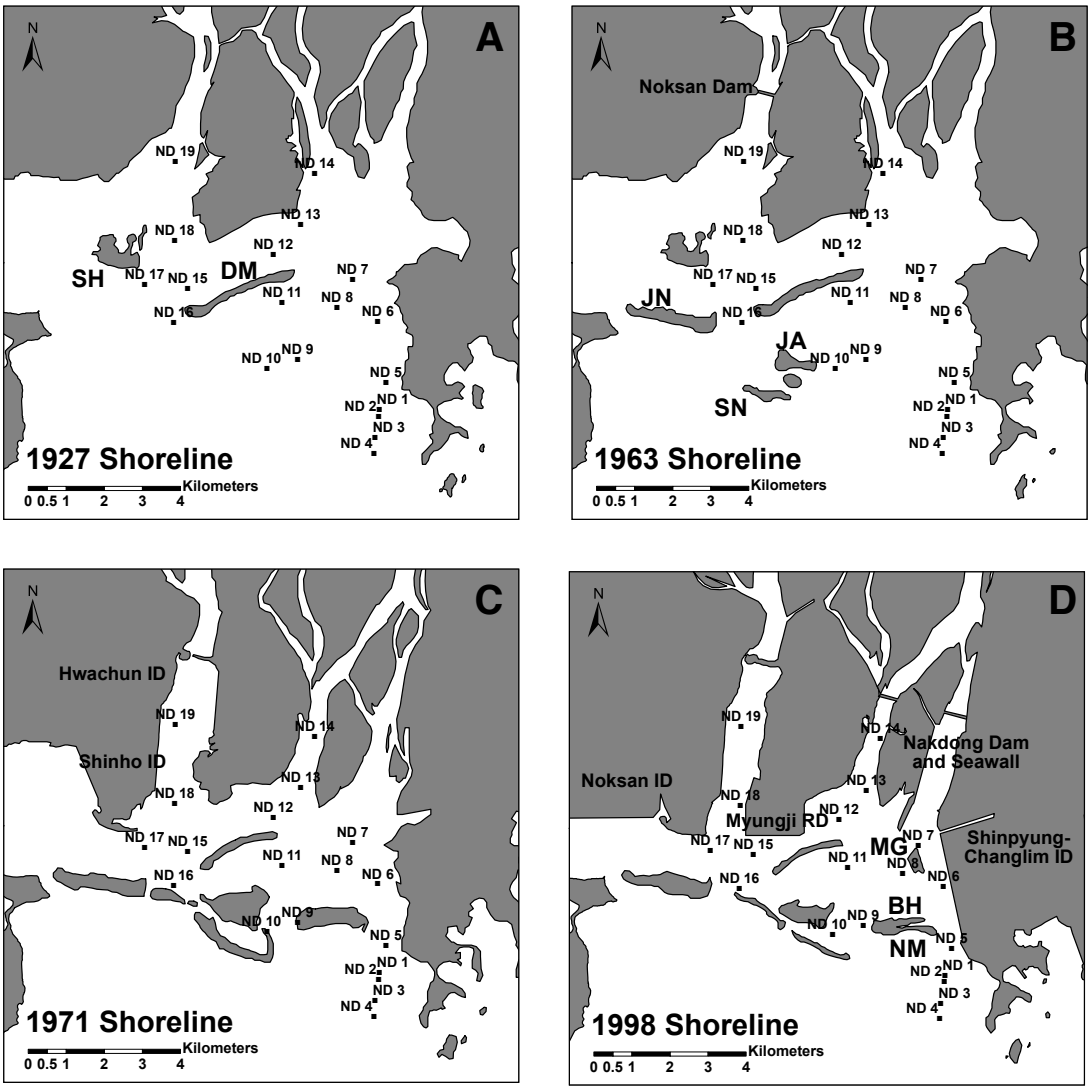


Figure 2.4 Historical shoreline changes of the Nakdong Estuary compiled from hydrographic charts. Construction and initiation of islands occurring between publication dates of charts are indicated on the following respective chart and abbreviations are given in Figure 2.1. Note: Figure 2.1 contains shoreline information for 2012 (SH=Shinhodo).

The seaward extent of the Nakdong Estuary in the southeastern Korean Straight, and the opening to the adjacent Jinhae Bay, have been shown to be the depocenter for fine grained sediments delivered by the Nakdong River. The depositional history of the Holocene sequence has been determined through high resolution seismic surveys and core analyses (Park and Yoo 1988, Kim et al. 2001, Lee et al. 2004, Lee et al. 2010). Sediment accumulation rates in the proximal area of the Korean Straight and Jinhae Bay have been found to be approximately 0.18-0.5 cm $yr^{-1}$ and have been shown to be primarily derived from the Nakdong River (Park and Lee 1996, Park et al. 1999, Lee et al. 2003, Wang et al. 2005, Lee et al. 2006). However, previous investigations of the Nakdong Estuary have focused primarily on spatial and temporal changes of the surficial expression of the barrier islands. These studies have utilized traditional Korean maps and historical marine charts to document the formation and movement of sand shoals within the estuary (Kwon 1973, Ban 1984). More recently, aerial photograph mosaics and synthetic aperture radar data have been employed to investigate shoreline changes (Oh 1999, Won et al. 1999, Kim et al. 2005, Kim 2005, Kim et al. 2007). However, due to uncertainties involved in the georectification of aerial photographs and the accuracy of historical charts, and dependent on the method used to track barrier island migration, debate exists over the rate of movement. Between 1971-2001, Kim et al. (2007) report shoreline advance rates between 20-40 m $y^{-1}$ based on aerial photographs and a digital shoreline analysis system that used 3 methods of rate calculations. Based on a series of published marine charts (1927-1995) and distance calculations to fixed land-based locations, Yoon et al. (2007) determined the barrier islands to be migrating at 7.4-26 m $y^{-1}$. By evaluating the movement based on an island centroid method rather than an advancing front, rates have also been postulated to be slower (Kim 2005). The Nakdong River watershed has also been modeled considering land use changes and soil erosivity, predicting the change in area of the barrier islands dependent on precipitation (Hwang et al. 2010).

## 2.3 Methods

### *2.3.1 Data Collection / Core Processing*

In order to examine the impacts of coastal construction, a total of 19 cores were obtained from the Nakdong Estuary using a standard vibracorer with 7.6 cm diameter aluminum core barrels between Oct. 9-12, 2011. Core locations were chosen at a roughly equidistant spacing throughout the estuary in order to sample all depositional environments and maintain high spatial resolution for correlation (Figure 2.1). Due to heavy dredging activities in the upper East Eulsuk Channel since the construction of the Nakdong Dam, this area was not sampled. Cores were sealed immediately upon recovery and processed within one week, and showed no signs of degradation from partial recovery or transportation. Each core was split in half lengthwise and high resolution digital photographs were taken at 20 cm intervals and mosaicked. X-radiographs were taken of core sections with significant fine grained material at an energy level of 64 kV and exposure time of 1.6 mAS with a portable Medison X-ray source and a Varian PaxScan® Amorphous Silicon Digital Imager. Subsamples were taken from the cores at 1 cm intervals and stored in sterile plastic bags until further processing.

### *2.3.2 Grain Size Analyses*

The distribution of grain size is a fundamental property of sediment and can be used to evaluate the dynamic conditions of transportation and deposition (Poppe et al. 2003). Samples were analyzed in the lab for grain size distribution using a Malvern Mastersizer 2000® laser particle diffractometer. Sediment samples were homogenized, and an approximately 3-5 g aliquot was placed in a 100 mL glass jar with 10 mL of a 5.5 g $L^{-1}$ sodium hexametaphosphate dispersant solution and subsequently sonicated for 30 minutes at 25°C at a frequency of 40 kHz. The fraction of sample larger than sand sized was removed by a 2 mm sieve and dry weighed for inclusion in the final distribution. The remaining slurry was diluted to a constant total volume of 200 mL and pipetted into the laser diffractometer until a calibrated level of obscuration was obtained, with an additional 10 mL aliquot removed and dried for weight percentage calculation. Triplicate

measurements of sand, silt, and clay fractions were made for each sample and the results were averaged and calculations made to include the fraction greater than 2 mm resulting in the final percentage grain size composition.

*2.3.3 Radioisotope Analyses*

Short-lived radioisotopes have been effective in quantifying sediment accumulation rates in marine and estuarine systems on decadal time scales by examining the rate of decay from a parent isotope with respect to depth ($^{210}$Pb), or identification of maximum activity associated with anthropogenic input due to nuclear fallout ($^{137}$Cs) (Nittrouer et al. 1979, Dellapenna et al. 2003). Respectfully, $^{210}$Pb and $^{137}$Cs have been chosen to evaluate accumulation rates within the Nakdong Estuary within the last century. Despite multiple pathways available for transport to the estuary, it is assumed that the isotopes are irreversibly adsorbed onto the surface of particles and that the residence time within the water column is negligible compared to the half-life (Nittrouer et al. 1979, Santschi and Honeyman 1989, Santschi et al. 1999).

Six cores (ND 11, 12, 13, 15, 18, and 19) were selected for radioisotope analyses based on recovered core depth, content of fine-grained material, and location to provide accumulation rates throughout the estuary. $^{210}$Pb ($t_{1/2}$ = 22.3 $yr^{-1}$) activities were measured indirectly using the $^{210}$Po method (Nittrouer et al. 1979, Santschi et al. 2001) where $^{210}$Po and $^{210}$Pb are assumed to be in secular equilibrium. Subsamples of cores were taken at 1 cm intervals and approximately 5 cm spacing for radioisotope analyses. Sediments were homogenized and wet sieved with a minimum amount of deionized water through a 38 μm sieve, and the smaller fraction was used in order to minimize the influence of changes in surface area on activity. Aliquots of dried sediment (1 g) were spiked with a $^{209}$Po tracer for yield determination of $^{210}$Po and chemically separated by complete digestion with concentrated HCl, $HNO_3$ and HF. Subsequently, $^{210}$Po and $^{209}$Po were spontaneously electroplated onto Ag planchets from the leachate for approximately 12 hr, and the activity of the Po isotopes was assayed by α-spectroscopy using a CANBERRA surface barrier detector. Determination of excess activity of $^{210}$Pb ($^{210}Pb_{xs}$)

was calculated by subtraction of supported level ($^{210}Pb_{sup}$) values from total activity ($^{210}Pb_{total}$) (Figures 2.5 and 2.6). Supported values were determined assuming that the activity at the bottom of the core where $^{210}Pb_{total}$ becomes asymptotic represents the supported value. Average sediment accumulation rates were determined by calculating a logarithmic regression line using the equation:

$$S_{Avg} = \frac{\lambda \cdot \Delta z}{\ln(A_0/A_z)}$$

where $S_{Avg}$ = average sediment accumulation rate (cm $y^{-1}$), $\Delta z$ = change in depth of the regression (cm), $A_z = {}^{210}Pb_{xs}$ activity at end of the regression (dpm $g^{-1}$), $A_o = {}^{210}Pb_{xs}$ activity at the beginning of regression (dpm $g^{-1}$), and $\lambda$ = radioisotope decay constant ($^{210}Pb$, 0.031 $y^{-1}$).

Activity of $^{137}Cs$ ($t_{1/2}$ = 30.17 $yr^{-1}$) was measured by gamma spectroscopy (662 keV) using a semi-planar intrinsic germanium detector coupled with CANBERRA DSA-1000 16K channel integrated multichannel analyzer using CANBERRA Genie 2000 spectroscopy software. Wet samples were homogenized and sealed in 70 mL petri dishes and counted for approximately 48 hr using identical geometries for gamma assay. Net count rates were converted to activities using predetermined efficiency factors for specific detectors at the intended gamma ray energy and normalized to wet weight of the sample counted. Average sediment accumulation rates derived from $^{137}Cs$ are based on peak nuclide concentration fallout rates in 1964 from atmospheric atomic bomb testing corresponding to a subsurface activity peak. As such, rates were calculated as the quotient of depth of maximum activity and the time difference between peak fallout and the date assayed (Figures 2.5 and 2.6).

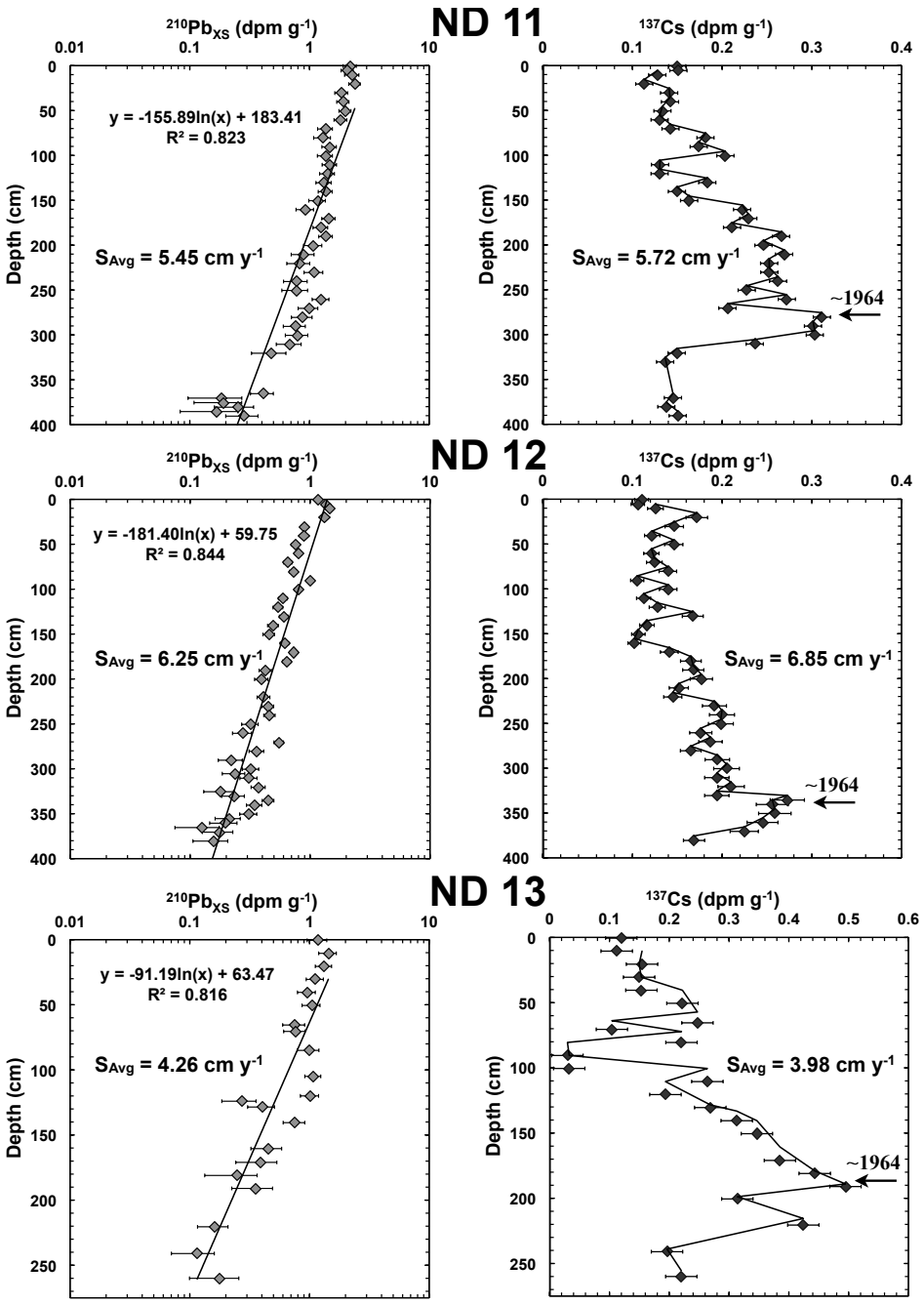


Figure 2.5 Excess $^{210}Pb$ and $^{137}Cs$ profiles for cores ND 11, 12, and 13. Core locations are shown in Figure 2.1. Error bars for activity are indicated or occur within the range of the plot symbol. Regression line for $^{210}Pb_{xs}$ and respective average accumulation rates ($S_{Avg}$) are shown within plot. Note different depth scales depending on core.

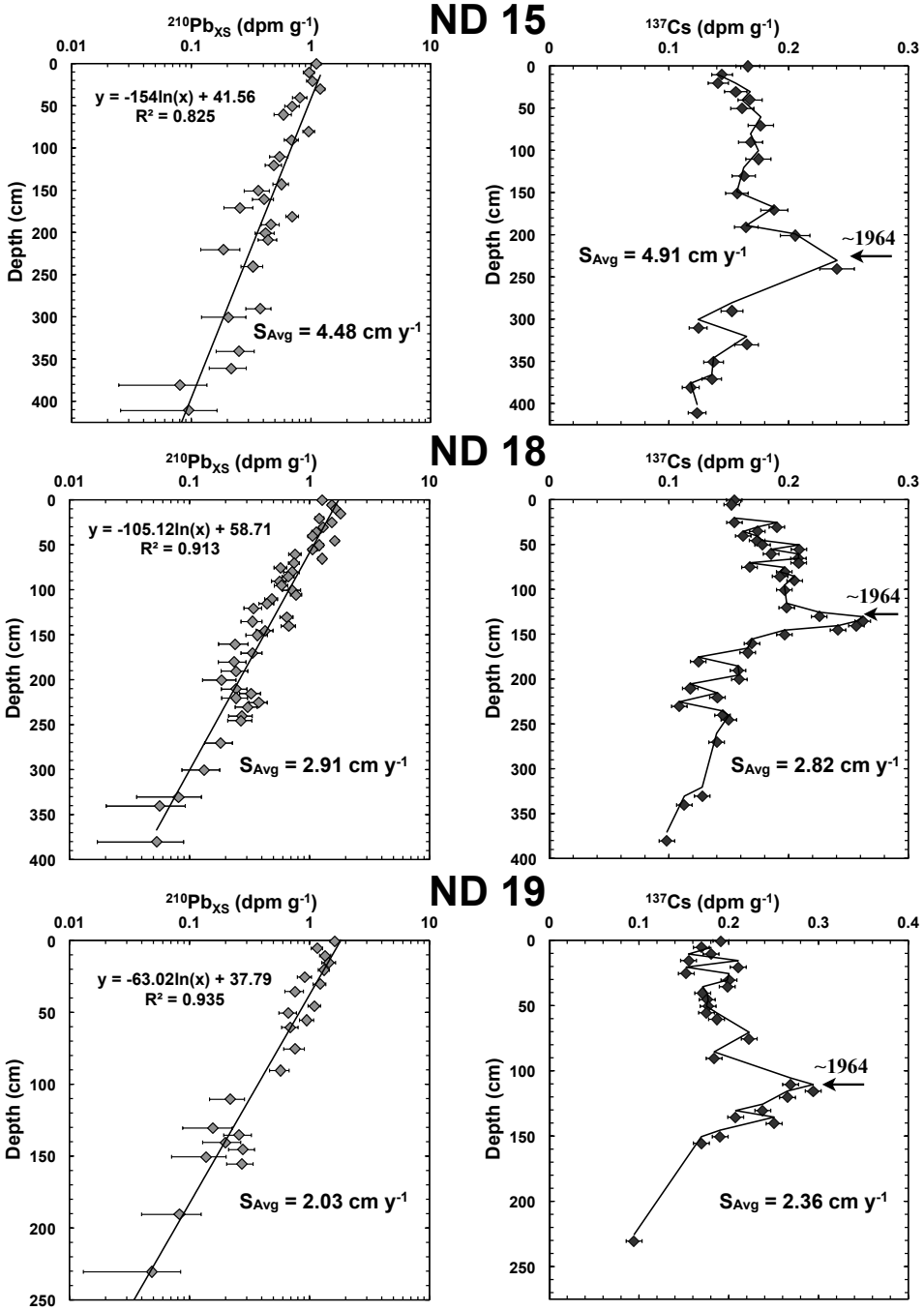


Figure 2.6 Excess $^{210}Pb$ and $^{137}Cs$ profiles for cores ND 15, 18, and 19. Core locations are shown in Fig. 1. Error bars for activity are indicated or occur within the range of the plot symbol. Regression line for $^{210}Pb_{xs}$ and respective average accumulation rates ($S_{Avg}$) are shown within plot. Note different depth scales depending on core.

*2.3.4 Bathymetric Data*

Data provided by the Korean Hydrographic and Oceanographic Administration (KHOA) from bathymetric surveys conducted in 1985 and 2009 were utilized to compare changes in seabed elevation and provide further support to geochemically derived accumulation rates. Data was compiled as a series of point measurements throughout the estuary and the nearshore region, and ESRI ArcGIS® software was employed to accurately compare values in a georeferenced environment. However, several caveats limited the extent to which this method could be applied. Spatial coverage of the surveys was not consistent, with point data not occurring at the same coordinates, and the majority of data was located within the channels or outside of the barrier islands. Additionally, since most cores were taken in less than 2 m water depth, accuracy of bathymetry data in these areas may be contentious. To limit the effects of these circumstances, a distance stipulation was required to consider data, in which bathymetric points from both surveys must be within 150 m of the core location. To determine accumulation rates ($S_{Bath}$), calculation of the change in depth over the respective time was made.

**2.4 Results**

*2.4.1 $^{210}Pb$ / $^{137}Cs$ Geochronology*

Profiles of $^{210}Pb_{xs}$ activity are typically variable throughout with multiple intervals of constant excess activity, suggesting the presence of mixing zones and non-steady state sediment deposition (Figures 2.5 and 2.6). Excess activities at the surface (0-20 cm) were consistently between 1.0-1.2 dpm $g^{-1}$ and decreased predominantly logarithmically with depth, with deviations representing bioturbation or episodic sedimentation. Due to the variability, sedimentation rates are assumed to be averaged of the time scale of the core and the regression line was fit from the base of the surface mixed zone to the $^{210}Pb_{sup}$ value. Although it is known this technique is averaging over multiple depositional events, sedimentation rates on a multi-decadal scale are assessed as valid based on sufficiently high $R^2$ values (> 0.8) of the regression line. However, several

intervals of constant decay can be observed within the profiles that are indicative of periods with comparatively steady state deposition. While generalities can be provided to describe the entirety of cores, distinctive characteristics warrant individual discussion. Accumulation rates acquired by $^{210}Pb$ and $^{137}Cs$ methods for each core are shown respectively in Figures 2.5 and 2.6, and have been summarized and averaged in Table 2.1.

| Core | $^{210}Pb$ $S_{Avg}$ (cm $yr^{-1}$) | $^{137}Cs$ $S_{Avg}$ (cm $yr^{-1}$) | Average (cm $yr^{-1}$) |
|---|---|---|---|
| ND 11 | 5.45 | 5.72 | 5.59 |
| ND 12 | 6.25 | 6.85 | 6.55 |
| ND 13 | 4.26 | 3.98 | 4.12 |
| ND 15 | 4.48 | 4.91 | 4.69 |
| ND 18 | 2.91 | 2.82 | 2.86 |
| ND 19 | 2.03 | 2.36 | 2.19 |

Table 2.1 Radioisotope accumulation rates for the Nakdong Estuary shown in cm $yr^{-1}$ derived from $^{210}Pb$xs and $^{137}Cs$ profiles. An average of the two rates was calculated and subsequently used for further correlation analyses.

Cores ND 11 and ND 12 are from the West Eulsuk Channel and exhibit similar accumulation rates and $^{210}Pb_{xs}$ profile attributes. The upper 20 cm displays nearly uniform activity, which is succeeded at depth with a series of alternating consistent decay and constant activity events. Boundaries between events are distinguished by offsets of 0.05-0.1 dpm $g^{-1}$. Significant sedimentation events can be delineated within ND 11, respectively at depths of 20, 60, 160, 220, 250, and 320 cm (Figure 2.5). Likewise, boundaries within ND 12 can be observed at depths of 20, 80, 150, 200, 260, 290, and 335 cm (Figure 2.5). Core ND 13, which is located closest to the dam in the West Eulsuk Channel, reveals a nearly uniform logarithmic decrease in activity to a depth of 70 cm, with an increase of 0.33 dpm $g^{-1}$ occurring near 110 cm. Steady decay

occurs throughout the rest of the core, with the exception of two outliers at 125 and 130 cm with considerably lower excess activities than samples immediately adjacent in depth (Figure 2.5). Core ND 15 exhibits intervals of constant decay apparent between 30-60 and 80-120 cm (Figure 2.6). In the West Nakdong River, cores ND 18 and ND 19 show substantially lower accumulation rates, with less discernible individual events of distinctive boundaries separating zones of variable decay (Figure 2.6). However, similar offsets of $^{210}Pb_{xs}$ activity magnitude are observed between samples, suggesting that due to lower sedimentation rates the sampling interval lacked the resolution to define multiple samples representing individual events. A noticeable shift in activity of 0.25 dpm $g^{-1}$ occurs within ND 18 at approximately 225 cm depth.

Profiles of $^{137}Cs$ activities for their respective cores are also shown in Figures 2.5 and 2.6 with values ranging from 0.02-0.5 dpm $g^{-1}$, with the majority of values occurring between 0.1-0.3 dpm $g^{-1}$. Data was fit with a 3-point moving average trendline in order to better observe the relationship between adjoining values. Peaks associated with the maximum fallout of the radionuclide in 1964 are apparent in all cores, with varying degrees of distinguishability. Activities trend rapidly towards negligible values below the maximum peak, and are gradually reduced towards the surface. Non-zero values prior to the highest value, and broader peaks than typically expected are possibly a result of diffusion due to the relatively high mobility of $^{137}Cs$ causing diffusion, and possible differences in the binding capability between freshwater and seawater environments (Santschi et al. 1999). Despite possible complications of $^{137}Cs$ geochronology in an estuarine environment with episodic deposition, accumulation rates obtained from this method corroborate $^{210}Pb$ derived rates. Since rates derived from both methods present similar values, the average is assumed to be the most accurate value. As such, all subsequent discussion herein refers to accumulation rates averaged from $^{210}Pb$ and $^{137}Cs$ methods (Table 2.1).

### *2.4.2 Sedimentary Structure*

Representative examples of sedimentary structures observed are exemplified by the X-radiographs of ND 12 shown in Figure 2.7. Generally, sections of cores with composition of sand percentage greater than 25% showed massive bedding (sand structures rarely visible on X-radiographs) or high degrees of bioturbation (Figure 2.7a). Frequently these type of structures were observed with small (1-2 cm) in-situ articulated mollusk shells. Other sections of cores with similar lithology showed less bioturbation and partial preservation of physical sedimentary structures (Figure 2.7b). In the example shown from 170-195 cm of ND 12, laminae can be discerned to a minimum of 0.5 cm. Overall grain size trends and some physical structures can be observed, such as erosional surfaces; however, they are partially obscured by bioturbation. Core sections with the highest levels of stratification preservation contained less than 15% sand, and commonly were found at greater depths within cores (Figures 2.7c and 2.7d). Large scale bedding features (2-10 cm) are apparent with much finer laminations (0.1-0.5 cm) interspersed within. Bedding planes dipping in differing directions within cores are indicative of alternating flow directions, which is consistent with a dynamic and tidally influenced estuary. Additionally, X-radiographs confirm that the edges of cores were not disturbed during the coring or transport process.

### *2.4.3 Grain Size Profiles*

All cores were analyzed for grain size with a maximum sampling interval of 5 cm, with fine-grained or laminated sections analyzed at 1 cm intervals, totaling 872 samples. Profiles of cores are shown as percent composition of shell, sand, silt, and clay with a consistent depth scale (Figures 2.8 and 2.9).

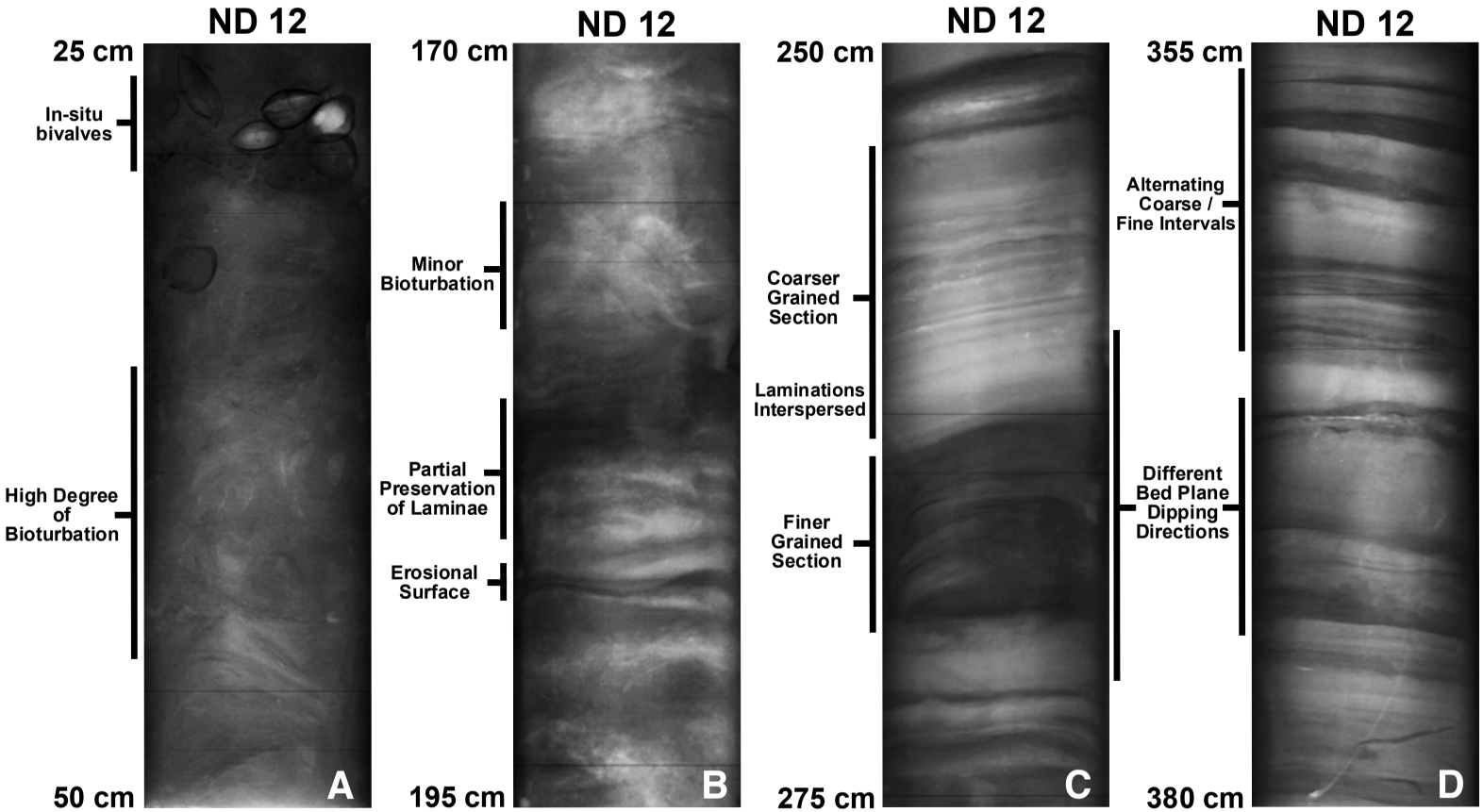


Figure 2.7 Representative X-radiograph sections from core ND 12. Location within core is shown in depth (cm) and key features are indicated. Descriptions correspond specifically to the X-radiograph found to the right.

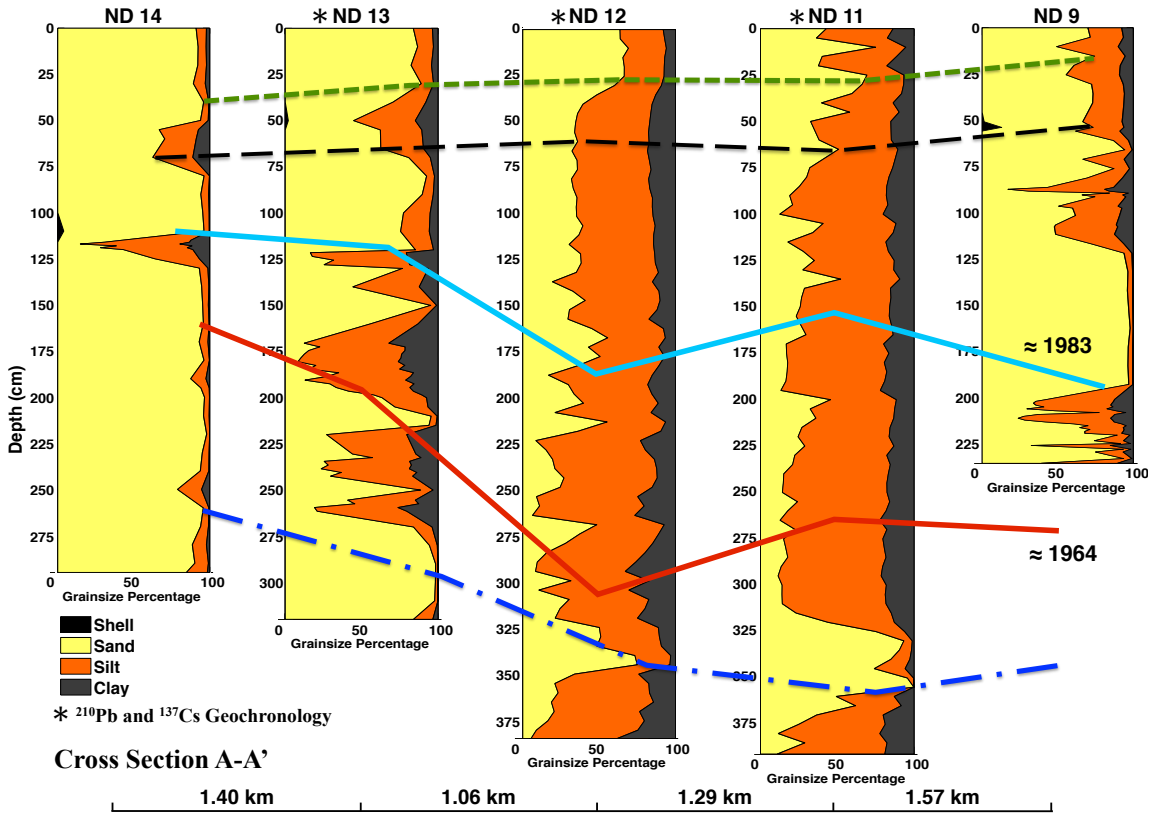


Figure 2.8 Shore normal cross section through the central channel of the Nakdong Estuary. Correlations are based on radiochemically derived data with minor depth change interpretations to respect grain size profiles. Transect location is shown in Figure 2.1 and isochron identification is maintained in Cross Section B-B' (Figure 2.9). Distances between cores are indicated below and grain size composition is represented as relative percentages.

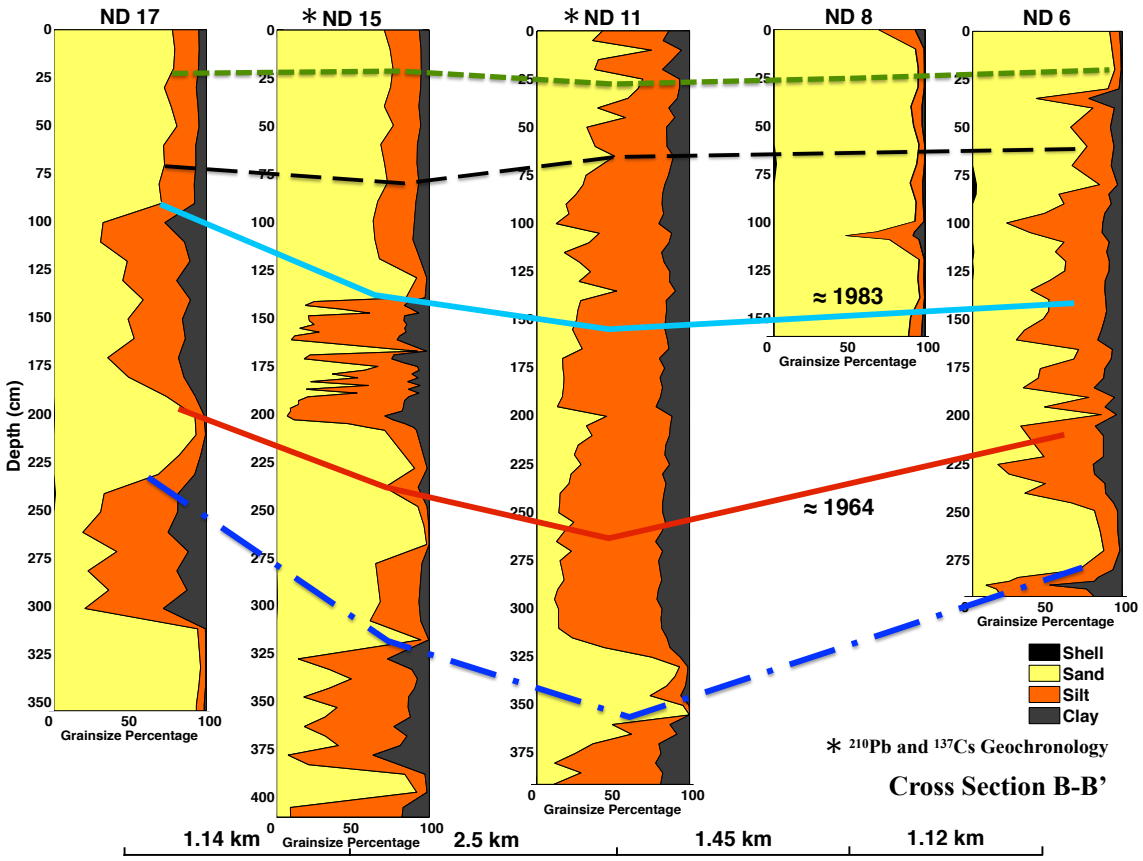


Figure 2.9 Shore parallel cross section across the central region of the Nakdong Estuary. Correlations are based on radiochemically derived data with minor depth change interpretations to respect grain size profiles. Transect location is shown in Figure 2.1 and isochron identification is maintained in Cross Section A-A' (Figure 2.8). Distances between cores are indicated below and grain size composition is represented as relative percentages.

Overall, each core exhibits a vast range of grain size distribution, commonly containing multiple intervals that vary with fluctuations in sand composition exceeding 60%. While precise composition changes are manifestly core specific, generalities can be described and attributed to core location within the estuary. Cores located in the middle of the estuary (ND 11 and ND 12) contain approximately 60% silt throughout with typical variations of 15% occurring at 5-10 cm intervals. In these cores, a distinctive increase in sand percentage (to > 70%) occurs between 300-375 cm, and a notable gradual increase occurs within the upper 75 cm.

Cores at the mouth of the West Nakdong River (ND 15, 16, 17, and 18) are composed predominantly of sand (> 60%) throughout with at least 2 significant fine-grained intervals approximately 60 cm thick. Due to higher accumulation rates, these intervals occur at greater depths in ND 15. Outside of these intervals, sand composition fluctuates by about 10%, consistently at 5 cm intervals. Although cores ND 13 and ND 14 are both located within the W. Eulsuk Channel and show similar characteristics, ND 13 is notably finer grained and is the more seaward of the two cores. Intervals characterized by a sharp increase in silt percentage occur in both cores at approximately 60 and 120 cm. Core ND 9 shows equivalent sedimentary attributes to ND 13, with the exception that finer grained intervals occur at different depths within the core. Several cores (ND 1, 2, 5, 7, 8, and 10) located immediately adjacent to the barrier islands are primarily composed of sand (>80%) with sparse fine-grained intervals. ND 8 exemplifies these cores and is shown in Figure 2.9. Cores ND 3 and ND 4 show similar characteristics to the barrier island cores, except with an overall decreased composition of sand and an increase in the frequency of finer grained intervals due to increased distance offshore. Within the eastern portion of the estuary located in the current primary channel (E. Eulsuk), ND 6 is characterized as a mixture of comparable features to cores in the western and middle region of the estuary. It consists of mostly (>60%) sand with variations of up to 20% occurring at 5-10 cm intervals. Additionally, a similarly characteristic high sand content interval occurs between 240-280 cm.

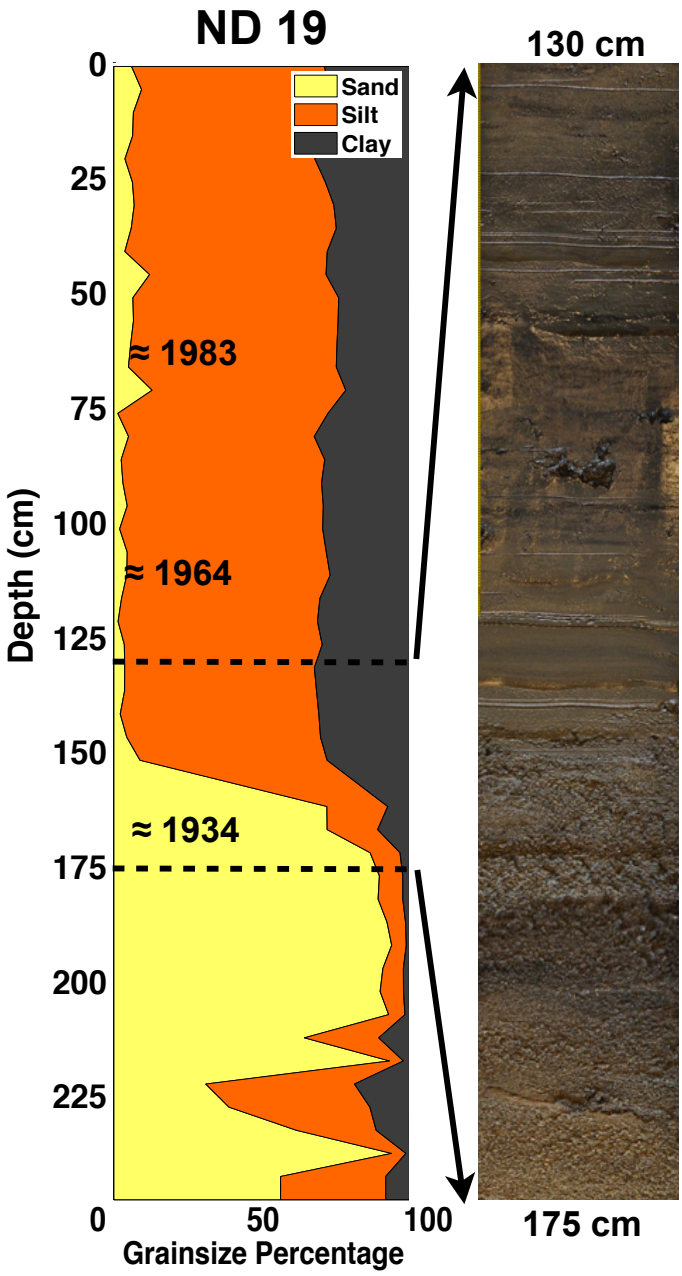


Figure 2.10 Complete grain size composition profile and core photograph for 130-175 cm section of core ND 19. Core location is proximal to the Noksan Dam and is shown in Figure 2.1. Approximate dates are based on $^{210}$Pb and $^{137}$Cs geochronology. A rapid increase in silt and clay percentage corresponds to the construction of the dam in 1934.

Located closest to the Noksan dam in the western channel, ND 19 exhibits an exceptionally distinctive shift in composition at approximately 160 cm depth (Figure 2.10). Over an interval of less than 20 cm, the grain-size composition changes rapidly from > 90% sand to <10% and subsequently remains at nearly uniform relative percentages to the top of the core, containing approximately 65% silt and 30% clay. Below this interval, grain-size composition and variability is similar to the cores at the mouth of the West Nakdong River.

| Core | Dist. (m) | 1985 Depth (m) | 2009 Depth (m) | $S_{Bath}$ (cm $yr^{-1}$) |
|---|---|---|---|---|
| ND 11 | 112 | -1.22 | 0.06 | 5.33 |
| ND 12 | 148 | -1.01 | 0.12 | 4.70 |
| ND 17 | 63 | -1.46 | -0.70 | 3.18 |
| ND 18 | 66 | -0.61 | 0.03 | 2.67 |

Table 2.2 Bathymetric survey data from 1985 and 2009 with distance from the closest core indicated. Sedimentation rates calculated as the depth change with respect to the time difference between surveys.

*2.4.4 Comparison of Bathymetric surveys*

Average accumulation rates determined by changes in bathymetry were able to be determined for 4 cores (ND 11, 12, 17, and 18) (Table 2.2). Comparison to the radioisotope derived dates (Table 2.1) indicates that despite uncertainties in bathymetric data, values are within a reasonable range and provide independent verification of accumulation rates. Values derived for cores ND 11 and 18 have less than a 7% relative difference between bathymetric and radioisotope derived rates. Core ND 12 shows a lower bathymetry derived rate (28% relative difference), but considering the distance is

at the maximum range of acceptance (148 m), the value is considered to provide significant evidence of rapid accumulation and substantiate radioisotope geochronology results. In addition to verification of these results, an accumulation rate for ND 17 was established; a core in which $^{210}$Pb and $^{137}$Cs geochronology was not applied.

## 2.5 Discussion

### *2.5.1 Episodic Sedimentation*

The results found in this study provide evidence for the impacts of anthropogenic alterations to the Nakdong Estuary. Significant variations in grain size composition and $^{210}Pb_{xs}$ activity within profiles indicate evidence of episodic sedimentation throughout an annual cycle. Episodic sedimentation within the estuary prior to anthropogenic alteration would also be expected due to the majority of rainfall and resultant discharge occurring during summer months. However, the hydrographic profile changes associated with controlling the discharge at the dam modulate the duration over which the discharge occurs. Within an undisturbed system, sediment deposition occurs primarily during the falling limb on a generally bell-shaped hydrograph, trapping sediment as the energy required for transport becomes insufficient. Discharge releases from estuarine dams have eliminated the build up and falling stages associated with a natural flood, resulting in a plateau shaped hydrograph. With immediate high flow velocities initiated with the opening of the dam, bed shear stresses increase rapidly rather than gradually as in natural systems, rapidly scouring the bed and flushing any fine material downstream. Consequently, sediment is delivered as a high intensity pulse during dam releases.

It has been demonstrated that seasonal variations in surficial grain size distribution are dependent on the volume discharged from the Nakdong dam and the incident wave climate. A sampling station within the estuary located between Daemadeung and Jangjado revealed a change of 52.9% relative sand content in surface sediments throughout an annual cycle (Summer 56% sand, Fall 71.7% sand, Winter 88.9%, Spring 36%; Yoon and Lee 2008). With this sampling station occurring approximately 0.5 km from core ND 11, similar variations would be expected within the sedimentary record,

provided net deposition and minimal disturbance due to bioturbation. With a sampling interval for grain size analyses of 5 cm, changes in sand composition of proximal samples were as high as 40%, and generally varied by approximately 15% (Figure 2.8). Variations similar in magnitude can also be seen in many of the other cores, particularly those within the central and western areas of the estuary (Figures 2.8 and 2.9). These grain size fluctuations within the cores give credence to the observations of a wide range in sand composition of surficial sediments, and suggest the preservation of flooding/discharge events. Although, with an average sedimentation rate for ND 11 determined to be 5.59 cm $yr^{-1}$, the resolution of the grain size analyses only provides an approximate annual rate. Consequently, with an annually varying sedimentation rate, 1 cm subsamples at a sampling interval of 5 cm only captures a particular event at an unknown point within the annual cycle. However, it can be postulated based on the observed seasonal surficial changes from Yoon and Lee (2008), that higher sand content intervals correspond to winter months while lower sand content intervals correspond to summer months. Additionally, due to the rapid sedimentation rates and visible structure within radiographs, the sampling interval is determined sufficient to discern the vertical grain size trends. Due to the large volume of fine sediment delivered to the estuary in summer during high discharge events, it is expected that relatively thick sequences of sediment deposited during this time account for the majority of annual deposition. Throughout the late autumn and winter, increased relative wave and tidal energy suspend fine-grained surficial sediments and advect them further offshore or towards the West Nakdong River channel. This process would winnow the fine material from the surficial sediments, resulting in a coarser grained interval.

Further evidence supporting seasonal episodic deposition can be observed within the $^{210}Pb_{xs}$ activity profiles (Figures 2.5 and 2.6). Deviations from the regression line and intervals of vertical excess activity could be the result of one or a combination of factors including: bioturbation, short term oscillations in the accumulation rate, and introduction of older/lower activity sediment. Intervals with higher or lower slopes than the regression line may respectively represent periods of increased or decreased

accumulation rates, which are observed in several cores with intervals ranging from 10-50 cm (particularly in ND 11 and 12). Short intervals (< 15 cm) that have exceedingly high or vertical slopes may be an indication of bioturbation or could conceivably represent a season of rapid accumulation or a single depositional event associated with a period of exceptional sediment flux. With prolonged periods of accumulation upstream of the dam and subsequent flushing that erodes sediment due to high current velocities, and dredging activities near the dam and in the main channel, it is likely that sediment with lower $^{210}Pb_{xs}$ activities could be exposed and mixed with younger sediments reducing the net activity. An example of this is observed in core ND 13 at depths of 125 and 130 cm, with $^{210}Pb_{xs}$ activities up to 0.7 dpm $g^{-1}$ below the average trend in values (Figure 2.5). When put in context of the grain size data, it can be seen that these data points occur within an interval of fine-grained sediment that can be approximately correlated to the construction of the Nakdong Dam (Figure 2.8). This interval is also observed in ND 14 allowing correlation of the event. While it is difficult to deduce the precise causes of departures from ideal exponential decay of $^{210}Pb$, the factors described here explain variations within the profiles and provide evidence for dynamic, event driven sedimentation.

### *2.5.2 Geochronology and Stratigraphy*

Two transects of cores were chosen for stratigraphic correlation that are representative of the depositional characteristics of the Nakdong Estuary, and are designated as cross sections A-A' and B-B' (Figure 2.1). Cross Section A- A' is a shore normal (Figure 2.8) transect through the E. Eulsuk Channel and Cross Section B-B' is a shore parallel (Figure 2.9) transect across the estuary. Based on averaged sediment accumulation rates, stratigraphic horizons corresponding to the initiation of construction of the Nakdong Dam in 1983 (light blue line; Figures 2.8 and 2.9) and the peak $^{137}Cs$ radionuclide fallout in 1964 (red line; Figures 2.8 and 2.9) were established within cores with radioisotopically derived rates. Grain size profiles and sedimentary structures were used to make correlations to cores without known accumulation rates, maintaining

isochron color designation in both transects (blue, black, and green lines; Figures 2.8 and 2.9). Considering that accumulation rates are averaged on a multidecadal scale, minor depth adjustments to horizons were interpreted based on depositional events inferred from grain size profiles. Since the 1964 horizon does not correspond to any particular local depositional event, correlation between cores occurs with contrasting sediment compositions. However, it does allow the timing of other depositional events to be constrained. While limited resolution of data exists for optically stimulated luminescence, an accumulation rate of 4.5 cm $yr^{-1}$ obtained between Doyodeung and Namutsitdeung for the last 49 years by Kim (2009) agrees well with the radioisotope derived results and extrapolated interpretations of this study.

Cross section A-A' reveals that a significant amount of fine-grained sediment (increased silt content) is accumulating within the middle region of the estuary (ND 11, 12), with a coarsening trend occurring both towards the dam and barrier islands (respectively ND 13, 14 and ND 9). A clear correlation can be made between cores ND 13 and ND 14 at the 1983 horizon corresponding to the top of a fine-grained interval with a sharp increase of sand content above. A similar observation made in ND 9 provides extension of this correlation seaward. Within cross section B-B' the 1983 isochron also corresponds to the top of a prominent fine grained interval in cores ND 15 and ND 17, based on respective accumulation rates. Additional correlations are made at shallower depths at the base of a fine grained interval and at the peak of an increase in sand at approximately 25 cm. A prominent feature seen throughout both cross sections is a sand interval that is approximately 50 cm thick in most cores occurring at varying depths based on respective accumulation rates (e.g. 320-375 cm depth in ND 11). Due to spatial scale of core proximity and the dynamic nature of sedimentation within estuaries, several minor isolated depositional events are difficult to correlate. However, these major grain size changes that have been correlated and constrained based on substantiated geochronology provide a framework in which to evaluate the following impacts resulting from engineered anthropogenic alterations.

*2.5.3 Impact of Dam and Seawall Construction*

Within the last century, the vast engineering of the Busan coastal zone has significantly altered the shoreline geometry and geomorphology of the Nakdong Estuary. Preceding the construction of the Noksan Dam (Figure 2.4a), the shoreline was recessed, the channels were significantly wider than at the present, and there were only two sand shoals (Shinhodo and Daemadeung). Without any other significant coastal development, the Noksan dam construction solely resulted in the formation of Jinudo and the initiation of the barrier islands Sinjado and Jangjado (Figure 2.4b). Further seawall construction associated with the development of the Hwachun and Shinho industrial districts, and the start of construction of the Shinnying-Changlim district greatly reduced the intertidal zone area and therefore the available accommodation space within the upper region of the estuary (Figure 2.4c). Coupled with the entire sediment flux being delivered through the W. and E. Eulsuk Channels, this resulted in the exceedingly rapid formation and expansion of barrier islands.

Following the emplacement of the Nakdong Dam and seawalls accompanying the development of the Noksan, Myungji, and Shinnying-Changlim districts, the intertidal zones were diminished further, the tidal prism was significantly reduced, and the controlled discharge altered the timing of sediment delivery. The reduction of the tidal prism can be approximated based on a mean tidal range of 1.07m and the difference in area from the 1927 historical chart to the current shoreline configuration, considering an areal extent 10 km upstream of the dam to the limit of the current barrier islands. This results in a very conservative estimate of a 54% reduction in the tidal prism attributed to land reclamation and dam construction. The emplacement of the Nakdong Dam also modified discharge rates/flow velocities at which sediment is delivered from a natural system by reducing the range of discharge associated with a single flood. These alterations to the natural system resulted in further geomorphologic changes, with the continued development of sand shoals near the mouth of the E. Eulsuk Channel.

Consequent to these shoreline changes, the sediment accumulation rates and depositional locations within the estuary have been modified. A compilation of average accumulation rates based on $^{210}Pb$ and $^{137}Cs$ radiochemical dating, bathymetric changes, and interpreted depths of isochrons reveals the general depositional distribution within the estuary (Figure 2.11). Interpolations of accumulation rates were achieved using a basic spline fit respecting the current shoreline boundaries. Two principal observations are made from these data: 1) the West Nakdong River has relatively lower accumulation rates (~2 cm $y^{-1}$) 2) high accumulation rates indicate the lower section of the W. Eulsuk Channel is the main depositional area (~5 cm $y^{-1}$). These accumulation rates are significantly higher than an equilibrium rate keeping pace with eustatic sea level rise, which has been estimated in this region to be approximately 2 mm $y^{-1}$ for at least the last 1000 years (Chang and Choi 2001). Considering the minimum accumulation rate derived in this study (2.19 cm $y^{-1}$), a conservative estimate would be at least an order of magnitude higher accumulation rates than eustatic sea level rise. At the current accumulation rates, most of the estuary would fill within 100 years, indicating these high local rates are a recent phenomenon attributed to engineered alterations. Currently, sediment is predominantly trapped within the estuary. If these high accumulation rates are sustained, the sediment trapping efficiency of the estuary will decrease as accommodation space is limited, and sediment flux seaward of the barrier islands will increase.

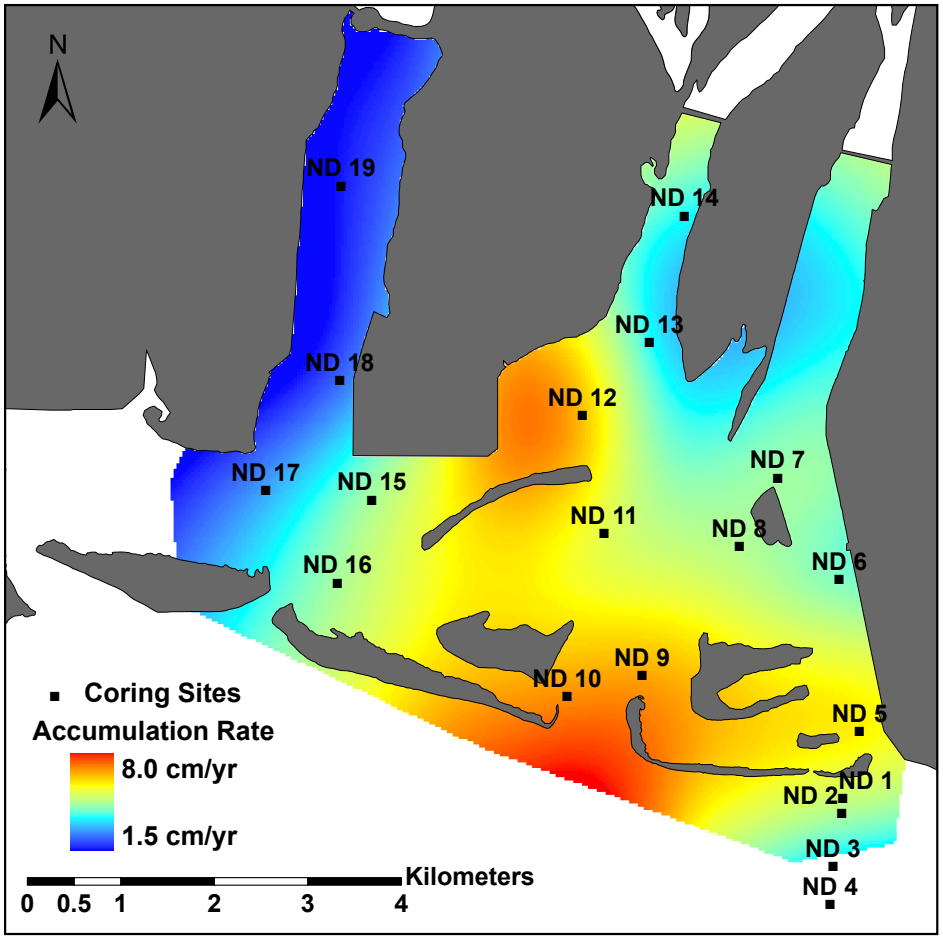


Figure 2.11 Interpolated sediment accumulation rates for the Nakdong Estuary. Known values are based on radiochemical dating (Figure 2.6) and correlations of isochrons between cores were used to calculate unknown rates.

The juxtaposition of accumulation rates and the rapid geomorphological changes indicate severe modification from a natural system, in which accumulation rates primarily vary axially dependent on total relative energy of marine and fluvial processes. In opposition, this highly altered system shows relatively low accumulation rates associated with the “river-dominated” end of the estuary, and varies significantly

transversely. Core ND 19 exemplifies the impacts on sedimentation of the Noksan dam (Figure 2.10). Prior to the construction of the dam and the cease of discharge in 1934, sediment was sand dominated with some fine-grained deposits interspersed. This represents typical estuarine tidal/fluvial channel fill with relatively high flow velocities due to river discharge and tidal currents. However, after the construction of the dam the area was isolated from channel discharge and tidal velocities were insufficient to transport coarse material to this location, resulting in relatively slow accumulation, primarily of silt and clay.

The rapid accumulation of sediment within the lower W. Eulsuk Channel is a result of several factors. After the construction of the Noksan Dam, the entirety of sediment flux was shifted to the E. and W. Eulsuk Channels making it the closest non-channelized area for sediment deposition. With the construction of the Nakdong Dam, the sediment source was further confined to the E. Eulsuk Channel. High flow velocity during discharge events from the dam is thus drastically reduced, allowing for the rapid accumulation of sediment. Ultimately, the anthropogenic alterations made to the Nakdong Estuary have resulted in a shift from a tide-dominated environment towards an increasingly wave-dominated system. Dalrymple and Choi (2007) described a tide-dominated environment geomorphologically as containing elongate tidal bars and tidal channels, by an absence or limited development of wave-generated shore parallel barrier islands, and typically displaying a funnel shaped geometry in which the width increases exponentially seaward. Despite the connotation of "tide-dominated" relating to high tidal ranges, several studies have demonstrated tidal currents being the relatively dominant energy source compared to wave and fluvial processes within microtidal environments (Cooper 2002, Davis Jr et al. 2003). The classification established here was based on historical bathymetric and shoreline charts, and we acknowledge the available data was limited. Examination of the pre-disturbed Nakdong Estuary coastline (Figure 2.4a) reveals the geomorphological characteristics required for classification as a tide-dominated estuarine system, which results in the described facies distribution of Dalrymple et al. (1992; Figure 2.12). This classification is demonstrated by the restricted

development of barrier islands, with only Shinhodo and the predominantly shore-normal elongated Daemadeung present, and distinctive funnel-shaped geometry. After the closure of the West Nakdong River with the Noksan Dam, the discharge and sediment source was shifted to the W. and E. Eulsuk Channels. The occlusion resulted in the reduction of the tidal prism and the reduction of accommodation space in the upper estuary due to land reclamation and channel bank hardening, thus forcing deposition of sediments seaward. Combined, these modifications resulted in the formation of several barrier islands (Figure 2.4b and 2.4c). At the same time, the reduction in intertidal zones caused the width of the estuary to be significantly reduced, narrowing the geometry from the original funnel-shape. With further land reclamation and the construction of the Nakdong Dam, tidal energy diminished significantly resulting in transition of the estuary from tide-dominated to wave-dominated.

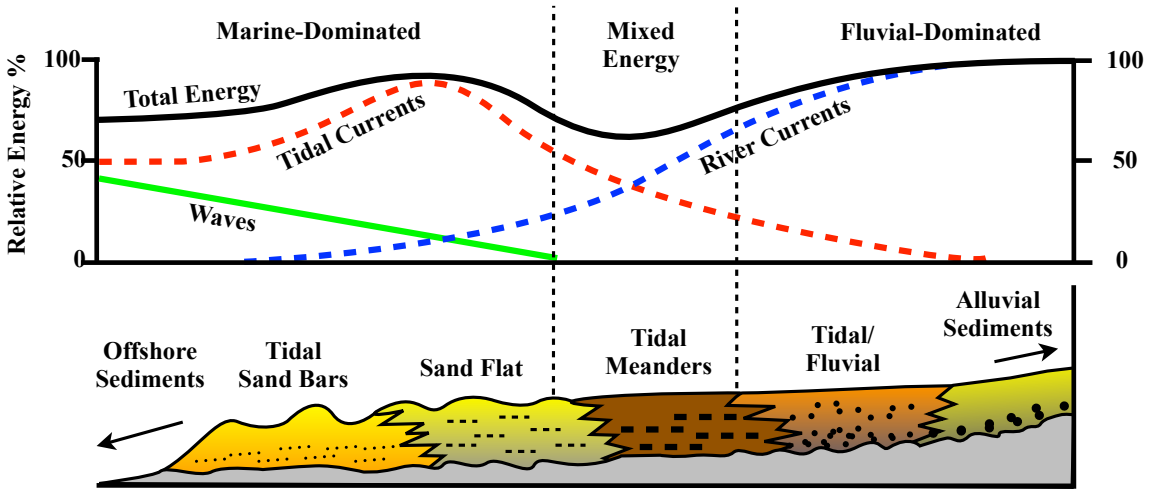


Figure 2.12 Idealized sedimentary facies and relative energy distribution for the axis of a tide-dominated estuary. Energy regimes are indicated as being either marine, mixed, or fluvial dominated, and relative energy inputs are time averaged. Facies extent may variable dependent on sediment supply, and model is vertically exaggerated. Modified from Dalrymple et al. (1992).

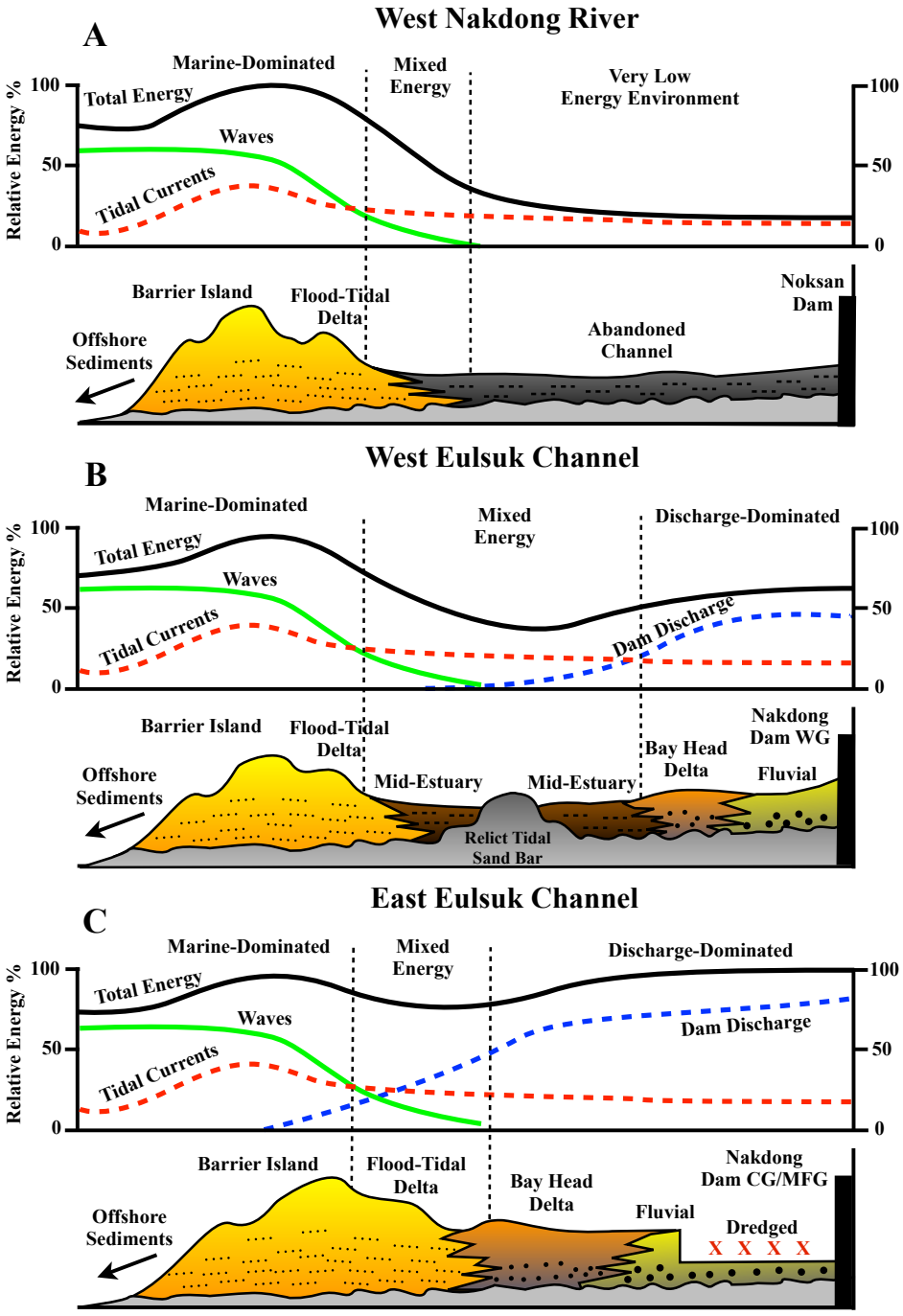


Figure 2.13 Conceptual model for relative energy and facies distribution depending on discharge from a dam for a wave-dominated estuary. A) No discharge released B) Periodic (weekly to monthly), low energy discharge C) Consistent (daily to weekly), high energy discharge.

These alterations resulted in a shift in facies distribution from tide-dominated (Figure 2.12) to a modified wave-dominated estuary, with facies dependent on the relative energy received through dam discharges (Figure 2.13). A new conceptual model is described here based on the Dalrymple et al. (1992) wave-dominated estuary model. It is important to note that our model differs as it applies to significantly anthropogenically altered systems, and is not intended to be applied to natural systems. There are several key differences that distinguish the models; however, several of the facies terms are adopted to maintain continuity. First, the relative energy input is significantly different from a typical river (e.g. Figure 2.12), because the discharge occurs over relatively short periods of time and is highly episodic with intervals of no discharge. This is opposed to a natural system in which a low discharge rate is maintained constantly. Second, this model assumes that a significant portion of the channels within the estuary have been altered by construction of seawalls or hardening of the shoreline. Lastly, a significant change is observed in relative tidal current energy due to the reduction of the tidal prism (Figures 2.12 and 2.13).

Therefore, based on the relative amount of energy received from dam releases, and subsequently the sediment flux, a conceptual model is described based on three discharge conditions: 1) No discharge released 2) Periodic (weekly to monthly), low energy discharge 3) Consistent (daily to weekly), high energy discharge. An example of each of these environmental conditions can be observed within the Nakdong Estuary. The facies shown within each model are assumed to overlay the pre-existing tide-dominated facies. While reworking of the underlying facies and redistribution of sediments likely occurred during the beginning of the transition from tide to wave-dominated, the accumulation of fluvial supplied sediments is assumed to have caused rapid burial. Included in each model is a sand dominated barrier island/flood tidal delta facies. Sediment supply for the formation of these facies is derived from fluvial delivered material, and reworking of pre-existing near shore sands and tidal bars.

The West Nakdong River exemplifies a no discharge impoundment (Noksan Dam) resulting in a predominantly very low energy environment in which very fine-grained sediment accumulates near the dam as an abandoned channel facies (Figure 2.13a). These sediments are predominantly silt and clay, containing < 10% sand. Since there is no sediment supply at the adjacent dam, the fine-grained sediment is advected from within estuary and offshore. A periodic discharge (weekly to monthly) of low energy is demonstrated by the W. Eulsuk channel (Figure 2.13b). Near the dam, sand dominated fluvial facies transition conformably to fine-grained sediments of a mid-estuary facies through a bay head delta. In this particular case, a relict tidal sand bar (Daemadeung) remains behind the rapidly formed barrier islands and mid-estuary facies sediment is accumulating in surrounding areas. The E. Eulsuk Channel demonstrates a consistent (daily to weekly) and high energy discharge environment (Figure 2.13c) resulting in sparse deposition of fine-grained material. Sediment flushed from the upstream portion of the dam rapidly accumulates as bay head delta deposits at the first point of reduced flow velocities. In the Nakdong Estuary, this process has developed Maenggeummeorideung since the construction of the dam (Figure 2.4d). Additionally, sediment deposited near the dam is dredged with large volumes being suspended and advected seaward. These models represent end-member environments for wave-dominated systems in which facies distributions can be evaluated after anthropogenic alterations and emplacement of estuarine dams based on the relative discharge energy. Estuaries experiencing a decrease in tidal currents and/or decreased sediment flux due to emplacement of dams, will subsequently encounter a redistribution of facies associated with a shift towards a relatively more wave-dominated system.

### *2.5.4 Future Research*

While multidecadal scales of sedimentation have been provided in this study, investigations on dynamics between floodgate discharge, wave and tidal energy on an annual scale are necessary to evaluate the erosion and deposition that may occur seasonally resulting in averaged sedimentation rates. A precise evaluation of seabed

elevation throughout the estuary on these time scales could link the timing and magnitude of depositional events to varying discharge volumes. Additionally, a detailed time series analysis of grain size coupled with altimeter data would greatly enhance the understanding of seasonal dynamics of sediment deposition. In combination with this type of study, an investigation utilizing very short lived radioisotopes such as $^{7}$Be could delineate the spatial extent of deposition during floodgate releases. This could be particularly useful during extreme discharge events in which large volumes of sediment may reach at least several kilometers offshore. Furthermore, a better understanding of the flow velocities produced throughout the estuary from high discharge events and normal tidal cycles could provide knowledge to support surficial sediment distributions and the formation of barrier islands.

**2.6 Conclusions**

Anthropogenic alteration to the Nakdong Estuary including the construction of numerous seawalls and estuarine dams has greatly modified the sediment transport dynamics. Construction of the seawalls eliminated large areas of intertidal zone and subsequently reduced the area for natural overbank flow and deposition during high discharge events. Consequently, sediment that previously could be trapped within the upper estuary and intertidal zones is confined to deposition within the middle of the estuary resulting in rapid accumulation rates. Construction of the Noksan Dam significantly reduced flow velocities and produced a severe depletion of coarse grained sediment in the West Nakdong River, resulting in the relatively slow accumulation of fine-grained sediments advected from the within the estuary and offshore. The occluding of the E. and W. Eulsuk Channels by construction of the Nakdong Estuarine Dam has resulted in alteration of the timing and discharge intensity at which sediment is delivered. Under current conditions, sediment flux to the estuary is restricted to floodgate releases which produce high flow velocities and episodic deposition. Furthermore, the source of sediment flux has been confined principally to the E. Eulsuk Channel instead of through three river channels that delivered sediment prior to coastal modification. Additionally, construction of the dams has prevented natural saltwater

intrusion to the Nakdong River which has appreciably reduced the tidal prism by at least 54%. This reduction in tidal energy and river discharge has resulted in a shift from a relatively tide-dominated system towards an increasingly wave-dominated system. Evidence for this change occurs as a series of barrier islands that have developed post-dam construction. The combination of these effects has resulted in extremely rapid geomorphologic changes and high accumulation rates within the estuary. These data provide insight to the increase in sediment trapping efficiency that ensued resulting from extensive coastal construction.

The observations made within this study have allowed the development of a conceptual model for facies distribution based on the relative amount of energy received from dam releases. These conditions include three discharge environments in which: 1) No discharge is released 2) there is periodic (weekly to monthly), low energy discharge and 3) there is consistent (daily to weekly), high energy discharge. Examples of each of these situations are seen within the Nakdong Estuary, respectively with the West Nakdong River, E. and W. Eulsuk Channels. The implications of anthropogenic alterations to estuarine systems is evident here based on a rapid geomorphologic reclassification from tide-dominated to wave-dominated, and high sediment accumulation rates within the middle estuary due to a reduction in accommodation space in the upper estuary as a result of seawall construction and land reclamation. A reduction of the tidal prism and modification of sediment delivery results in vast geomorphological changes accompanied by a redistribution of facies. With significant anthropogenic alterations occurring in natural estuarine systems, these observations are likely to increase and be amplified with continued development of coastlines.

# CHAPTER III
# SEDIMENTARY IMPACTS OF ANTHROPOGENIC ALTERATIONS ON THE YEONGSAN ESTUARY, SOUTH KOREA*

## 3.1 Introduction

Most of the world's ports and coastal cities reside adjacent to estuaries, with approximately 65% of cities of population greater than 5 million located less than 10 m above sea level (McGranahan et al. 2007). Throughout the last century, rapid socioeconomic development has resulted in significant engineered alterations to coastal areas, and severe degradation of ecosystems (Lotze et al. 2006, Cooper 2009, Wong et al. 2014). The industrial and urban development of estuaries has resulted in changes to shoreline configuration, fluvial discharge, tidal characteristics, and sediment dynamics (Byun et al. 2004, Crossland et al. 2005, Syvitski et al. 2005, Walling 2006, Cuvilliez et al. 2009, Gao et al. 2012, Jackson 2013, Wang et al. 2013, Williams et al. 2013, Liu et al. 2014, Pye and Blott 2014). With 37% of the world's population living within 100 km of the coast (Cohen et al. 1997), and a predicted rise in sea level of between 0.3 and 1.0 m within the next century (Church et al. 2014), it is anticipated that there will be an increase of engineered structures within estuaries globally. In order to predict the results of future anthropogenic alterations, we need to understand how systems that have already undergone comparable alterations have responded. The Republic of Korea provides an ideal natural laboratory to address such issues, because many of the watersheds and estuaries have been highly modified (Lee et al. 2011). Among the 463 estuaries identified in S. Korea, Lee et al. (2011) determined that approximately half are classified as closed estuaries due to an estuarine dam or sluice gate.

The construction of estuarine dams to impede saltwater intrusion and regulate discharge, along with vast emplacement of seawalls has considerably modified many coastal areas within the last century (Yoon and Woo 2000, Choi et al. 2005, Yoon et al.



*Reprinted with permission from "Sedimentary Impacts of Anthropogenic Alterations on the Yeongsan Estuary, South Korea" by Williams, J. R., Dellapenna, T. M., Lee, G., and Louchouarn, P., 2014, *Marine Geology*, 357, 256-271, Copyright (2014) by Elsevier B.V.

2007). The impacts of estuarine dams and/or reservoirs constructed in coastal zones on sediment deposition have been investigated in numerous studies. Sedimentation rates proximal to the Keum estuarine dam (S. Korea) were reported to have increased as much as three times (<6 cm $yr^{-1}$ to ~20 cm $yr^{-1}$) due to hydrodynamic changes that resulted in a decrease in overall current velocity (Kim et al. 2006). Within the Netherlands Haringvliet Estuary, several coastal engineering projects and dam construction resulted in increased sediment volume and a decrease in the tidal prism (Tönis et al. 2002). Anthropogenic alterations to the Nakdong Estuary (S. Korea) have also led to a similar reduction in the tidal prism. Geomorphological changes due to seawall and estuarine dam construction ultimately caused a shift in classification from a tide to wave-dominated estuary, resulting in a dramatic increase in sedimentation rates below the dam and re-distribution of bottom types and associated benthic habitats (Williams et al. 2013). Additionally, several studies have documented changes in sediment transport dynamics due to coastal dam construction (Barusseau et al. 1998, Yoon et al. 2007, Gao et al. 2012, Zamora et al. 2013). Management (dredging operations, etc.) and monitoring of estuarine sediment in macrotidal systems, particularly in estuaries of Northern Europe (Mitchell and Uncles 2013), has been addressed and the need for further sediment accumulation research is apparent.

The Yeongsan Estuary (S. Korea) is a prime example of an estuary that has undergone significant coastal construction within the last century. Built to divert and impound fresh water for agricultural practices, impede the intrusion of saltwater, and provide flood prevention, the Yeongsan Estuarine Dam was constructed in 1981. As a result, approximately 98 $km^2$ of total estuarine area was eliminated above the dam with the cessation of tidal exchange, creating the freshwater Yeongsan Lake (Figure 3.1).

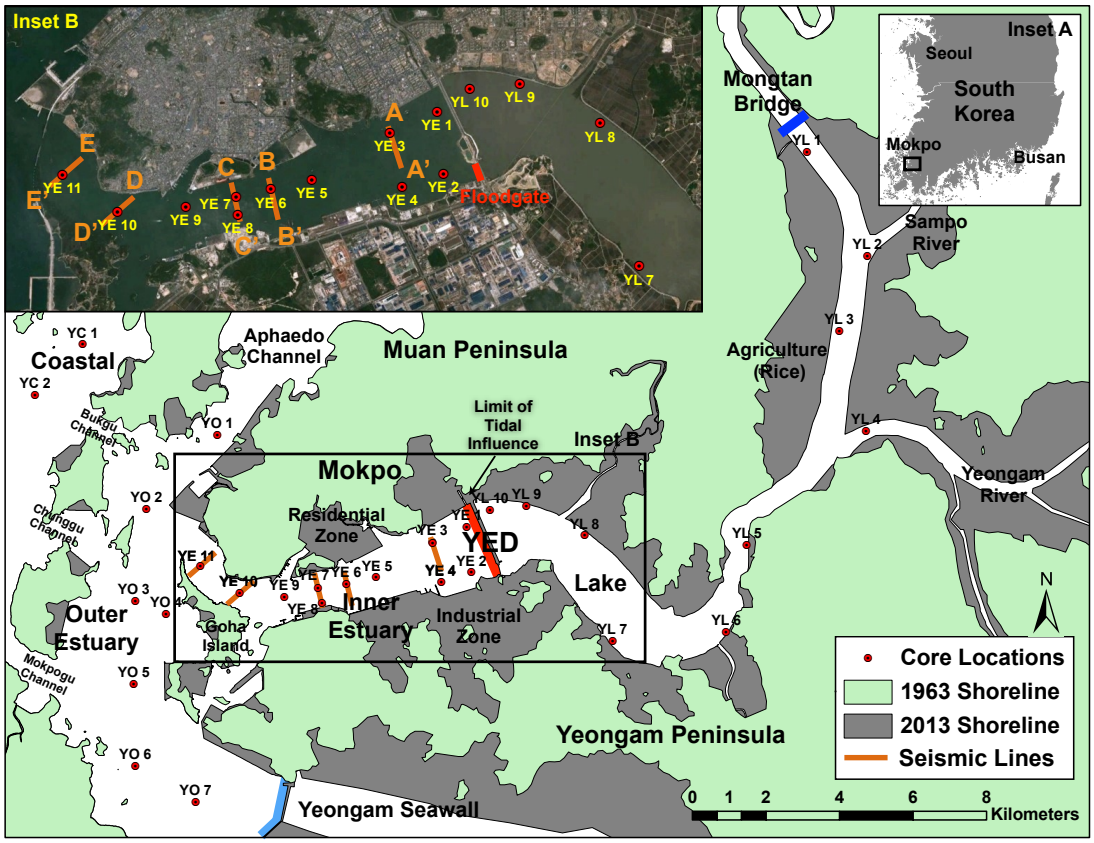


Figure 3.1 Detailed study area map showing location of the Yeongsan Estuary within South Korea and all core sampling locations. Inset A identifies study location within South Korea. Detailed location of cores proximal to the Yeongsan Estuarine Dam (YED) is shown within Inset B (extent has been outlined). The location of discharge release at the floodgates has been indicated within Inset B. Cores are labeled according to respective environments, including Yeongsan Lake (YL 1-10), Inner Estuary (YE 1-11), Outer Estuary (YO 1-7), and Coastal (YC 1-2) cores. The total reclaimed area is represented by the change in shoreline pre-development (1963) to the current configuration (2013), such that the difference in area represents reclaimed intertidal zones (gray zones).

Prior to occlusion, tidally influenced environments spanned approximately 63 km upstream from the dam (Lee et al. 2009). Additionally, during land reclamation projects throughout the 1980's, tidal flats were filled and 90 km of seawalls/embankments were added. With a current reservoir area of 34.3 $km^2$, the reduction in intertidal area above the dam is estimated to be 63.2 $km^2$ (65%). Below the dam, land reclamation projects have reduced intertidal zones by 16.5 $km^2$, resulting in a total reduction of nearly 80 $km^2$. Seawalls have also been constructed in the region south of the Yeongsan Estuary including the Youngam seawall in 1991, and the Keumho seawall in 1994, eliminating an additional 130 and 60 $km^2$ of intertidal zones respectively (Kang 1999).

Several studies have been conducted on the Yeongsan Estuary and Lake examining the changes in tidal characteristics, water structure/mixing, and biogeochemistry. In a multidisciplinary study of Yeongsan Lake, Lee et al. (2009) showed significant anthropogenic organic compound loading and oxygen depletion due to thermal and haline stratification, a reduction in fish diversity, and an increase in sediment deposition based on bathymetric change analyses. Through observational data and numerical analysis, Kang (1999) reported an increase in extreme high tide of 60 cm and a decrease in extreme low tide of 43 cm as a cumulative result of construction of the estuarine dam and seawalls. Furthermore, tidal current velocities decreased due to a reduction in tidal choking (Kang 1999). Byun et al. (2004) also reported a significant increase in tidal amplitude and an advance in tidal phase due to the reduction in storage capacity associated with a shift towards a non-choked system. These alterations have severely impacted estuarine circulation by eliminating natural mixing of fresh and saltwater above the dams, resulted in severe water quality degradation, and dramatically changed the sediment dynamics of the region (Lee et al., 2009).

Although these studies have provided insights into the hydrodynamic, biological, and chemical alterations, there remains a paucity of data investigating the historical changes within the recent stratigraphic record. While predictive or modeled shifts in sediment dynamics and historical bathymetric changes provide substantial information,

evaluating the changes in sedimentary processes through core analyses remains crucial to characterize the impacts of human alterations to these systems.

This study aims to determine the effects of anthropogenic alterations on sedimentation within the Yeongsan Estuary. Specifically, we aim to determine 1) how environmental changes have impacted sedimentary organic matter signatures 2) the system response in terms of sediment distribution and accumulation, 3) the deposition of sediment associated with a large discharge, and 4) how current accumulation rates compare to average rates throughout the Holocene. The results herein provide a case study on how macrotidal estuaries respond to significant anthropogenic alterations. These findings are not only poignant regionally, as many estuaries in East Asia have recently and are continuing to undergo significant coastal construction, but have future global implications with continued industrialization in developing countries and predicted sea level rise (Church et al. 2014).

### 3.2 Regional Setting

The Yeongsan Estuary is located within the city of Mokpo, with an approximate population of 250,000 and consists of the Yeongsan Lake, Inner Estuary, Outer Estuary, and Coastal zones (Figure 3.1). The Yeongsan River has a drainage basin area of 3,468 $km^2$ with a total length of 137 km, making it the sixth longest river in the country. The river debouches to the Yellow Sea through a relatively shallow (predominantly <50 m depth) intricate coastline of islands. The Inner Estuary is situated between the Muan and Yeongam peninsulas with an average depth and width of 19 m and 1.3 km, respectively for a length of 6.7 km. At the mouth of the estuary, the main channel splits around Goha Island opening to a series of islands separated by four main channels (Bukgu, Chunggu, Mokpogu, and Aphaedo) (Figure 3.1). Wave height is typically suppressed within the estuary due to the orientation of the estuary and the many nearshore islands blocking the open sea (Byun et al. 2007). With an approximately 4.5 m tidal range the estuary is classified as macrotidal, with primarily semidiurnal ebb dominated tides (Byun et al. 2004). The Yeongsan Lake spans 23.4 km in length from the estuarine dam to the

Mongtan Bridge, decreasing in width from 1.2 to 0.6 km with an average depth of 10 m with two main tributaries, the Sampo and Yeongam Rivers, connecting from the east (Lee et al. 2009).

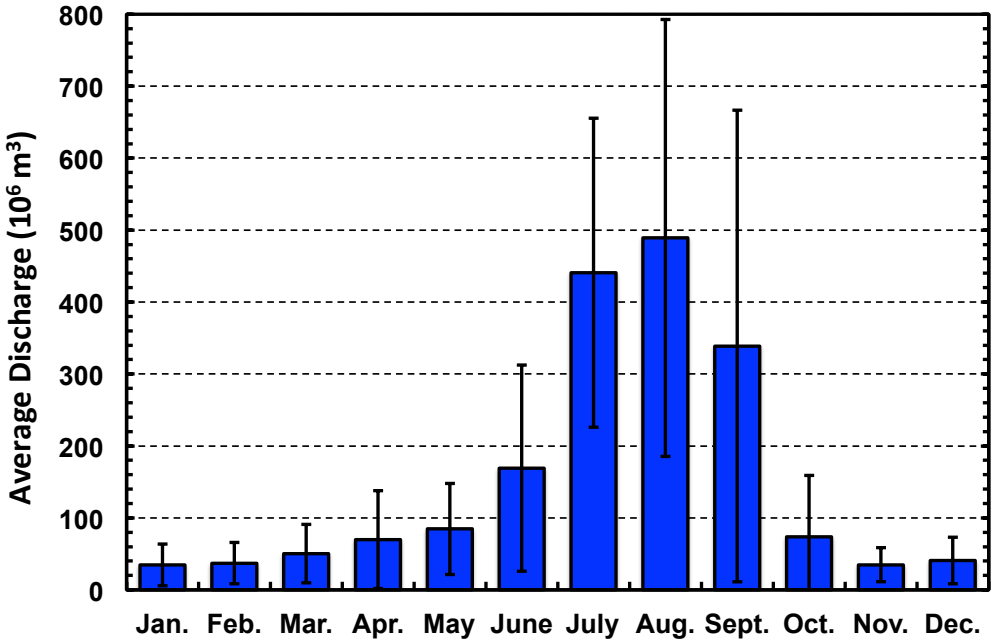


Figure 3.2 Average monthly discharge from the Yeongsan Estuarine Dam for the period of Jan. 1997 - Sept. 2013. Note that discharge scale units are $10^6$ $m^3$. Error bars are shown as 1σ.

On the Korean peninsula, climatic conditions are dominated seasonally by monsoons. During winter months, strong north to northwesterly winds are accompanied by minimal precipitation. Conversely, summer months typically experience relatively weak south to southeasterly winds, heavy precipitation, and occasional typhoons (Chang 2004). This seasonal variability in precipitation results in a predominance of freshwater releases from the dam during summer months. Discharge data from 1997-2013 reveals

that nearly 80% of the discharge occurs between late June and early September (Figure 3.2). However, the total annual discharge varies significantly and is highly dependent on annual precipitation (Figure 3.3), resulting in large standard deviations in monthly averages, particularly in summer months (Figure 3.2). Since 2000, on average the dam has been opened every 1.7 days during the summer months for 154 min. resulting in an average total discharge of 10.4 x $10^6$ $m^3$ per dam release, and opened every 7.4 days during the dry season for 123 min. resulting in an average total discharge of 2.6 x $10^6$ $m^3$ per dam release (Kang et al. 2009, Rhew and Lee 2011).

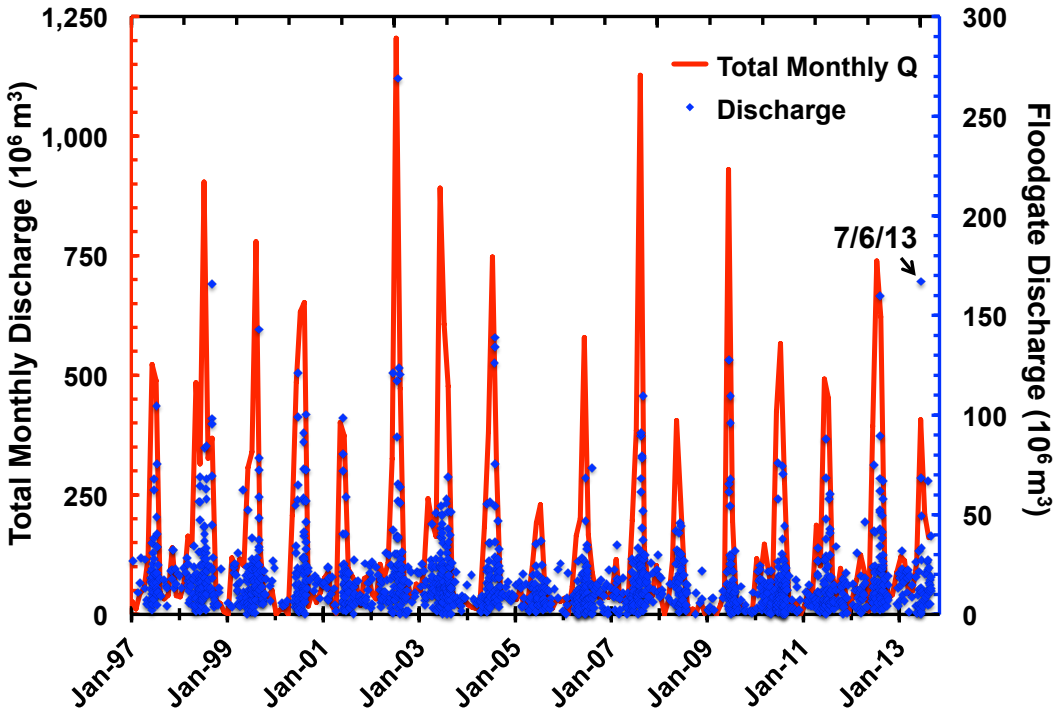


Figure 3.3 Total monthly discharge (red) and individual floodgate discharge events (blue) for the period of Jan. 1997 - Sep. 2013. The large discharge event (7/6/2013) that occurred between sampling times is indicated. Note that discharge scale units are both $10^6$ $m^3$, but there are significantly different discharge ranges on respective axis.

## 3.3 Methods

### *3.3.1 Data Collection / Core Processing*

A total of 30 gravity cores were collected between May 15-16, 2012 using a 6.0 cm diameter core barrel with PVC liners and have been nominally assigned to either lake (YL 1-10), inner estuary (YE 1-11), outer estuary (YO 1-7), or coastal (YC 1-2) environments (Figure 3.1). Additionally, 10 cores were collected by a scientific diver using 7.2 cm diameter acrylic cores on June 7 and Aug. 5, 2013, respectively at core locations YE 1, 3, 7, 11 and YO 3, 6. Cores were sealed immediately upon recovery, and showed no signs of degradation from partial recovery or transportation. X-radiographs of diver cores were taken using a MinX-Ray HF100+ Amorphous Silicon Imaging System 4030R X-Ray unit at an energy level of 60 kV with exposure time of 1/20 second. Subsamples were taken at 1 cm intervals, homogenized, and stored in Whirl-Paks® until further processing. Additional 10 g aliquots were desiccated for determination of water content.

### *3.3.2 Radioisotope Analyses*

$^{210}$Pb ($t_{1/2}$ = 22.3 $yr^{-1}$) activities were measured indirectly using the $^{210}$Po method (Nittrouer et al. 1979, Appleby 2001, Santschi et al. 2001, Williams et al. 2013). Briefly, sediments were sieved at 38 μm, spiked with $^{209}$Po, chemically separated via digestion with concentrated HCl and $HNO_3$, and electroplated onto Ag planchets. Activities of Po isotopes were assayed by α-spectroscopy using a CANBERRA surface barrier detector. Determinations of unsupported levels of $^{210}$Pb ($^{210}Pb_{xs}$) were calculated by subtraction of supported level ($^{210}Pb_{sup}$) values from total activity ($^{210}Pb_{Tot.}$). Supported values were determined from averaged activities at the base of the core, where $^{210}Pb_{Tot.}$ becomes asymptotic. For cores not reaching supported levels, an average regional value of 0.93 dpm $g^{-1}$ was applied. Average sediment accumulation rates were determined applying a constant supply of $^{210}$Pb model (Appleby and Oldfield 1978, Appleby 2001).

Activities of $^{7}$Be ($t_{1/2}$ = 53.2 $d^{-1}$) were measured by gamma spectroscopy at 477 keV using a CANBERRA High-Purity Germanium (HPGe) well detector coupled with a

DSA-1000 16K integrated multichannel analyzer. Dry samples were counted using identical geometries for gamma assay and net count rates were converted to activities using calibrated detector efficiencies. With these methods, the assumptions are made such that isotopes are irreversibly adsorbed onto particles regardless of transport pathway to the estuary, and the residence time within the water column is negligible compared to the half-life (Nittrouer et al. 1979, Santschi et al. 1989).

### *3.3.3 $\delta^{13}C$ and $\delta^{15}N$*

Sediment samples for bulk carbon and nitrogen stable isotope analyses were dessicated, HCl acidified, and analyzed via combustion with a Costech Elemental Analyzer at the Baylor University Stable Isotope Laboratory using USGS-40/41 as international standards for normalization. Standard deviations for standard reference materials were 0.01‰ and 0.02‰ for $\delta^{13}C$ and $\delta^{15}N$ respectively. Standard delta notations of isotopic values are relative respectively to Vienna Pee Dee Belemnite and atmospheric $N_2$ values.

### *3.3.4 Grainsize Analyses*

Samples were homogenized, sieved at 2 mm, sonicated with sodium hexametaphosphate dispersant, and analyzed for grainsize distribution using a Malvern Mastersizer 2000® laser particle diffractometer at a calibrated level of obscuration. Sieved fractions were dry weighed for inclusion in the final distribution. Reported results are an average of triplicate measurements of sand, silt, and clay fractions.

### *3.3.5 Bathymetric Data*

Relative changes in seabed elevation were determined from bathymetric survey data provided by the Korean Hydrographic and Oceanographic Administration (KHOA) from 1983 and 1997. Using ESRI ArcGIS®, discrete measurements were converted to bathymetric surfaces and the differences are reported as relative change in bed level, with positive and negative values representing accretion and erosion or dredging, respectively (Figure 3.4). The horizontal spatial resolution of survey data is

approximately 10 m, with no information provided on vertical resolution. Considering the precision of available survey equipment, the accuracy of data on or below decimeter scales is contentious.

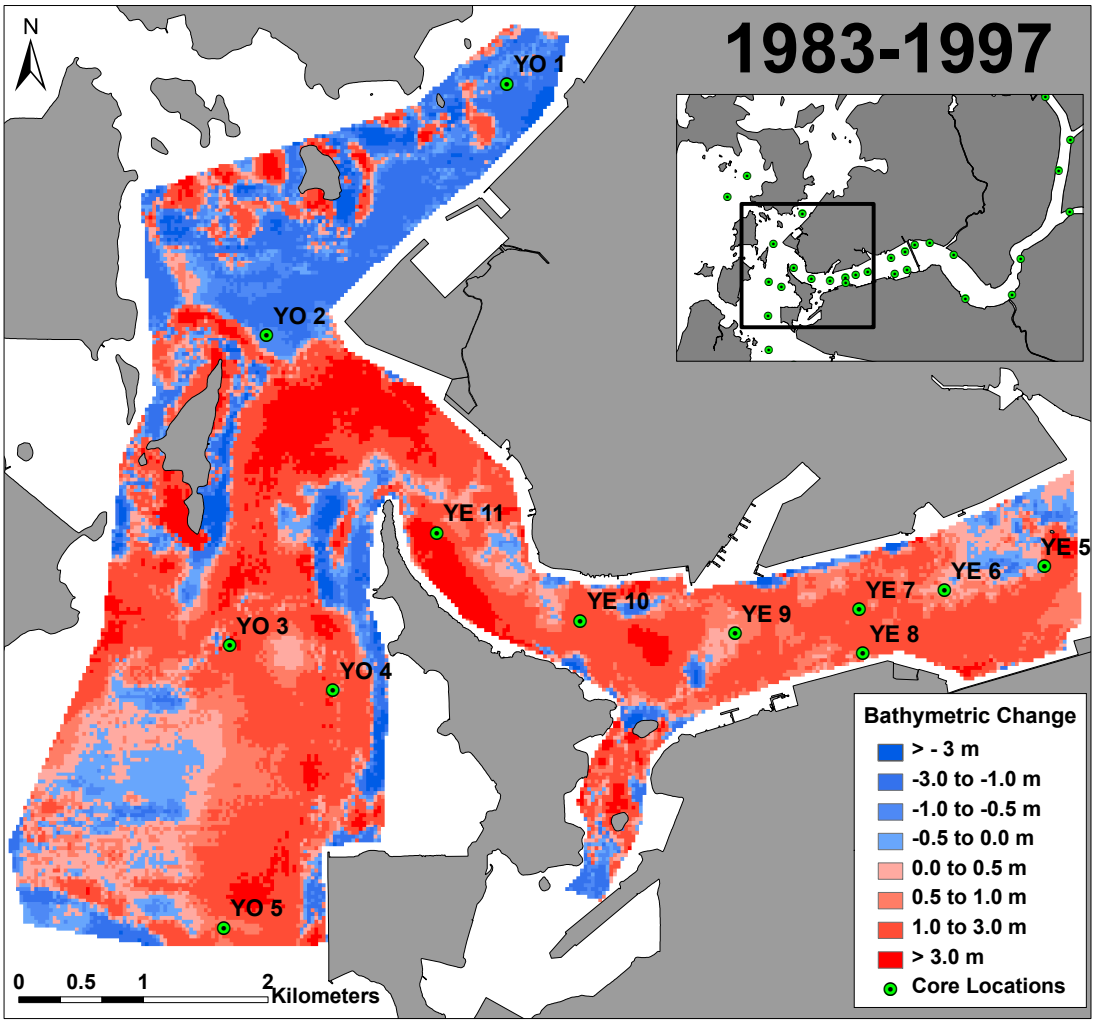


Figure 3.4 Calculated bathymetric change from 1983 to 1997 based on surveys conducted by the Korean Hydrographic and Oceanographic Administration. Areas of net accumulation are indicated in red, while areas of net erosion are indicated in blue. Color bar indicates magnitude of bathymetric change in meters. Note: Some areas of apparent erosion may be the result of dredging activity.

*3.3.6 Geophysical Data*

Side-scan sonar data were collected using a DSME E&R Ltd. T-150A SonarBeam at 400 kHz perpendicular to the axis of the estuary at 100 m line spacing using constant gain and range settings. Mosaic compilation was completed in Chesapeake Technology Inc. SonarWiz 5 utilizing nadir blanking and time variable gain. Grainsize data from surface intervals of cores and surface grab samples (unpublished data) were used to calibrate backscatter intensities.

High-resolution sub-bottom seismic data were collected with an Edgetech 3100 and SB-216S CHIRP towfish operating with a swept acoustic frequency range of 2-16 kHz. Post-processing of seismic data was conducted in Chesapeake Technology Inc. SonarWiz 5 software applying water-column blanking, sediment interface tracking, time variable gain, and trace stacking.

**3.4 Results**

*3.4.1 Geochronology*

Examination of $^{210}Pb_{xs}$ activity revealed 3 distinctive profiles that have been characterized herein as core types A, B, and C. Representative examples displaying typical $^{210}Pb$ characteristics are shown in Figures 3.5, 3.6, and 3.7. Sedimentation rates on a decadal timescale are assessed as valid based on sufficiently high $R^2$ values (>0.7) of the regression line. Water content profiles were also used to corroborate geochronology results. Qualitatively, high water content sediments have not undergone significant gravitational compaction, and are interpreted as recently deposited. Conversely, compacted sediment containing low interstitial pore-water is interpreted to have undergone sufficient loading to reduce water content with extended burial time. Geochronology data, total core length, and core classification type have been summarized by region in Table 3.1.

| Region | Core | Type | Length (cm) | Avg. Sand % | Avg. Silt % | Avg. Clay % | $^{210}$Pb $S_{Avg}$ (cm yr$^{-1}$) |
|---|---|---|---|---|---|---|---|
| Lake | YL 1 | B | 208 | 10.7 ± 16.9 | 64.4 ± 13.0 | 24.9 ± 5.7 | 1.3 ± 0.6 |
| | YL 2 | B | 214 | 0.8 ± 3.3 | 63.6 ± 3.5 | 35.6 ± 4.1 | 2.0 ± 0.4 |
| | YL 3 | B | 154 | 6.5 ± 14.0 | 65.2 ± 10.6 | 28.3 ± 6.7 | 2.3 ± 0.4 |
| | YL 4 | B | 198 | 9.2 ± 12.2 | 65.5 ± 8.4 | 25.2 ± 4.5 | 2.5 ± 1.3 |
| | YL 5 | B | 143 | 6.5 ± 6.2 | 63.7 ± 5.1 | 29.8 ± 4.4 | 1.9 ± 1.3 |
| | YL 6 | C | 182 | 2.4 ± 1.6 | 73.7 ± 2.2 | 23.8 ± 1.6 | - |
| | YL 7 | C | 131 | 1.5 ± 1.6 | 69.7 ± 1.2 | 28.8 ± 1.7 | - |
| | YL 8 | B | 97 | 12.1 ± 11.4 | 70.0 ± 13.0 | 17.9 ± 4.9 | 2.7 ± 0.5 |
| | YL 9 | B | 163 | 5.8 ± 1.8 | 71.6 ± 5.1 | 22.6 ± 6.1 | 1.4 ± 0.8 |
| | YL 10 | B | 157 | 4.6 ± 2.2 | 68.7 ± 3.7 | 26.7 ± 3.8 | 2.0 ± 0.4 |
| Inner Estuary | YE 1 | B | 212 | 4.4 ± 2.2 | 65.4 ± 4.5 | 30.2 ± 3.8 | 0.9 ± 0.6 |
| | YE 2 | C | 106 | 13.4 ± 3.3 | 69.3 ± 2.6 | 17.3 ± 1.3 | - |
| | YE 3 | B | 201 | 4.1 ± 1.1 | 63.1 ± 6.7 | 32.7 ± 6.4 | 2.4 ± 0.6 |
| | YE 4 | A | 162 | 9.5 ± 3.9 | 71.4 ± 3.9 | 19.2 ± 1.8 | 4.8 ± 1.9 |
| | YE 5 | A | 167 | 8.1 ± 11.8 | 57.1 ± 7.7 | 34.8 ± 6.6 | 10.0 ± 2.9 |
| | YE 6 | A | 96 | 4.1 ± 3.1 | 59.9 ± 4.7 | 36.0 ± 3.6 | 7.0 ± 2.2 |
| | YE 7 | A | 118 | 3.4 ± 1.9 | 64.0 ± 2.2 | 32.7 ± 2.4 | 8.2 ± 2.1 |
| | YE 8 | A | 124 | 3.5 ± 1.0 | 66.2 ± 2.2 | 30.3 ± 2.4 | 4.1 ± 1.2 |
| | YE 9 | A | 139 | 5.0 ± 2.5 | 64.9 ± 1.5 | 30.1 ± 1.3 | 6.0 ± 1.1 |
| | YE 10 | A | 157 | 3.9 ± 1.3 | 66.4 ± 3.3 | 29.7 ± 3.8 | 8.8 ± 1.4 |
| | YE 11 | A | 153 | 0.6 ± 0.3 | 67.3 ± 1.0 | 32.1 ± 1.1 | 8.1 ± 1.2 |
| Outer Estuary | YO 1 | C | 112 | 19.8 ± 19.7 | 57.8 ± 13.9 | 22.4 ± 6.0 | - |
| | YO 2 | C | 181 | 9.2 ± 3.9 | 71.3 ± 4.8 | 19.5 ± 3.8 | - |
| | YO 3 | B | 149 | 9.8 ± 5.8 | 66.1 ± 4.2 | 24.1 ± 3.6 | 3.1 ± 0.7 |
| | YO 4 | A | 158 | 4.8 ± 1.8 | 68.8 ± 1.1 | 26.4 ± 1.9 | 4.5 ± 1.3 |
| | YO 5 | A | 110 | 4.6 ± 3.5 | 66.0 ± 2.5 | 29.5 ± 1.4 | 7.8 ± 1.5 |
| | YO 6 | A | 119 | 0.2 ± 0.2 | 66.5 ± 0.9 | 33.3 ± 1.0 | 9.4 ± 2.3 |
| | YO 7 | C | 162 | 9.8 ± 8.1 | 68.7 ± 7.1 | 21.6 ± 2.1 | - |
| Coastal | YC 1 | C | 113 | 5.9 ± 1.5 | 73.3 ± 1.5 | 20.9 ± 1.7 | - |
| | YC 2 | B | 189 | 2.6 ± 1.7 | 71.9 ± 1.6 | 25.5 ± 2.9 | 1.7 ± 0.6 |

Table 3.1 Summary of grainsize and average sediment accumulation data derived from $^{210}$Pb geochronology. Cores are separated by region (locations shown in Fig. 1) and core lengths are shown in cm. Sand, silt, and clay percentages represent averages calculated from all samples within each core at a maximum sampling interval of 5 cm with errors shown as 1σ. Note: Accumulation rates were not able to be calculated for cores with no $^{210}Pb_{xs}$ activity (type C).

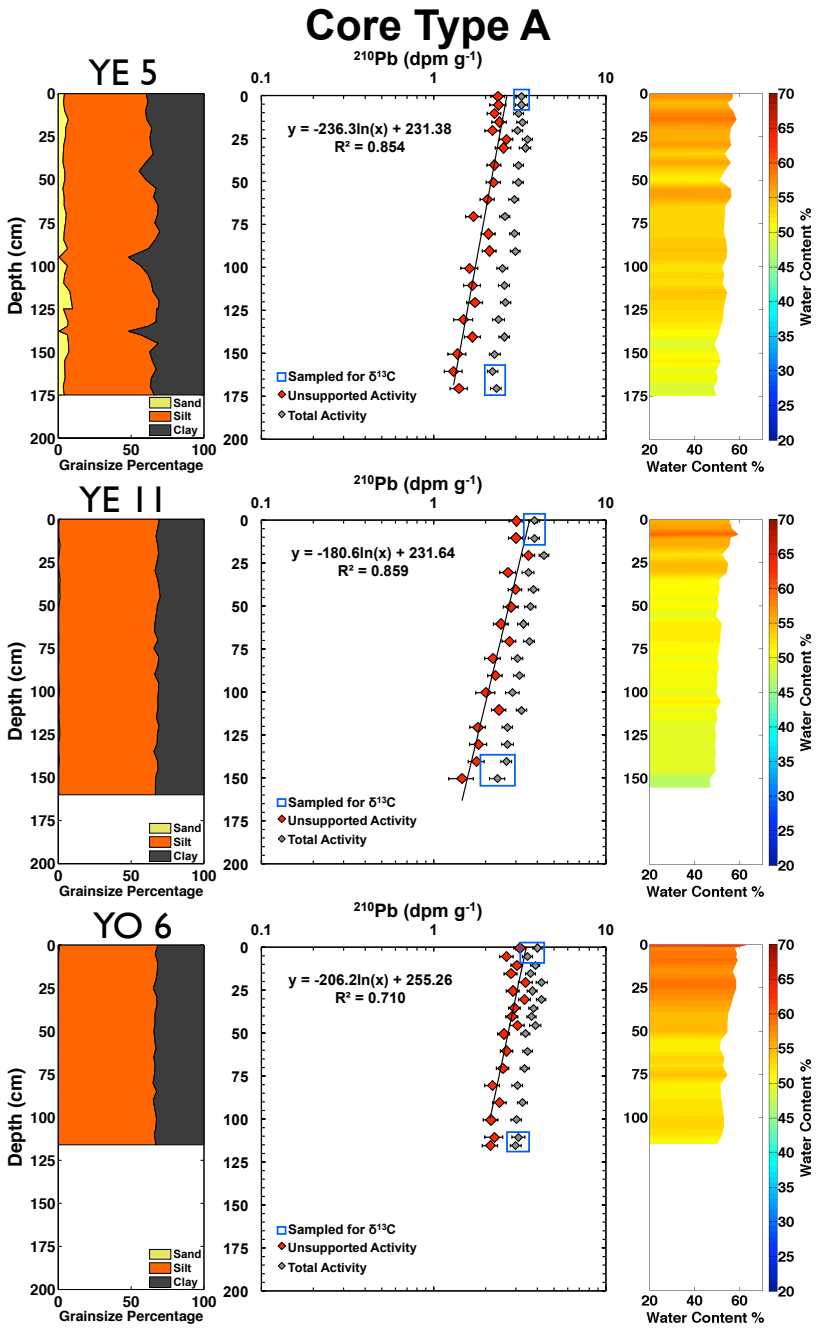


Figure 3.5 Representative examples of Core Type A (Core locations are shown in Figure 3.1). Left panel indicates relative grainsize percentage. Middle panel displays total ($^{210}Pb_{Tot.}$) and unsupported ($^{210}Pb_{xs}$) activities of $^{210}Pb$ in dpm $g^{-1}$. Regression line for $^{210}Pb_{xs}$ and $R^2$ value are shown within plot. Samples chosen for $\delta^{13}C$ and $\delta^{15}N$ analyses are also indicated. Right panel shows water content percentage throughout each core.

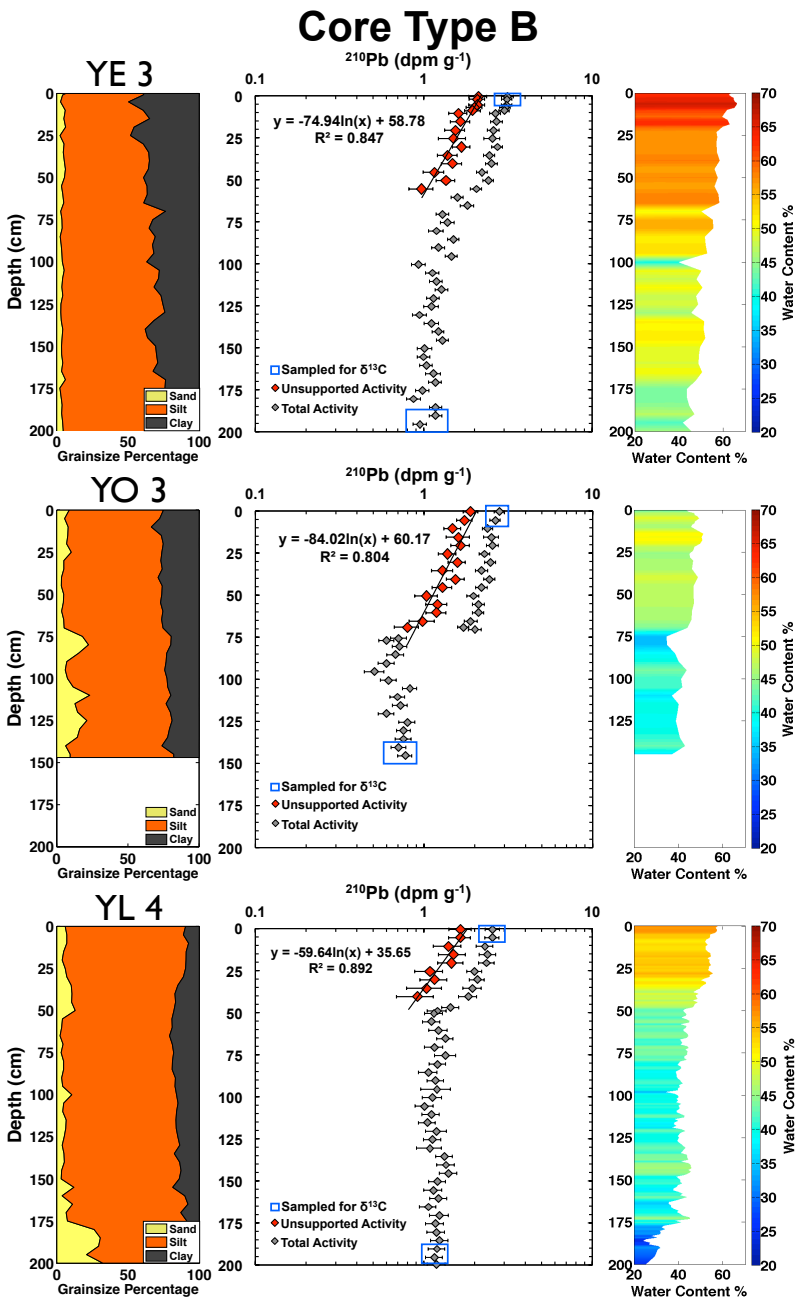


Figure 3.6 Representative examples of Core Type B (Core locations are shown in Figure 3.1). Left panel indicates relative grainsize percentage. Middle panel displays total ($^{210}Pb_{Tot.}$) and unsupported ($^{210}Pb_{xs}$) activities of $^{210}Pb$ in dpm $g^{-1}$. Regression line for $^{210}Pb_{xs}$ and $R^2$ value are shown within plot. Samples chosen for $\delta^{13}C$ and $\delta^{15}N$ analyses are also indicated. Right panel shows water content percentage throughout each core.

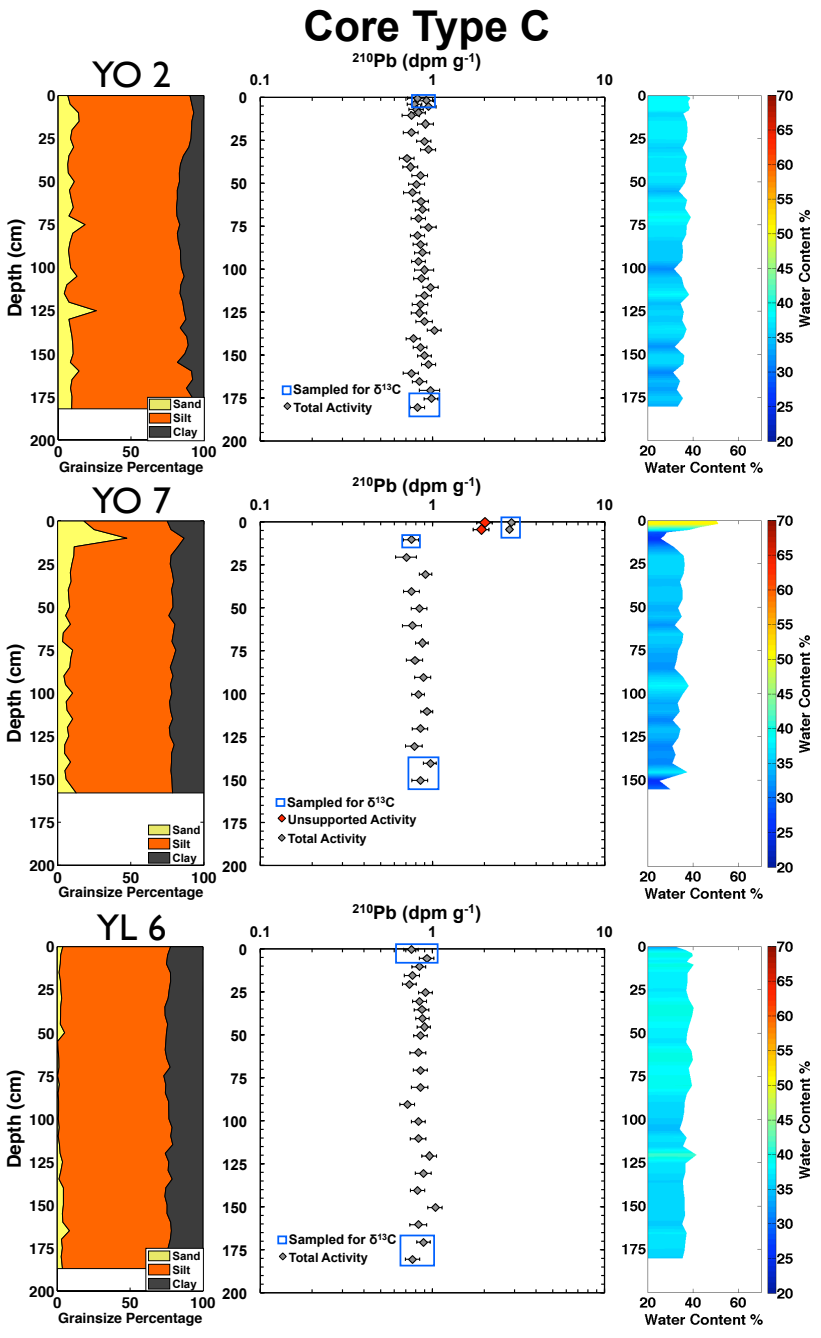


Figure 3.7 Representative examples of Core Type C (Core locations are shown in Figure 3.1). Left panel indicates relative grainsize percentage. Middle panel displays total ($^{210}Pb_{Tot.}$) and unsupported ($^{210}Pb_{xs}$) (YO 7 only) activities of $^{210}Pb$ in dpm $g^{-1}$. Samples chosen for $\delta^{13}C$ and $\delta^{15}N$ analyses are also indicated. Right panel shows water content percentage throughout each core.

Core type A exhibits $^{210}Pb_{Tot.} > 2.0$ dpm $g^{-1}$ throughout the core, indicating activities are significantly above supported levels (Figure 3.5). These 11 cores have been determined to have relatively high average sedimentation rates of > 4 cm $yr^{-1}$, with values ranging from 4.1 ± 1.2 cm $yr^{-1}$ (YE 8) to 10.0 ± 2.9 cm $yr^{-1}$ (YE 5). Water contents are high (> 50%) throughout, indicative of rapid sediment accumulation. Core type B displays relatively moderate average sediment accumulation rates, with $^{210}Pb_{Tot.}$ activities decreasing from approximately 2.0 to < 1.0 dpm $g^{-1}$ at depth, reaching supported levels (Figure 3.6). The 12 cores classified as type B represent a range in average accumulation rates from 0.9 ± 0.6 cm $yr^{-1}$ (YE 1) to 3.1 ± 0.7 cm $yr^{-1}$ (YO 3). Type B cores also showed a decrease in water content from approximately 60% at the surface to 35% at the base of the core, supporting the interpretation of relatively moderate accumulation rates. Cores of type C contain $^{210}Pb_{Tot.} < 1.0$ dpm $g^{-1}$ throughout, representing only supported activity (Figure 3.7). The low $^{210}Pb_{xs}$ and water content values (< 40%) throughout suggest the lack of sediment accumulation. However, an exception exists in the upper 8 cm of YO 7 with samples containing $^{210}Pb_{Tot.}$ activities of approximately 2.0 dpm $g^{-1}$ and water content of 53%.

Examination of the distribution of core type reveals a clustering of type A within the inner estuary and proximal outer estuary, type B cores dominating the upper lake region and areas near the dam, and type C cores occurring in varying locations throughout the system. Accordingly, the highest accumulation rates are within the inner estuary, averaging approximately 8 cm $yr^{-1}$ throughout, while relatively moderate accumulation rates are observed through the majority of Yeongsan Lake, averaging approximately 2 cm $yr^{-1}$ (Figure 3.8). In order to understand the spatial distribution and variability in average sediment accumulation rates, interpolation of these data were conducted using a standard Kriging method (Figure 3.8). While this method identifies trends, it is based solely on interpolation and it is presented as an interpretation. However, we believe the spatial density of core locations is sufficient to provide an accurate portrayal, and consistency between this approach (Figure 3.8) and bathymetric

change analyses (Figure 3.4) supports the reconstruction of accretion versus eroding regions.

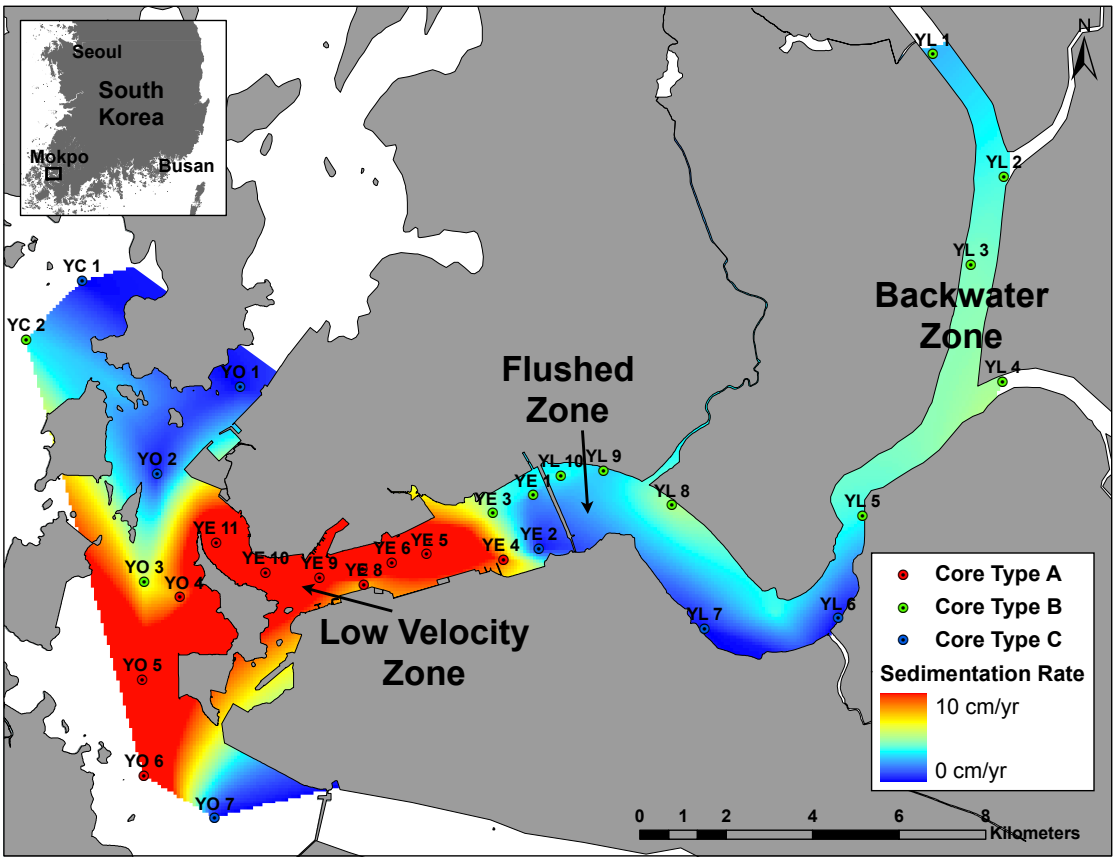


Figure 3.8 Interpolated average sediment accumulation rates for the Yeongsan Estuary. Input data obtained from $^{210}$Pb geochronology from all cores shown. Core type (A, B, C) is indicated by color. Core type C was assumed as 0 cm yr$^{-1}$ for interpolation.

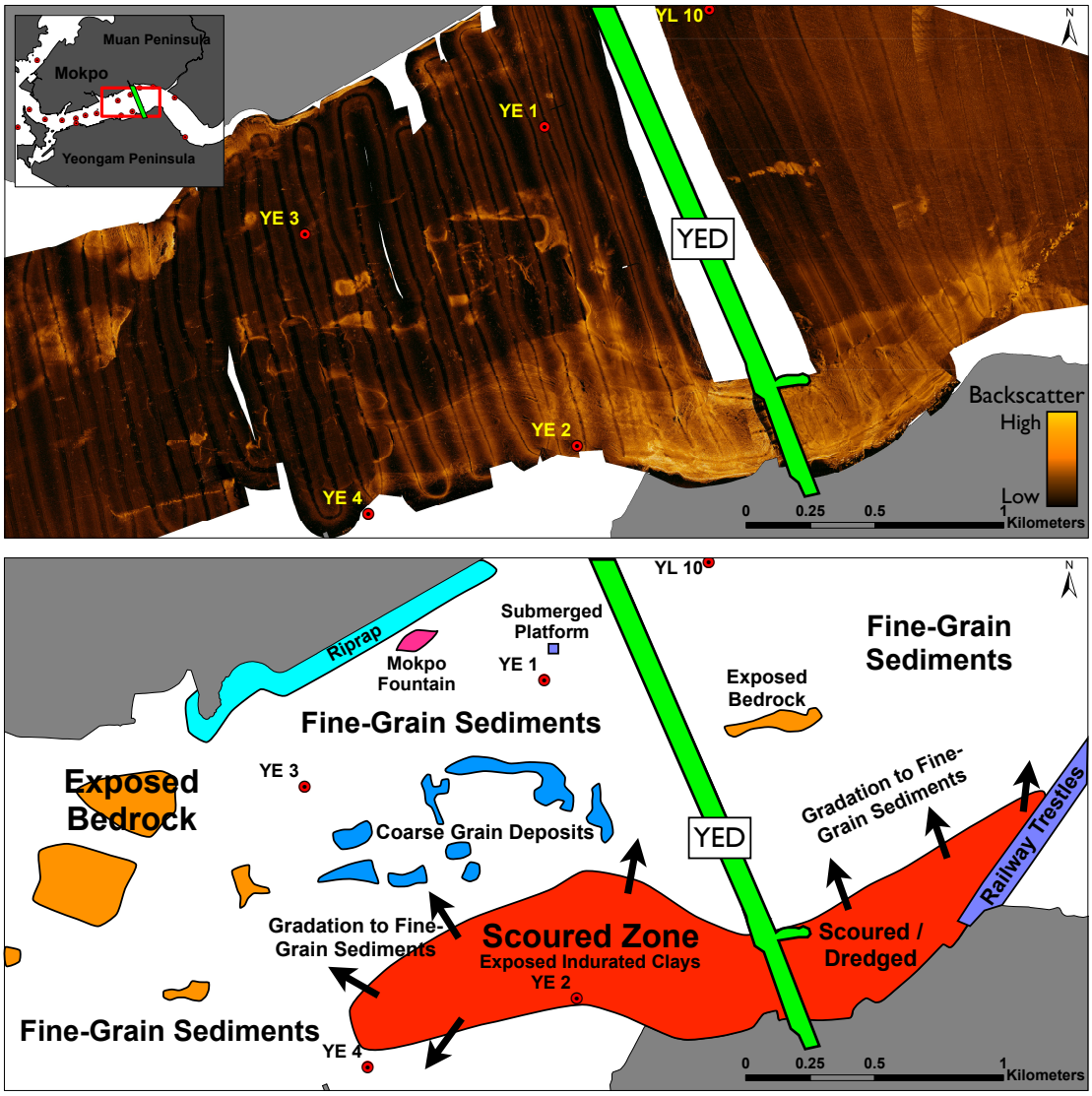


Figure 3.9 Side scan sonar mosaic (top panel) and interpretations (bottom panel) of area immediately adjacent to the Yeongsan Estuarine Dam (YED). Figure extent is outlined and panels are identical in scale. Interpretations are color coded by type throughout survey area.

*3.4.2 Surficial Sediment Distribution*

The surficial distribution of sediment adjacent to the dam has been investigated by side scan sonar mosaic analyses (Figure 3.9). A range in backscatter intensity occurs throughout the survey, with the majority of the region displaying very low backscatter with several high backscatter targets distributed predominately in the inner estuary. Confirmed by grainsize distributions of surficial sediment (YE 1-4, YL 10), the low backscatter represents unconsolidated fine-grained sediment. High backscatter targets observed within the survey area were identified visually as bedrock at low tide during subaerially exposure. In the central region of the estuary, numerous irregularly shaped, relatively high backscatter targets have been interpreted as coarser grain sediment.

*3.4.3 Stable Isotope Signatures*

Organic matter source was evaluated using stable isotopic analyses of $\delta^{13}C$ and $\delta^{15}N$, with samples taken at surface and bottom intervals of 15 cores (Ex. Figures 3.5, 3.6, and 3.7) and summarized as interval averages in Table 3.2. Signatures for $\delta^{13}C$ and $\delta^{15}N$ ranged from -26.2‰ to -15.8‰, and 4.7‰ to 10.2‰, respectively. Based on $^{210}Pb$ geochronology, isotopic values are interpreted as deposited pre-dam (<1981) if sampled from the bottom of core types B or C, and post-dam if sampled from the surface of core types A or B (Figure 3.10). While a gradient in pre-dam $\delta^{13}C$ signatures exists from lake to coastal samples (-22.3‰ to -15.8‰), a notably higher range is observed in post-dam sediment (-26.2‰ to -16.4‰) (Figure 3.10). Additionally, enrichment in $\delta^{15}N$ signature is apparent with pre-dam samples (4.7‰ to 6.5‰) exhibiting a smaller and relatively depleted range compared to post-dam samples (5.3‰ to 10.2‰). Statistical analyses (heteroscedastic T-test) reveal there are significant shifts ($p < .01$) in $\delta^{13}C$ and $\delta^{15}N$ signatures of pre and post dam sediments within the lake and inner estuary. In the outer estuary, no significant differences for $\delta^{13}C$ and $\delta^{15}N$ are observed ($p = 0.67$ and $p = 0.27$, respectively).

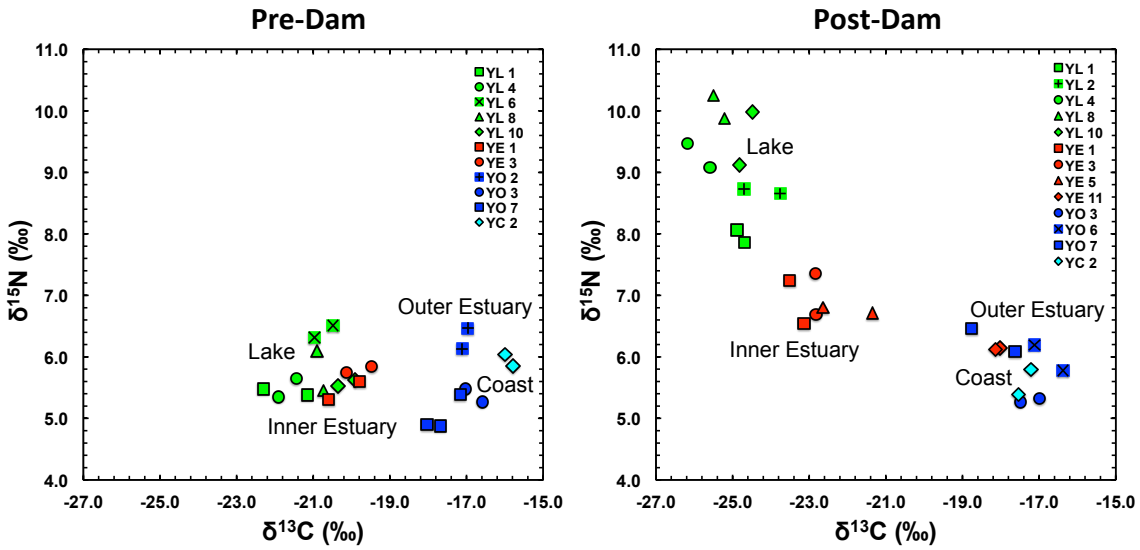


Figure 3.10 $\delta^{13}C$ and $\delta^{15}N$ signatures for pre and post-dam sediment. Samples are color coded according to region (Yeongsan Lake = Green, Inner Estuary = Red, Outer Estuary = Blue, Coast = Teal) and symbols for cores (Type B) in both panels are consistent. Pre-dam samples were taken from the bottom of cores type B and C, and post-dam samples were taken from the tops of cores type A and B. An exemption to this is core YO 7 (Type C) where the upper two surface samples are considered post dam sediments. Selected sample depths in cores are indicated in Figures 3.5, 3.6, and 3.7.

### *3.4.4 Grainsize Profiles*

Grainsize profiles are shown as relative percent composition of sand, silt, and clay and exhibited relatively minor changes throughout individual cores, with only slight variation between cores regardless of depositional environment (Figures 3.5, 3.6, and 3.7). The average relative grainsize distribution for all cores is summarized in Table 3.1. The preponderance of samples are composed of fine silt and clay with minor amounts of sand present. Considering averaged data from all cores, the sediment composition data yields an average sand (6.2 ± 4.3%), silt (66.7 ± 4.1%), and clay (27.1 ± 5.4%) content, respectively (errors shown as 1σ).

| Region | Core | Type | Sample | $\delta^{15}N$ | $\delta^{13}C$ | %TOM | Δ%TOM |
|---|---|---|---|---|---|---|---|
| Lake | YL 1 | B | SF | 8.0 ± 0.15 | -24.8 ± 0.14 | 88.1 | 29.9 |
| | | | BT | 5.4 ± 0.07 | -21.7 ± 0.81 | 58.2 | |
| | YL 2 | B | SF | 8.7 ± 0.05 | -24.2 ± 0.67 | 82.6 | 21.3 |
| | | | BT | 6.2 ± 0.12 | -22.1 ± 0.25 | 61.3 | |
| | YL 4 | B | SF | 9.3 ± 0.27 | -25.9 ± 0.42 | 98.9 | 41.3 |
| | | | BT | 5.5 ± 0.21 | -21.7 ± 0.33 | 57.6 | |
| | YL 6 | C | SF | 5.7 ± 0.33 | -21.5 ± 0.18 | 55.8 | 7.4 |
| | | | BT | 6.4 ± 0.13 | -20.7 ± 0.34 | 48.4 | |
| | YL 8 | B | SF | 10.1 ± 0.26 | -25.4 ± 0.20 | 93.7 | 44.5 |
| | | | BT | 5.8 ± 0.45 | -20.8 ± 0.11 | 49.3 | |
| | YL 10 | B | SF | 9.5 ± 0.61 | -24.7 ± 0.25 | 86.8 | 44.3 |
| | | | BT | 5.6 ± 0.07 | -20.1 ± 0.31 | 42.5 | |
| Inner Estuary | YE 1 | B | SF | 6.9 ± 0.49 | -23.3 ± 0.26 | 73.8 | 30.7 |
| | | | BT | 5.4 ± 0.21 | -20.2 ± 0.57 | 43.1 | |
| | YE 3 | B | SF | 7.0 ± 0.47 | -22.8 ± 0.01 | 69.0 | 29.7 |
| | | | BT | 5.8 ± 0.07 | -19.8 ± 0.47 | 39.4 | |
| | YE 5 | A | SF | 6.8 ± 0.06 | -22.0 ± 0.92 | 60.8 | -3.5 |
| | | | BT | 6.7 ± 0.22 | -22.4 ± 0.25 | 64.3 | |
| | YE 11 | A | SF | 6.1 ± 0.02 | -18.1 ± 0.08 | 22.4 | 1.5 |
| | | | BT | 5.9 ± 0.13 | -17.9 ± 0.27 | 20.9 | |
| Outer Estuary | YO 2 | C | SF | 5.3 ± 0.21 | -17.5 ± 0.61 | 17.0 | 4.8 |
| | | | BT | 6.3 ± 0.24 | -17.0 ± 0.11 | 12.3 | |
| | YO 3 | B | SF | 5.9 ± 0.04 | -18.2 ± 0.35 | 14.2 | 4.2 |
| | | | BT | 4.8 ± 0.15 | -17.9 ± 0.31 | 10.1 | |
| | YO 6 | A | SF | 6.0 ± 0.29 | -16.8 ± 0.53 | 9.4 | -1.9 |
| | | | BT | 6.3 ± 0.05 | -16.9 ± 0.01 | 11.3 | |
| | YO 7 | C | SF | 6.3 ± 0.26 | -17.9 ± 0.80 | 23.5 | 5.5 |
| | | | BT | 5.1 ± 0.29 | -17.6 ± 0.44 | 18.0 | |
| Coastal | YC 2 | B | SF | 5.6 ± 0.29 | -17.4 ± 0.23 | 15.5 | 14.5 |
| | | | BT | 5.9 ± 0.13 | -15.9 ± 0.14 | 1.0 | |

Table 3.2 Summary of organic matter $\delta^{13}C$ and $\delta^{15}N$ signatures and interpreted terrestrial organic matter (TOM) percentages. Cores are separated by region (locations shown in Fig. 1) and core types are indicated. Values shown represent averages for surface (SF) and bottom (BT) intervals of cores with errors are shown as 1σ. The change (Δ%TOM) was calculated as the difference in surface and bottom %TOM for each core. Note: Core YO 7 surface samples are post-dam sediments although core is classified as Type C.

### *3.4.5 High Resolution Seismic Stratigraphy*

The record of Holocene sedimentation has been evaluated through CHIRP seismic on a series of cross estuary transects intersecting with cores YE 3, 6, 7, 8, 10, and 11 (Figure 3.1). These profiles reveal a prominent reflector extending continuously through the survey at approximately 3 to 7 m sediment depth, with reflectors primarily indistinguishable below. Where identifiable, this reflector has been traced. Above this point, an unconformable stratigraphic sequence with numerous continuous internal reflectors is observed throughout the inner estuary. While the thickness of the strata within this sequence varies, a strong correlation to the depth of the acoustic basement is apparent, suggesting control of antecedent topography (i.e. accumulation space) on sediment accumulation.

### *3.4.6 $^{7}$Be Deposition and X-radiographs*

To determine the timing of sediment deposition in relation to discharge, cores were collected and assayed for $^{7}$Be activity. In order to characterize the dry/low discharge season, 4 cores were collected (6/7/13) prior to the beginning of the summer monsoon. Although high discharge events may occur through Sept. (Figure 3.2), to minimize time after a large discharge event (7/6/13, Figure 3.3), 6 subsequent cores were collected (8/5/13) before the end of the average high discharge/monsoon period. In locations with data from both sampling periods (YE 1, 3, 11 and YO 3), the results prior to high discharge events (6/7/13) have been depth offset to interpreted depths of sediment deposition observed in temporally successive cores (8/5/13). Additional core results with pre-flooding data unavailable (YE 7 and YO 6) are also reported (Figure 3.11).

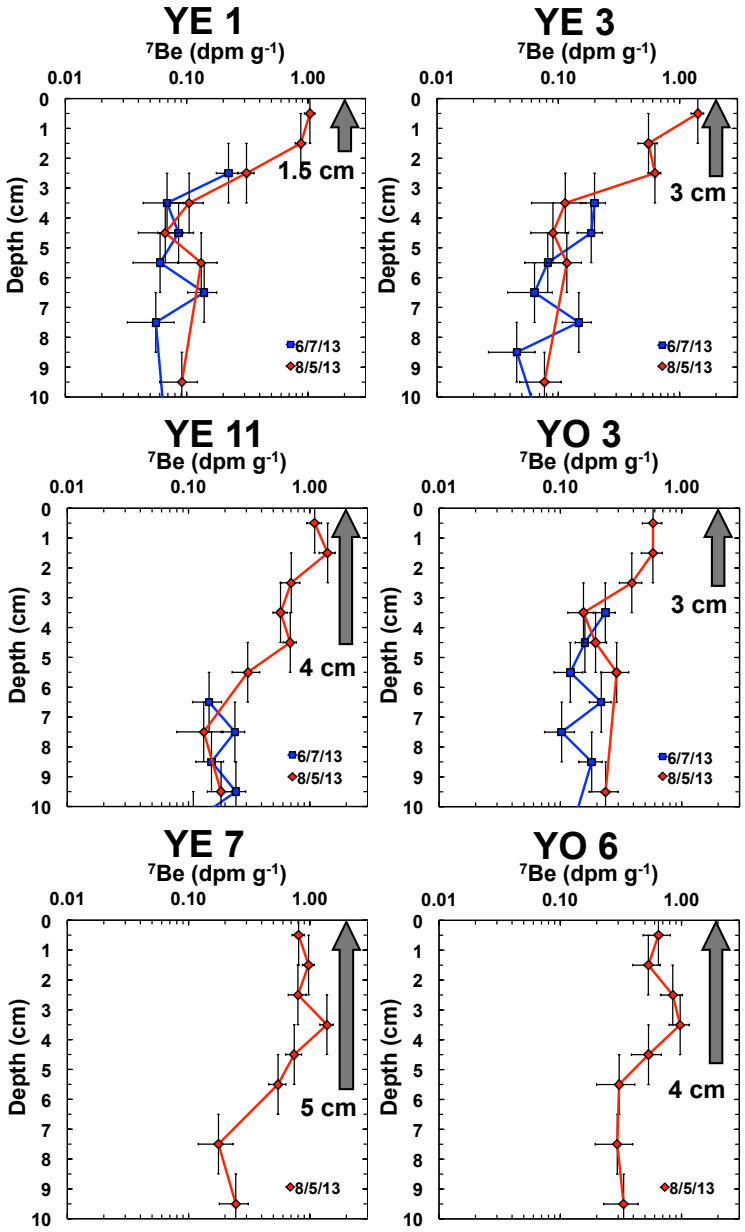


Figure 3.11 $^{7}$Be activities with depth for cores obtained from the Yeongsan Estuary on 6/7/13 (Blue) and 8/5/13 (Red). Cores were taken at the same location (within GPS error), except YE 7 and YO 6 for which only data from 8/5/13 are available. Cores from 6/7/13 have been depth offset to the interpreted depth of new sediment deposition, which is shown by arrows within. Note: Large discharge event occurring between sampling times (7/6/13) is indicated in Figure 3.3.

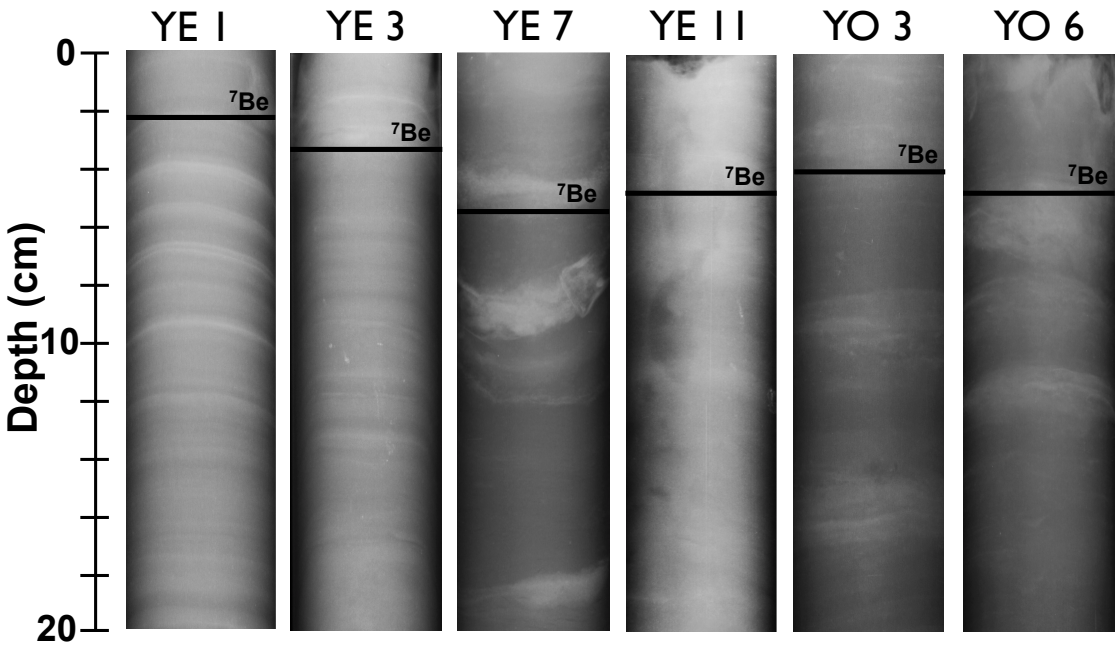


Figure 3.12 Representative X-radiographs for cores shown in Figure 3.11. Depth of $^{7}$Be penetration is indicated (also shown in Fig. 11). 7Be depths were allowed slight depth adjustment (< 1 cm) to coincide with observed bedding features to compensate for sampling procedure error.

Cores taken in June display relatively depth constant $^{7}$Be activities near detection limits between 0.06 and 0.25 dpm $g^{-1}$, suggesting sediment deposition prior to at least 2 half-lives (> ≈ 100 d). $^{7}$Be activities from cores taken in August are elevated in surface intervals (0.8 to 1.2 dpm $g^{-1}$), and display abruptly decreased activities at depth, suggesting recently deposited surface sediments. Sediment deposition occurring between sample collection dates is interpreted as the offset depth corresponding to maximum penetration (1.5 to 5 cm) of elevated $^{7}$Be activities (Figure 3.11), and has been indicated on core X-radiographs (Figure 3.12). Considering potential mixing and the complexity involved in sampling surface sediment, these estimates should be regarded as maximum deposition depths. X-radiographs reveal minor to absent bioturbation throughout, with

laminations ranging in size from millimeters to centimeters. Specifically, in cores located proximal to the estuarine dam (YE 1, 3), small scale laminations (< 2 cm) predominate. Sediment texture is similar in cores with higher $^{7}$Be penetration depths (YE 7, 11, YO 3, 6), displaying coarser (1-3 cm) laminations interspersed with massive bedding.

## 3.5 Discussion

### *3.5.1 Evidence of Environmental Change from Organic Matter Isotopic Signatures*

There have been extensive studies utilizing stable isotopes as tracers for organic matter, specifically to delineate terrestrial versus marine sources, within coastal and estuarine sediments (Schelske and Hodell 1995, Louchouarn et al. 1999, Zimmerman and Canuel 2002, Bianchi 2007, Brandenberger et al. 2011). In the Yeongsan Estuary and Lake, severe anthropogenic alteration to the system has resulted in a significant shift in stable isotopic signatures (Figure 3.10).

To further assess these changes, the proportion of terrestrial organic matter (TOM) has been evaluated through a binary mixing model, applying end-member sources of $\delta^{13}C$ to determine relative abundances. The terrestrial and marine end-member values have been respectively chosen based on the maximum depleted value found within the surface sediment of the lake (-26.2‰), and the most enriched value found offshore (-15.8‰). These values correspond with recognized signatures from terrigenous C3 plants and marine plankton (Bianchi 2007). The contribution from the terrigenous end-member (%TOM) to the total organic carbon in sediment is determined by:

$$\frac{\left[\delta^{13}\mathrm{C}\right]_X - \left[\delta^{13}\mathrm{C}\right]_M}{\left[\delta^{13}\mathrm{C}\right]_T - \left[\delta^{13}\mathrm{C}\right]_M}$$

where subscripts represent the sample (X), terrestrial end-member (T), and marine end-member (M) signatures. The %TOM for all samples is summarized in Table 3.2. The proportion of TOM in pre-dam sediment ranges from 43-61% in the lake, 39-43% in

the inner estuary, and 10-20% in the outer estuary. Post-dam sediment TOM ranges from 82-99% in the lake, 22-74% in the inner estuary, and 9-14% in the outer estuary. Changes in terrigenous input (Δ%TOM) from surface to bottom of cores are shown to compare pre and post dam signatures (Table 3.2). Notably, the Δ%TOM is sufficiently small (-3.5 to 7.4%) for core types A and C, indicating minor environmental changes, and providing corroborating evidence for core characterization.

Based on these calculations, there has been a significant increase in %TOM (≈ 30-45%) in lake and inner estuary sediments since the construction of the estuarine dam (Figure 3.10 and Table 3.2). The elimination of marine phytoplankton, the primary source of relatively enriched $\delta^{13}C$, above the dam with the cessation of tidal mixing increased the relative abundance of TOM in lake sediments. Moreover, the influence of organic matter derived from the lake is apparent within surface sediment of the inner estuary, displaying high %TOM in the majority of cores (YE 1, 3, 5) (Figure 3.10). Combined, this suggests that reduced tidal inflow (lake) and increased flux of TOM (inner estuary) has resulted in increased proportions of TOM to lake and inner estuary sediments.

However, defining organic matter source based solely on $\delta^{13}C$ data has been shown to be problematic (Louchouarn et al. 1999, Gordon and Goñi 2003, Bianchi 2007, Bianchi and Canuel 2011). First, end-members may vary with changing environmental conditions. Second, contributions from additional sources such as terrigenous soils, $C_4$ salt marsh plants, or freshwater phytoplankton could alter $\delta^{13}C$ signatures. Expansion of the model herein to include soil and biomarker data (lignin phenols and/or lipids), and completed profiles of elemental and molecular analyses would further elucidate organic matter sources and the transition from historical to current conditions.

Similarly, $\delta^{15}N$ values show a marked shift in lake and inner estuary samples after impoundment (Figure 3.10). Typically, a shift from higher relative contribution of marine/estuarine phytoplankton to terrigenous vascular plants results in a depletion of $\delta^{15}N$; however, post-dam sediment reveals enrichment. Several studies have shown that

enriched $\delta^{15}N$ signatures are caused by isotopically heavy nitrogen loading from agricultural runoff (fertilizers) and/or sewage waste (Heaton 1986, Macko and Ostrom 1994), or from recycling/regeneration under anaerobic conditions (Struck et al. 2000, Zimmerman and Canuel 2002, Bratton et al. 2003). Recently, severe oxygen depletion due to eutrophication has been observed within Yeongsan Lake (Smith et al. 2006, Park et al. 2008, Lee et al. 2009). Therefore, with the introduction of highly fertilized agricultural plots and sewage waste input, the enriched $\delta^{15}N$ signatures are interpreted as a combination of these processes.

### *3.5.2 Sediment Accumulation and Distribution*

The cumulative effects of appreciably reducing tidal current velocities, altering river discharge characteristics, and hardening shorelines have drastically altered sediment accumulation and distribution within the Yeongsan Estuary and Lake. With water and sediment flux restricted to the dam, the effects on sediment distribution are apparent within side scan sonagrams (Figure 3.9). Flow velocities of approximately 1.5 m $s^{-1}$ recorded 1.8 km from the dam during moderate discharge events (Shin and Lee 2014) support the interpretation of the prominent high backscatter area extending approximately 1 km on each side of the dam as a zone of intense scouring. Indurated clays obtained from this area (Core YE 2 and a surficial grab) suggest exposure of early to mid Holocene deposits (Nahm et al. 2008). On the edges of the scoured zone, the gradation in backscatter is interpreted as a transition from erosion to accumulation of fine-grained sediment.

Throughout the estuary and lake, the loss of intertidal zones resulted in a substantial reduction of accommodation space. Apparent from geochronological and bathymetric change analyses, this resulted in the inner estuary accreting sediment at high rates since the construction of the dam (Figures 3.4, 3.8, 3.11, and 3.12). Previously dominated by tidal processes, the lake was excluded from macrotidal influence and estuarine mixing post dam. Contribution of sediment from the Sampo and Yeongam tributaries has resulted in relatively moderate accumulation rates (compared to inner

estuary) in upper portions of the lake. Increased accumulation due to trapping of sediment upstream of dams has been widely documented (Kummu et al. 2010, Gupta et al. 2012, Ran et al. 2013, Vukovic et al. 2014), and it is emphasized that this phenomenon is occurring in the Yeongsan Lake. Holistically, due to anthropogenic activities, modern accumulation rates within the Yeongsan Estuary and Lake are considerably higher than rates reported in many natural estuarine systems (Santschi et al. 2001, Pekar et al. 2004, Lu and Matsumoto 2005, Álvarez-Iglesias et al. 2007, Osterman and Smith 2012).

Results from subsurface seismic analyses reveal an unconformity apparent throughout the inner estuary, which has been interpreted as the Holocene-Pleistocene unconformity surface (Figure 3.13). The stratigraphic sequence above this surface is interpreted as Holocene estuarine fill (H.E.F.) (Figure 3.13). The thickness and age of these strata correspond well to units identified as deposited during the Holocene marine transgression within the Yeongsan Estuary, that unconformably overly a paleosol determined to be exposed during the Last Glacial Maximum (Nahm et al. 2008). Additionally, the depth of the Holocene-late Pleistocene boundary and the thickness of this stratigraphic sequence (<10 m) are consistent with other studies within the region (Park et al. 1991, Khim et al. 2000, Choi et al. 2002, Lim and Park 2003, Lim et al. 2004, Choi et al. 2012a, Kwon 2012).

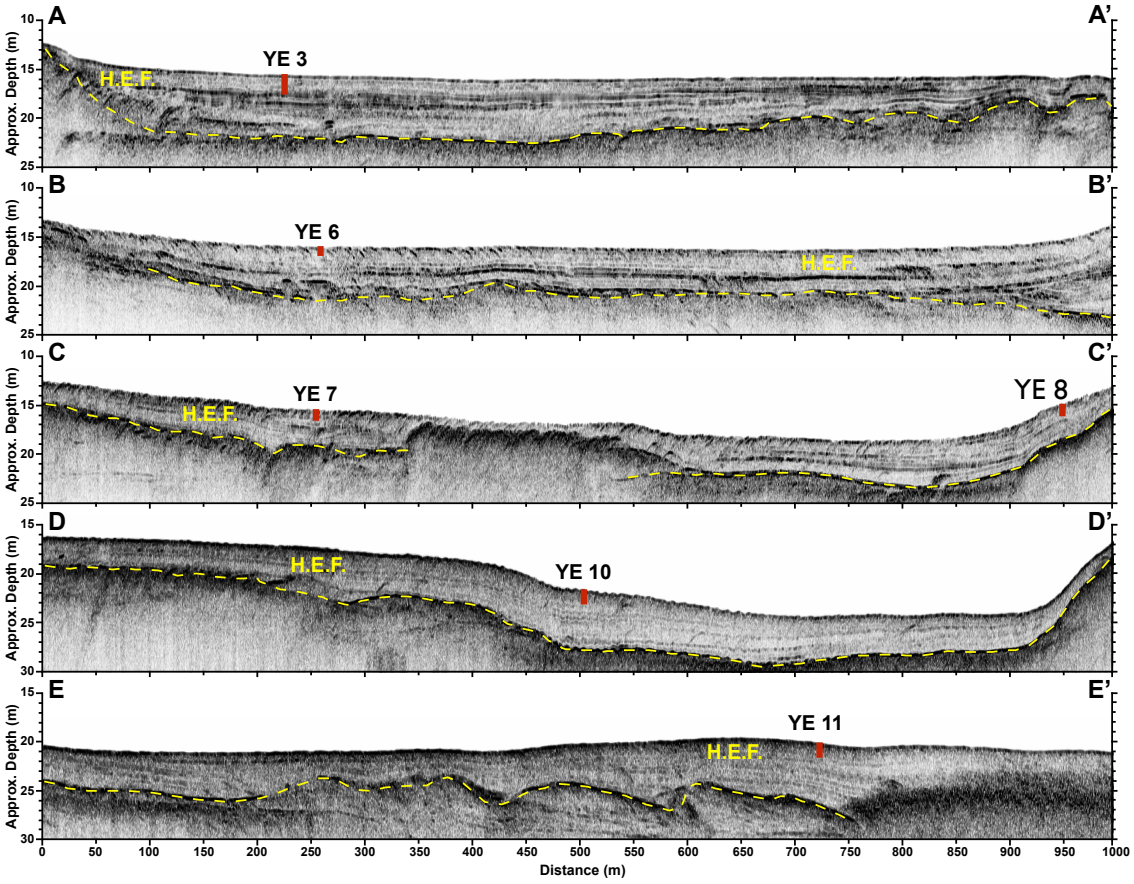


Figure 3.13 High-resolution CHIRP seismic subsurface profiles from within the inner estuary. Profile locations are indicated in Figure 3.1, and maintain consistent scales at a vertical exaggeration of approximately 10:1. A prominent reflector identified throughout the survey has been traced, and all sediment above this point has been interpreted as Holocene estuarine fill (H.E.F.). Cores YE 3, 6, 7, 8, 10, and 11 are indicated with appropriate penetration depths. All seismic profiles are displayed as viewing upstream.

With rising sea levels, many of the world's estuaries formed between 5-10 ka (Wolanski and Chappell 1996, Long et al. 1998, Kench 1999, Lario et al. 2002, Rodriguez et al. 2005). Relative sea level rise rates within the region have been estimated to be approximately 0.5-2 mm $y^{-1}$ for at least the last millennia (Park 1983,

Bloom and Park 1985, Park and Yi 1995, Yoo and Park 2000, Chang and Choi 2001). Using these local sea level curves, the initiation of estuarine conditions to our study area can be conservatively estimated at 6 ka. While modern (post dam) sediment accumulation rates have been determined herein, it is clear sediment deposited at these rates represents only a small fraction of the total estuarine fill throughout the Holocene (e.g. core penetration depths, Figure 3.13).

However, considering the variable thickness of the H.E.F., we can conclude the average Holocene sedimentation rates in the estuary to be on the order of 0.5-1.5 mm $yr^{-1}$. These rates are consistent with an estuary in equilibrium with relative sea level rise, and are typical of reported values throughout the Holocene (Park et al. 1991, Park et al. 1995, Park and Yi 1995, Lario et al. 2002, Klingbeil and Sommerfield 2005, Frouin et al. 2007, Schneider et al. 2010). Therefore, this indicates at least an order of magnitude increase from Holocene averages to modern accumulation rates, suggesting the rates reported in this study are not sustainable and are distinctively a recent phenomenon as a result of anthropogenic alteration.

*3.5.3 Episodic Sedimentation*

Elevated $^{7}Be$ activities in surface intervals and laminations in X-radiographs are indicative of event driven sedimentation (Figures 3.11 and 3.12) (Sommerfield et al. 1999, Mullenbach and Nittrouer 2000, Mullenbach and Nittrouer 2006, Carlin and Dellapenna 2014). Combined with a lack of visible bioturbation (Figure 3.12), this suggests deviations in $^{210}Pb_{xs}$ profiles may represent temporal variability in sediment deposition (Figure 3.5). The highly variable and non-rhythmic nature of the lamination thickness suggests tidal processes are not the primary deposition control; however, tidal advection likely plays a role in the distribution of sediment. Episodic sedimentation is not necessarily an impact of anthropogenic alteration; however, the timing and intensity of discharge are markedly different after emplacement of an estuarine dam. The typical hydrographic profile of a flooding event in a natural system displays a normal distribution curve, with the majority of sediment deposition occurring on the falling limb

with decreasing flow velocity. A relatively short, high intensity discharge pulse from a dam differs in that the build up and falling stages have been eliminated, resulting in extremely rapid introduction of sediment to a quiescent environment.

If a constant supply of sediment is deposited and undisturbed (i.e. limited or no physical or biological mixing), exponential decay of $^{7}$Be activity with depth is expected. However, our data display relatively constant activity throughout surface intervals suggesting sediment was deposited synchronously (Figure 3.11). Comparing the thickness of this interval to decadally averaged annual accumulation rates (Table 3.1) reveals that a singular event may represent a significant fraction of the annual rate. Therefore, assuming a direct correlation to sediment accumulation in the estuary, the amount of sediment deposited annually should reflect discharge (Figure 3.3). However, this assumption does not account for sediment supplied to the system from other sources, such as advection from offshore. Considering the high sediment accumulation rates in the central portion of the outer estuary, this process is likely a contributing factor. Additionally, this is supported by isotopic data with %TOM significantly lower in the outer estuary and core YE 11, with intermediate values of the inner estuary, suggesting a combination of sources.

Relative to average values, the low total discharge in the summer of 2013 seems insufficient to produce the deposition recorded by $^{7}$Be activities (Figures 3.3 and 3.11). This implies the amount of sediment deposited is not strictly a function of total discharge. Although the vast majority of discharges release < 30 x$10^{6}$ $m^{3}$ per event, the event occurring on 7/6/13 of 167 x$10^{6}$ $m^{3}$ accounts for nearly half of the total summer discharge and represents the second highest discharge event recorded from 1997-2013 (Figure 3.3). Over this time period, there were 18 discharge events exceeding 100 x$10^{6}$ $m^{3}$, with the largest event occurring in 2002 (268 x$10^{6}$ $m^{3}$)(Figure 3.3). This suggests the magnitude of discharge events may be equally important as total annual discharge when considering sediment deposition. Hence, the sediment observed with elevated $^{7}$Be activities is interpreted as primarily sourced from the 7/6/13 event.

Several other factors could also impact sediment deposition on an annual basis. The concentration of suspended sediment in the water column prior to opening floodgates, and the erodibility of the bed adjacent to the dam would impact sediment availability. To summarize, the amount deposited in any given year is likely dependent on total amount of discharge, quantity and volume of individual events, and suspended sediment concentration prior to discharge.

### 3.6 Conclusions

Anthropogenic alteration to the Yeongsan Estuary has dramatically changed the shoreline geometry, accumulation rates, depositional environments, and distribution of organic matter. The primary modifications to the system that have resulted in these changes include construction of an estuarine dam and massive land reclamation projects. Additionally, construction of seawalls have hardened shorelines and restricted overbank deposition. Due to the loss of intertidal zones, the accommodation space was significantly reduced resulting in rapid accumulation rates and an increase in sediment trapping efficiency. The average accumulation rates derived from this study indicate that rates have increased over average Holocene by at least an order of magnitude, with most areas displaying more than a 20x increase. Sediment delivery mechanisms, including the timing and intensity of discharge, have also been modified from a natural system. The high flow velocities associated with discharge have resulted in scouring adjacent to the dam, and episodic sedimentation associated with discharge is apparent. The distribution of organic matter throughout the system shifted in accordance with the construction of the estuarine dam. Organic matter source signature in pre and post-dam lake and inner estuary sediments display an increase in %TOM, reflecting the elimination of natural estuarine circulation and the influence of discharge, respectively.

Significant environmental changes have occurred throughout the Anthropocene, and many are represented within the Yeongsan Estuary. It is predicted that coastal engineering will continue to rapidly increase globally over the next century. Impacts on estuarine systems, such as those observed in this study, are likely to be magnified with

increasing coastal population, industrialization, and rising eustatic sea level. Continued observation is necessary for increased understanding of how multiple feedback mechanisms drive natural responses to anthropogenic alterations. These results provide advancement in the knowledge of how estuarine sedimentation processes respond to severe coastal construction within estuaries, and can be used to advise and develop future estuarine management strategies throughout the world.

# CHAPTER IV
# HISTORICAL RECONSTRUCTION OF ANTHROPOGENIC MERCURY INPUT FROM SEDIMENTARY RECORDS: YEONGSAN ESTUARY, SOUTH KOREA

## 4.1 Introduction

Mercury (Hg) is found in the environment from both natural and anthropogenic sources, and have been shown to severely deteriorate ecosystem and human health under sufficiently high concentrations (Mergler et al. 2007, Driscoll et al. 2012, Karagas et al. 2012). Industrialization over the last two centuries has caused global mercury inventories to increase rapidly (Schuster et al. 2002, UNEP 2013). Previous estimates of total annual anthropogenic inputs of Hg vary depending on calculation method, particularly emission factors, with estimates for the years 1990-2010 ranging from 1010-4070 ton $yr^{-1}$ (Pacyna and Pacyna 2001, Pacyna et al. 2010, UNEP 2013, Muntean et al. 2014). In 2005, relative contributions of global anthropogenic Hg emissions were estimated at 45.6% from fossil fuel combustion, 18.2% from gold production, 10.4% from other metals production, and 9.8% from cement production combined with all other sources (AMAP/UNEP 2008). Once emitted to the atmosphere, the behavior and transport of anthropogenic mercury depends highly on speciation (Schroeder and Munthe 1998, Selin 2012, Swartzendruber and Jaffe 2012, UNEP 2013). Gaseous elemental mercury ($Hg^0$) comprises >90% of atmospheric mercury, and has a high volatility and low water solubility (Han et al. 2014). Depending on environmental conditions, $Hg^0$ can be deposited locally, or remain in the atmosphere for up to a year allowing global transport (Schroeder and Munthe 1998, Pirrone and Mason 2009). More reactive forms, such as gaseous oxidized ($Hg^{+2}$) and particle bound ($Hg^P$) mercury, have shorter atmospheric residence times (hours-days) and are typically deposited close to their emission source (Pirrone and Mason 2009, Rothenberg et al. 2010, Swartzendruber and Jaffe 2012, Han et al. 2014).

Currently, nearly 40% (1960 ton $yr^{-1}$) of global anthropogenic mercury emissions are attributed to East and Southeast Asian countries (UNEP 2013). However, within S. Korea there is a paucity of historical atmospheric mercury measurements to evaluate emissions from local sources, with the majority of records coming from urban areas near Seoul (Kim and Kim 2000, Kim and Kim 2002, Kim et al. 2013). Generally, these studies report higher values of total gaseous mercury ($Hg^0 + Hg^{+2}$) concentrations (0.2-150 ng $m^{-3}$) near highly urbanized regions than within rural areas (0.26-10.8 ng $m^{-3}$) (Kim et al. 2013, Han et al. 2014), although within the last decade concentrations have been decreasing due to increased emission regulation (Kim et al. 2013). Long-range transport of anthropogenic and natural Hg to Korea has also been observed from China, Japan, and Russia (Fang et al. 2008, Choi et al. 2009, Nguyen et al. 2010). Recently, a comprehensive study evaluated mercury emission factors and sectorial concentrations from the major anthropogenic sources in S. Korea and determined that of the total average of 12.8 ton $yr^{-1}$ (6.5-20.2 ton $yr^{-1}$) approximately 26% was emitted from coal fired power plants, 25% from oil refineries, 21% from cement kilns, 20% split between medical, sludge, industrial, and municipal waste incinerators, 7% from iron manufacturing, and the remaining 1% combined from glass, pulp/paper, and nonferrous metal manufacturing (Kim et al. 2010). These sources are primarily concentrated near the major industrial areas of Seoul (Northwest) and Busan (Southeast) (Figure 1 of Han et al., 2014).

It has been well documented that through wet and dry deposition, atmospheric Hg is ultimately accumulated within sediments, typically transported associated with fine particles and organic matter (Sanei and Goodarzi 2006, Weiss-Penzias et al. 2011, Lasorsa et al. 2012, Zhang et al. 2012, Connan et al. 2013, Chakraborty et al. 2014, Sanei et al. 2014). Numerous studies have investigated the historical record of Hg input to sedimentary systems throughout the world, and the impact of localized deposition and varying source input is apparent in the wide range of timing for onset of increased mercury and peak concentrations (Table 4.1).

| Location | $t_{INT.}$ | $t_{Peak}$ | T-$Hg_{Bkg.}$ | T-$Hg_{MAX}$ | Source |
|---|---|---|---|---|---|
| N. America | | | | | |
| San Francisco Bay, USA | < 1900 | 1960's | < 60 | 434 | Donovan et al. (2013) |
| Galveston Bay, USA | 1940's | 1971 | 30 | 2,375 | Al Mukaimi et al. (2013) |
| St. Lawrence Estuary, Canada | 1940's | 1965 | 30 | 6,000 | Louchouarn and Lucotte (1998) |
| Sagua la Grande Estuary, Cuba | 1970's | 1985 | 35 | 312 | Alonso-Hernández et al. (2012) |
| S. America | | | | | |
| Guaratuba Bay, Brazil | 1950's | 2000 | 15 | 44 | Sanders et al. (2006) |
| Laguna del Plata, Argentina | 1970's | 1993 | 13 | 131 | Stupar et al. (2014) |
| Europe | | | | | |
| United Kingdom | 1850's | 1970's | 20 | 1,606 | Yang and Rose (2003) |
| Portuguese Margin | 1850's | 1990's | 50 | 594 | Mil-Homens et al. (2013) |
| Straight of Sicily | 1950's | 1975 | 38 | 202 | Leonardo et al. (2006) |
| Asia | | | | | |
| Pearl River Estuary, China | 1950's | 1960's | < 80 | 201 | Shi et al. (2010) |
| Shanghai, China | 1940's | 1990's | 43 | 867 | Li et al. (2013) |
| Jinhae-Masan Bay, Korea | 1940's | 1940's | 19 | 150 | Lim et al. (2012) |
| Thane Estuary, India | 1950's | 1975 | 70 | 10,500 | Jha et al. (2003) |
| Ulhas Estuary, India | 1960's | 1991 | 60 | 20,000 | Ram et al. (2003) |
| Africa/Arabia | | | | | |
| Berg Estuary, S. Africa | 1970's | 2003 | 22 | 48 | Kading et al. (2009) |
| Kuwait Bay, Kuwait | 1960's | 1985 | 15 | 36,500 | BuTayban et al. (2004) |

Table 4.1 Summary of numerous studies investigating the historical input of anthropogenic Hg in coastal sedimentary records. The timing of initial significant increase in detected Hg ($t_{INT.}$), the timing of peak concentrations ($t_{Peak}$), average background value (T-$Hg_{Bkg.}$), and maximum reported concentration (T-$Hg_{MAX}$) are indicated. Note: this list is not comprehensive, but is only representative of all investigations.

While in some regions the increase in total global anthropogenic mercury (mid 1800's) due to industrialization is recorded, many studies have not reported increases above background levels until well into the 20$^{th}$ century. Furthermore, considerable variation exists in background and maximum total mercury concentration (Louchouarn and Lucotte 1998, Jha et al. 2003, Ram et al. 2003, Yang and Rose 2003, BuTayban and Preston 2004, Leonardo et al. 2006, Sanders et al. 2006, Kading et al. 2009, Shi et al. 2010, Alonso-Hernández et al. 2012, Lim et al. 2012, Al Mukaimi 2013, Donovan et al. 2013, Li et al. 2013, Mil-Homens et al. 2013, Stupar et al. 2014). Several studies have investigated mercury (and other heavy metal) contamination within estuaries, rivers, and

lakes of S. Korea; however, they have been primarily focused on surface sediment concentration and distribution (Joo et al. 2000, Lee et al. 2008, Oh et al. 2010, Kim et al. 2011, Choi et al. 2012b, Lim et al. 2013, Kim et al. 2014), with few reporting historical input from core data (Lim et al. 2012, Park et al. 2012b). The variation within these data indicates that the type and proximity of mercury source are strong controls on the historical record of input to the sedimentary record.

Without significant policy intervention, estimates of global mercury emissions are projected to increase significantly (up to 98%) by 2050 (Streets et al. 2009, Pacyna et al. 2010, Rafaj et al. 2013). In order to understand the implications of future increased anthropogenic mercury emission, the sedimentary record of deposition and the relative influence of long-range transport and local sources must be evaluated regionally. The rapid development and industrialization of Asian countries, particularly China and Korea, within the last few decades has caused a significant increase in sources of atmospheric Hg (Pacyna et al. 2010, UNEP 2013, Muntean et al. 2014). Thus, this study aims to determine 1) the sedimentary record of historical input of anthropogenic Hg to the Yeongsan Estuary, 2) the distribution of Hg concentration in surface sediments, and 3) the potential utility of Hg as a geochronological tool. The results herein provide a case study on how an anthropogenically altered estuary has recorded increasing anthropogenic Hg throughout the last half-century. These findings are not only significant regionally, as many depositional environments in East Asia have been accumulating anthropogenic Hg, but have global implications for the fate of anthropogenic Hg with continued industrialization in developing countries.

### 4.2 Regional Setting / Background

The Yeongsan Estuary is separated respectively into the Yeongsan Lake, Inner Estuary, Outer Estuary, and Coastal zones (Figure 4.1). Located on the southwestern tip of the Korean Peninsula, the Yeongsan River has a drainage basin area of 3,468 $km^2$ and a total length of 137 km, making it the sixth longest river in the country. The estuary has undergone significant coastal construction within the last century, including the

construction of an estuarine dam in 1981 and the addition of approximately 90 km of seawalls/embankments. The estuarine dam resulted in cessation of tidal exchange with the creation of the freshwater Yeongsan Lake (Figure 4.1) (Lee et al. 2009). Additionally, 80 km$^2$ of tidal flats were filled during land reclamation projects throughout the 1980's, causing a reduction in intertidal area by at least 65% (Williams et al. 2014). In the region adjacent to the outer Yeongsan Estuary, 190 km$^2$ of intertidal zones were also eliminated with the construction of the Youngam seawall in 1991, and the Keumho seawall in 1994 (Kang 1999).

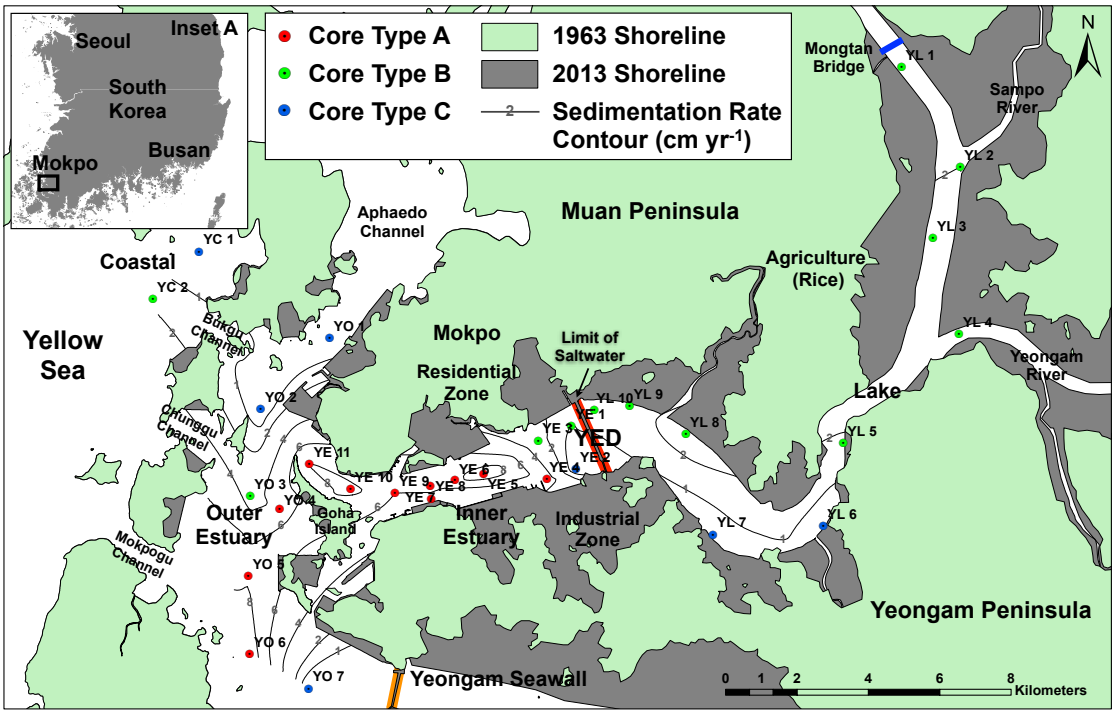


Figure 4.1 Detailed study area map showing location of the Yeongsan Estuary and all locations of core samples. Cores are labeled according to respective environments, and identified by core type adopted from Williams et al. (2014).

Currently, the Yeongsan Lake spans 23.4 km in length from the estuarine dam to the Mongtan Bridge, decreasing in width from 1.2 to 0.6 km with an average depth of 10 m (Lee et al. 2009) with two main tributaries, the Sampo and Yeongam Rivers, entering from the east (Figure 4.1). The Inner Estuary has average depth and width of 19 m and 1.3 km, respectively for a length of 6.7 km, and is positioned between the Muan and Yeongam peninsulas. Entering the outer estuary, the main channel splits around Goha Island and opens to a series of islands separated by four main channels (Bukgu, Chunggu, Mokpogu, and Aphaedo) which continue to the Yellow Sea through a relatively shallow (predominantly <50 m depth) intricate coastline of islands (Figure 4.1). With an approximately 4.5 m tidal range the estuary is classified as macrotidal, with primarily semidiurnal ebb dominated tides (Byun et al. 2004).

The impact of the major anthropogenic alterations on sediment distribution and accumulation, and organic matter source input has recently been investigated by Williams et al. (2014). The average sediment accumulation rates and core types reported in that study have been incorporated herein, utilizing sediment samples from the same cores. Briefly, Williams et al. (2014) categorized cores based on profiles of water content and $^{210}$Pb activity into 3 types. Respectively, core types A, B, and C display characteristics of relatively high (> 4 cm yr$^{-1}$), moderate (≈1-3 cm yr$^{-1}$), and null (0 cm yr$^{-1}$; eroding/recently dredged) average sediment accumulation rates. Generally, the inner estuary displayed the highest rates, with moderate accumulation throughout the majority of the lake and outer estuary (Figure 8, Williams et al. 2014). The geochronology and depositional history previously derived from these cores provides a framework to investigate the record of anthropogenic Hg input to the Yeongsan Estuary (Figure 4.1).

## 4.3 Methods

### *4.3.1 Data Collection / Core Processing*

A total of 30 gravity cores were collected between May 15-16, 2012 using a 6.0 cm diameter core barrel with PVC liners and have been nominally assigned to either lake

(YL 1-10), inner estuary (YE 1-11), outer estuary (YO 1-7), or coastal (YC 1-2) environments (Figure 4.1). Cores were sealed immediately upon recovery, and showed no signs of degradation from partial recovery or transportation. Subsamples were taken at 1 cm intervals, desiccated, homogenized, and stored at 4 °C until further processing.

*4.3.2 Grainsize Analyses*

Grainsize distribution of samples was determined using a Malvern Mastersizer 2000® laser particle diffractometer at a calibrated level of obscuration. Prior to sample injection by a Malvern Hydro 2000G, samples were wet sieved at 2 mm and sonicated with sodium hexametaphosphate dispersant to minimize flocculation. When applicable, sieved fractions were dry weighed for inclusion in the final distribution. Reported results are an average of triplicate measurements.

*4.3.3 Hg Analyses*

Total mercury concentrations were analyzed on a Milestone SLR Direct Mercury Analyzer (DMA-80) by atomic absorption spectrometry. Samples were sieved at 38 μm prior to analyses in order to reduce grainsize effects (Ackermann et al. 1983). The average fraction of sediment larger than 38 μm for all samples (n = 1015) measured 13.12% ± 10.50% (error as 1σ), and results reported herein as total mercury (T-Hg) concentration do not reflect any correction for this fraction. However, Hg concentrations in sediments >20 μm have been shown to be considered negligible (Barghigiani et al. 1996). Analyses were conducted according to U.S. EPA Method 7473 (EPA 1998). Briefly, approximately 300 mg of dried sediment was thermally decomposed at 615°C to liberate mercury from sediments. Through continuous flow of oxygen, all mercury species were transferred in vapor phase to a catalyst, and reduced to elemental form. Hg is isolated via a gold amalgamator at 900°C, then cooled to 125°C and carried to cuvette cells to quantify concentration by absorption at 253.7 nm wavelength (EPA 1998). The instrument was calibrated using four prepared standard solutions (0.1, 1, 10, 100 ppm Hg) and the calibration curve verified with three Standard Reference Materials (SRM) (MESS-3 Marine sediment [0.091 ± 0.009 ppm, National Research Council of Canada],

NIST 2702 Inorganics in Marine Sediment [0.4474 ± 0.0069 ppm, National Institute of Standards and Technology], and PACS-2 Marine Sediment [3.04 ± 0.2 ppm, National Research Council of Canada]). Quality assurance/quality control measures during sample analyses include an SRM and a blank every 10 samples, with sample duplicates every 5 samples. The relative standard deviation of SRMs was ± 3.5% (n = 98), with an average recovery rate of 103.1%.

### *4.3.4 Total Organic Carbon*

The total organic carbon content (TOC) was determined by combustion using a Costech Analytical Technologies, Inc. ECS 4010 CHNSO elemental analyzer. Prior to analyses, inorganic carbon was removed from sediments by HCl vapor phase acidification for 24 h with subsequent drying at 40°C (Harris et al. 2001). Calibration of the instrument was done with a 4-point calibration using acetanilide as a standard. NIST SRM 1941b (Organics in Marine Sediment) was used for quantification verification, and the SRM was analyzed every 10 samples as a verification standard. Quality assurance/quality control measures included an SRM every 10 samples, and sample duplicates every 5 samples. Replicate analyses resolved the mean analytical variability for TOC as ± 2.2% (n = 31).

## 4.4 Results

### *4.4.1 Hg Profiles*

Profiles of T-Hg for all cores are shown in Figures 4.2 and 4.3, with both bulk and clay normalization indicated. Bulk values ranged from 4.9 to 60.4 ng $g^{-1}$, with the highest concentrations found in surface samples within the upper portions of the lake (YL 1-3, note different scale).

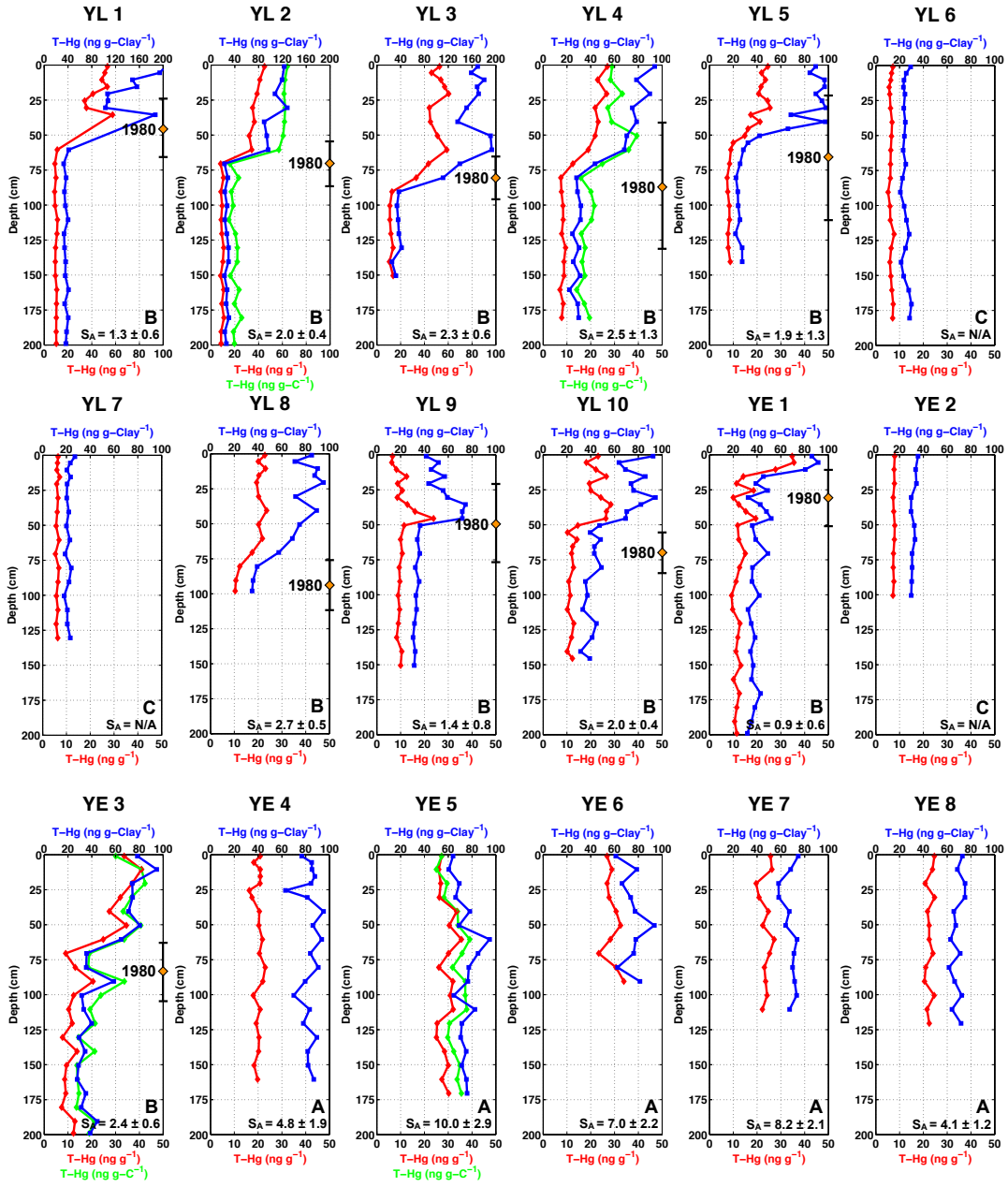


Figure 4.2 Profiles of bulk total Hg (red), clay normalized total Hg (blue), and carbon normalized total Hg (green) for cores YL 1-10 and YE 1-8. Within each plot, the average sediment accumulation rate (SA) (when applicable) and core type adopted from Williams et al. (2014) is indicated. Based on these rates, the depth of 1980 including confidence interval is shown. Core locations are displayed in Figure 4.1. Note the different scale for cores YL 1-3.

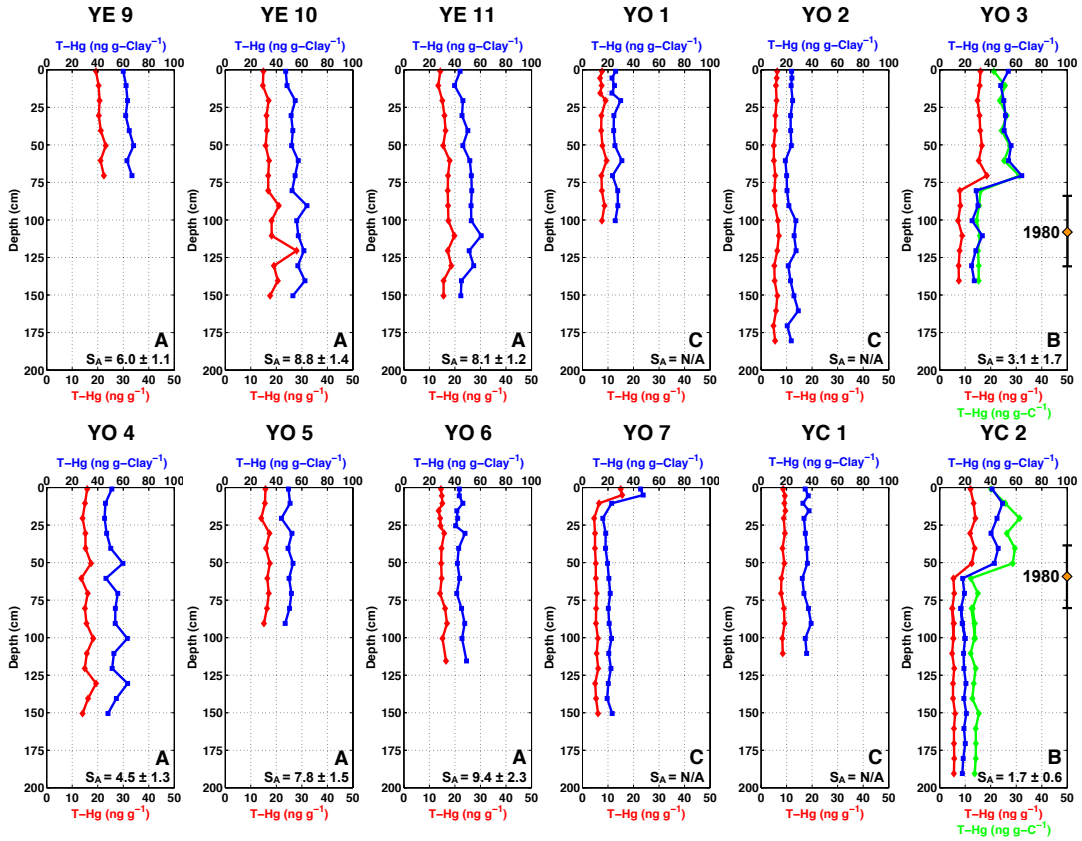


Figure 4.3 Profiles of bulk total Hg (red), clay normalized total Hg (blue), and carbon normalized total Hg (green) for cores YE 9-11, YO 1-7, and YC 1-2. Within each plot, the average sediment accumulation rate (SA) (when applicable) and core type adopted from Williams et al. (2014) is indicated. Based on these rates, the depth of 1980 including confidence interval is shown. Core locations are displayed in Figure 4.1.

The profile types described in Williams et al. (2014) are apparent, with core type A displaying relatively elevated T-Hg throughout core depth (n =11), core type B showing a distinct decrease in concentration with depth (n =12), and core type C having consistently low concentrations at all depths (n =7) (Figures 4.2 and 4.3). Based on the average sediment accumulation rates derived for these cores, the increase in Hg (core type B) occurs consistently around 1980 (Figures 4.2 and 4.3). While profiles display

similar characteristics, showing minimal variability with depth, observed T-Hg concentrations are consistently higher (≈ > 15 ng $g^{-1}$) in core type A than C (< 10 ng $g^{-1}$).

Grainsize distribution remained relatively constant with depth for most cores, resulting in a consistent offset in T-Hg profiles when normalized to clay content. However, one exception occurs in YL 9, with lower clay content above 50 cm depth creating a discernible increase in clay normalized T-Hg. Comparing T-Hg to clay content for all samples analyzed (n = 540) reveals a very weak correlation, indicating that the increased mercury content observed is not a function of grainsize variability within cores (Figure 4.4).

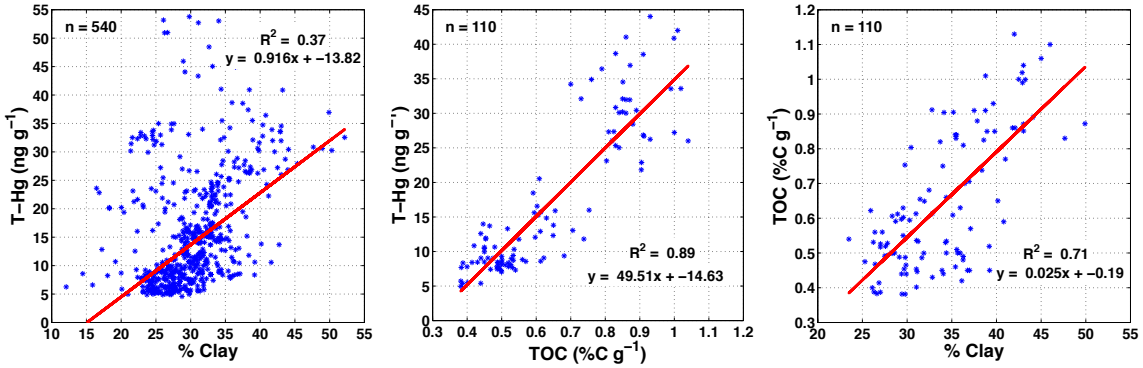


Figure 4.4 Correlation plots for total Hg and clay content, total Hg and total organic carbon, and total organic carbon and clay content. The number of samples (n), $R^2$ value, and robust fit equation are indicated on respective plots.

### *4.4.2 Organic Matter*

Considering TOC as a proxy for organic matter abundance, six cores were analyzed to determine the relationship to T-Hg concentration (YL 2, 4; YE 3, 5; YO 3; YC 2), and have been plotted with T-Hg normalized to carbon (Figures 4.2 and 4.3).

Values for TOC ranged from 0.36% to 1.12%, with mean of 0.63 ± 0.19%. Examination of T-Hg concentration versus TOC reveals a strong positive correlation (Figure 4.4), which is similar to the preponderance of data found within the literature (Lambertsson and Nilsson 2006, Hung et al. 2009, Ethier et al. 2010, Swartzendruber and Jaffe 2012, Taylor et al. 2012). Additionally, there is a positive correlation of TOC to clay content (Figure 4.4). Profiles of carbon normalized T-Hg display similar trends to clay normalized T-Hg, predominantly causing an offset from bulk values. Combined with the very weak correlation to clay content, this suggests that the elevated mercury concentrations are not due to increases in carrier phase (i.e. clay/TOC), but to increased source input.

## 4.5 Discussion

### *4.5.1 Historical Input of Anthropogenic Hg*

Using the published geochronology determined for these cores, the data can be separated into two distinguishable groups representing modern and pre-industrial sediments, with relatively elevated and background values, respectively (Figure 4.5). In core type B, this transition occurs at approximately 1980, while core type A represents all modern sediment, and core type C contains entirely pre-industrial sediment (Figures 4.2 and 4.3). Comparing these groups (heteroscedastic t-test) reveals significant difference ($p < 0.001$) between modern and pre-industrial lake, inner estuary, outer estuary and coastal sediments (Table 4.2). While the sediments of the Yeongsan Estuary would not currently be considered contaminated (Long et al. 1995), these data show a significant increase in T-Hg concentrations within the last half-century. The concentrations found for both post-industrialization sediments and background levels are consistent with previously reported values for the region (Joo et al. 2000, Choi et al. 2012b, Kim et al. 2014). However, due to the relatively low T-Hg values compared to several other similar environments (Table 4.1), and regional studies conducted closer to major sources (Lee et al. 2008, Oh et al. 2010, Kim et al. 2011, Lim et al. 2012, Park et al. 2012b, Lim et al. 2013) the increase in anthropogenic Hg observed represents a rather

weak signal. However, there is a significant enrichment factor (E.F.; ratio of modern over pre-anthropogenic concentrations) in all sites (1.8 to 3.5) with a decreasing gradient downstream from the lake.

| Region | Modern Hg (ng $g^{-1}$) | n | Pre-Ind. Hg (ng $g^{-1}$) | n | p-value | E.F. |
|---|---|---|---|---|---|---|
| Lake | 31.1 ± 12.9 | 68 | 8.8 ± 2.1 | 125 | < 0.001 | 3.5 |
| Inner Estuary | 23.3 ± 6.1 | 136 | 10.9 ± 3.1 | 58 | < 0.001 | 2.1 |
| Outer Estuary | 15.6 ± 1.2 | 60 | 6.7 ± 1.4 | 63 | < 0.001 | 2.3 |
| Coastal | 12.8 ± 0.7 | 9 | 7.1 ± 1.8 | 28 | < 0.001 | 1.8 |
| All Samples | 23.2 ± 9.6 | 273 | 8.6 ± 2.7 | 274 | < 0.001 | 2.7 |

Table 4.2 Statistical results comparing modern to pre-industrialized sediments from the Yeongsan Estuary. Modern sediments are considered those deposited subsequent to 1980 (core type A and surface of B), and pre-industrial deposited prior to this point (core type C and bottom of B). The distinction between these sediments has been indicated (dashed line) in Figures 4.2 and 4.3. The number of samples (n), mean and standard deviation (1σ) are shown, with *p*-values calculated from a heteroscedastic t-test. Enrichment factor (E.F.) determined as ratio of modern to pre-industrialized concentrations.

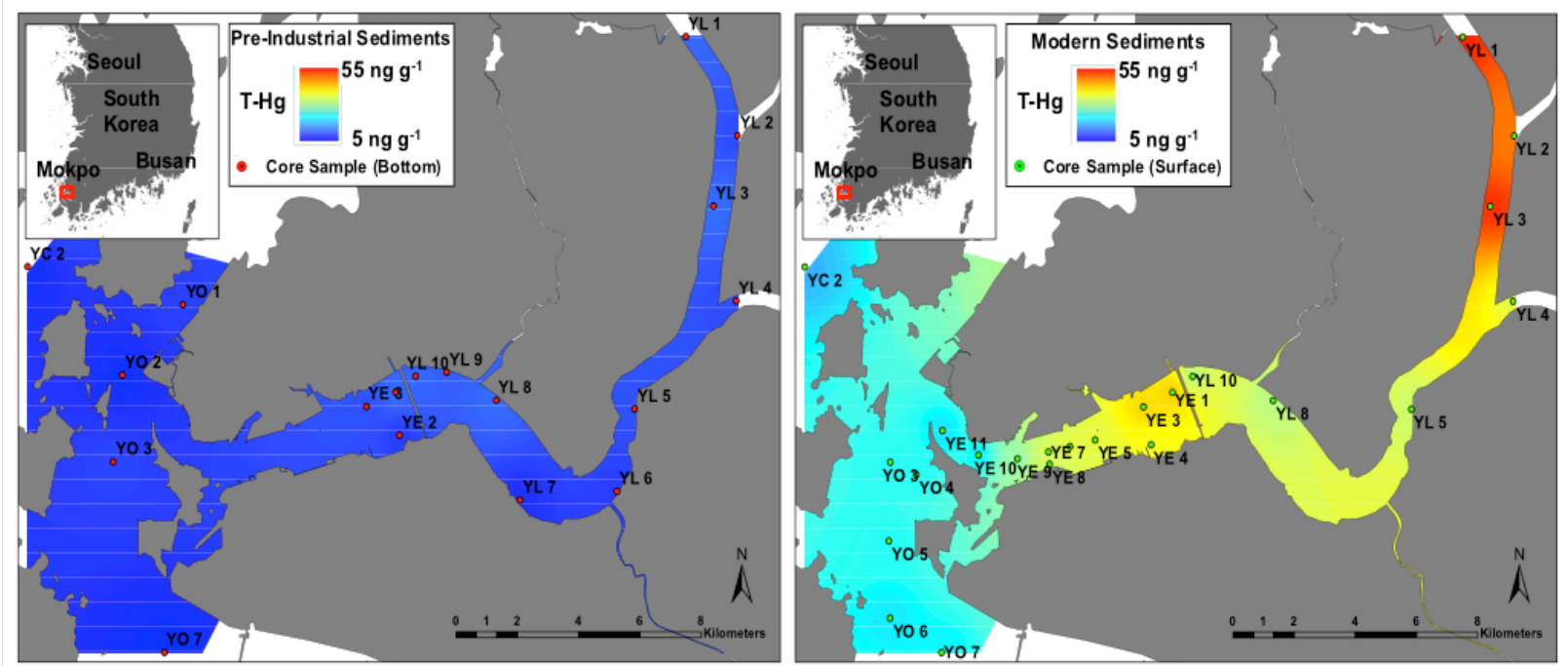


Figure 4.5 Historical and current distribution of total Hg within the Yeongsan Estuary. Samples used for interpolation of historic data represent the bottom of cores type B and C, with all cores utilized displayed. Samples used for interpolation of modern data represent the surface of cores type A and B, with all cores utilized displayed. Note: For comparison, the scale is the same in both panels.

With significant anthropogenic Hg accumulation within the Yeongsan Estuary not commencing until at least the 1970's, it is apparent that the primary sources to the watershed are likely regional. Combined, fossil fuel combustion (anthracite/bituminous coal and petroleum oil) and cement production comprise 72% of atmospheric anthropogenic Hg emissions within S. Korea (Kim et al. 2010). Within the last 40 years, these sources have dramatically increased (Figure 4.6) and are interpreted to be the cause of increased T-Hg concentrations within the Yeongsan Estuary. Prior to the 1980's, total coal consumption was dominated by anthracite mainly used for residential heating (Lim et al. 2012). However, the rapid consumption of bituminous coal by thermal power plants since then has caused total consumption to increase five fold (Figure 4.6).

Consumption of petroleum, primarily by oil-fired power plants, has also increased by nearly 4 fold since the 1980's (Figure 4.6). Despite high Hg removal efficiencies (68-91%) by air pollution control devices in these modern power plants, there is still a substantial proportion of anthropogenic Hg emitted (Kim et al. 2010, Pudasainee et al. 2010). Cement production in kilns, the third highest emitter of anthropogenic Hg in S. Korea, also exponentially increased from 1970 to 1995, remaining relatively constant since (Figure 4.6). The rapid increase in these indicators reflects the dramatic economic growth S. Korea experienced from the 1970-90's, and the consequence of industrialization on anthropogenic Hg emissions. Ultimately, the history of these increases is evident within the sedimentary record of the Yeongsan Estuary.

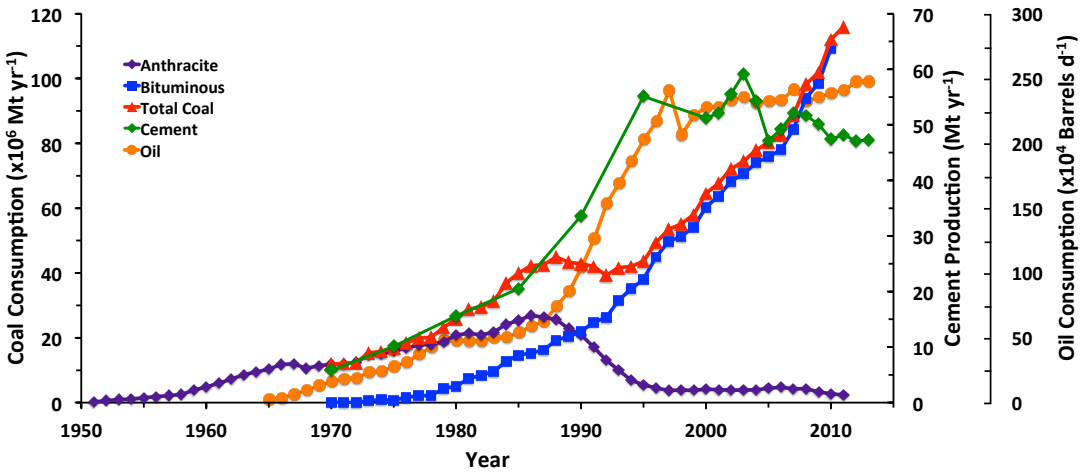


Figure 4.6 Historical trends of potential anthropogenic Hg sources since 1950 in S. Korea. Total coal is represented as the sum of anthracite and bituminous coal. Data represents a compilation from (KEEI 2013, BP 2014, EIA 2014, KCoal 2014) (oil and coal) and (Worrell et al. 2001, KCA 2013) (cement).

### *4.5.2 Spatial Distribution*

In order to understand the spatial distribution and variability of T-Hg, interpolation of these data were conducted using a standard Kriging method (Figure 4.5). The trends identified are presented as an interpretation; however, we believe the spatial density of core locations is sufficient to provide suitable representation. The pre-industrialization distribution utilized average data from the bottom of respective type B and C cores (Figure 4.5a), while the modern distribution is taken from surface sediment of core types A and B (Figure 4.5b). One exception occurs with a modern sample used from the surface of YO 7 (core type C) (Figure 4.3).

The distribution of pre-industrialized sediments shows minor variability between regions, predominantly reflecting the average background value ($8.6 \pm 2.7$ ng $g^{-1}$) (Figure 4.5 and Table 4.2). However, modern sediments display a gradient from the

upper portions of the lake to the coastal zone with a decrease in T-Hg concentration, respectively (Figure 4.5b). During freshwater discharge events, Park et al. (2012a) showed that the highest salinity gradient occurs within the inner estuary. It has also been shown that both dissolved (minor fraction of T-Hg) and particulate bound Hg typically have an inverse relationship with salinity (Han et al. 2006), with approximately 90% of T-Hg sourced from rivers being deposited in coastal sediments (Sunderland and Mason 2007). Combined with the highest sediment deposition rates occurring within the inner estuary (Williams et al., 2014), this suggests that the high gradient in T-Hg is the result of particle scavenging during releases from the estuarine dam. Additionally, T-Hg concentrations are similar on both sides of the dam, indicating that discharged water likely contains sediment sourced from proximal areas within the lake. Evidence of scouring from side-scan sonagraphs in this region provides support for this interpretation (Williams et al., 2014).

Above the estuarine dam, the freshwater Yeongsan Lake does not contain a salinity gradient yet still displays a noticeable T-Hg increase in post-industrialized sediment within the uppermost portions (Figure 4.5b). The strong correlations suggest higher organic matter or clay input to this area would result in increased T-Hg concentrations (Figure 4.4), yet cores from the lake (YL 2, 4) displayed consistently lower clay content and TOC values than those of the inner estuary (YE 3, 5). However, examination of the ratio of TOC to clay content reveals that the cores in the lake contain the highest values (Figure 4.7), suggesting changes in carrier phase characteristics. Possible explanations for the increased relative amounts of TOC are higher agricultural runoff in this region, or input from the Sampo River. Additional organic matter source characterization (molecular analyses, lignin phenols and/or lipids) may further elucidate the cause of these differences.

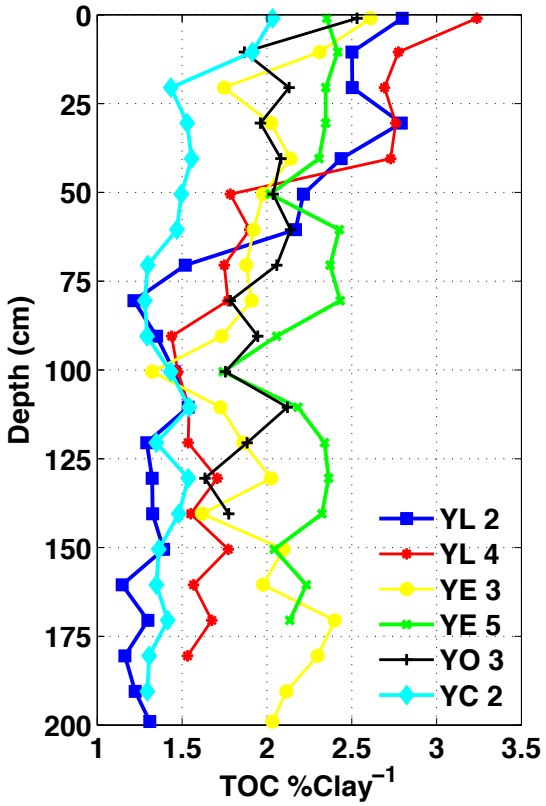


Figure 4.7 Profiles of total organic carbon normalized to clay content for 6 cores used in this study. Core locations are indicated in Figure 4.1.

*4.5.3 Applying Hg as a Geochronologic Tool*

There have been numerous studies examining anthropogenic Hg input to the sedimentary record, with vast differences in timing and concentration results (Table 4.1). However, the majority of these studies reference local sources regarding the onset of discernible anthropogenic Hg input. Within the Yeongsan Estuary, geochronology determined by $^{210}$Pb analyses reveals an increase in anthropogenic Hg at approximately 1980 (Figures 4.2 and 4.3). With no prior geochronologic data available, examination of the rapid increase in local anthropogenic Hg emissions (Figure 4.6) would likely result

in similar interpretation of the age-depth model. Thus, in this case, Hg acts as a pseudo-independent geochronologic marker.

Review of data published from similar studies (e.g. such as those in Table 4.1), indicates this method would be equally well applied in several cases. Therefore, due to the relatively low cost and sample processing time, it is proposed T-Hg analyses be more widely incorporated to studies of recent (< 200 yrs.) sedimentary process as an additional geochronologic tool. Due to uncertainty in the relative influence of local and global (long-range transport) sources, this method may not be used independently. However, although being conditional on having sufficient historical records of regional anthropogenic Hg emission, this practice provides independent and corroborating evidence to traditional isotopic methods (e.g. $^{210}$Pb, $^{137}$Cs, $^{239,240}$Pu). Similar to Hg, numerous studies have used input of anthropogenic metals (Pb, As, etc.) for chronostratigraphic markers (Shotyk et al. 2003, Lima et al. 2005, Hao et al. 2008, Kemp et al. 2012, Gobeil et al. 2013, Walraven et al. 2014, Xu et al. 2014). In addition to further constraining geochronology, the broader usage of Hg analyses in modern sedimentary process studies would continue the development of a global inventory regarding the fate of total atmospheric anthropogenic Hg emission.

### 4.6 Conclusions

Anthropogenic Hg input to the Yeongsan Estuary has significantly increased and has accumulated within the sedimentary record, with the transition from background values to enriched sediment occurring during the late 1970-80's. Coincident with the timing of T-Hg enrichment, the major sources of atmospheric anthropogenic Hg (i.e. coal, oil, and cement production) dramatically increased, reflecting the rapid economic and industrial growth of S. Korea at this time. The relatively low concentrations observed in this study are likely the result of the location of the primary S. Korean Hg sources being located near Seoul (NW) and Busan (SE), outside of the Yeongsan watershed (SW). Current spatial distribution of T-Hg displays highest values in the upper lake region, with a gradient to lower values within the inner estuary. The region of

highest concentration within the lake corresponds to the highest ratios of TOC to clay content, while high accumulation rates and a strong salinity gradient during freshwater discharge suggests the transition to lower T-Hg in the inner estuary is a result of particle scavenging. The contemporaneous timing of sediment enrichment and increased emissions suggests that regional sources dominate the Hg input to the Yeongsan Estuary, rather than long range transport. Similar reports of locally influenced increases indicate that with sufficient regional historic emission data, T-Hg may be utilized as a geochronologic tool.

Globally, increased anthropogenic Hg input has significantly increased within the last two centuries, primarily due to fossil fuel consumption, cement production, and mining practices. These increases are apparent in the sedimentary record, reflecting proximity and type of source in variable concentrations and timing of enrichment depending on environment and location. Continued regional investigation on the impacts of anthropogenic Hg accumulation in sediments is imperative not only for ecosystem analyses and inventorying historical Hg production, but understanding the fate of predicted increased emissions in the future.

# CHAPTER V
# CONCLUSIONS

## 5.1 Nakdong Estuary

Within the Nakdong Estuary, anthropogenic alteration has greatly modified the sediment transport processes, with primary engineering including the construction of numerous seawalls and estuarine dams. Large areas of intertidal zone were eliminated with the construction of the seawalls, and subsequently reduced the area for natural overbank flow and deposition during high discharge events. This resulted in rapid accumulation rates as sediment that previously could be trapped within the upper estuary and intertidal zones became confined to deposition within the middle of the estuary. The construction of the Noksan Dam caused a depletion of coarse grained sediment in the West Nakdong River due to reduced flow velocities. In addition, this resulted in the relatively slow accumulation of fine-grained sediments, likely advected from the eastern portion of the estuary and offshore. The construction of the Nakdong Estuarine Dam occluded the E. and W. Eulsuk Channels and has resulted in alteration of the timing and discharge intensity of sediment delivery. After the construction of the estuarine dam, sediment flux to the estuary was limited to floodgate releases. This pulsed discharge causes high flow velocities and episodic deposition. Moreover, the source of sediment has been reduced from three river channels prior to coastal modification, to flux principally through the E. Eulsuk Channel. The construction of the estuarine dams has appreciably reduced the tidal prism, preventing natural saltwater intrusion and estuarine circulation. The resultant reduction in tidal energy and river discharge caused a shift from a relatively tide-dominated system towards an increasingly wave-dominated system. A series of barrier islands that have developed post-dam construction provides evidence for these changes. Thus, the extremely rapid geomorphologic changes, high accumulation rates, and increased sediment trapping efficiency within the estuary are a result of a combination of these anthropogenic alterations.

The development of a conceptual model for facies distribution based on the relative amount of energy received from dam releases has been made from observations within this study. The conditions include three discharge environments in which: 1) No discharge is released 2) there is periodic (weekly to monthly), low energy discharge and 3) there is consistent (daily to weekly), high energy discharge. Examples of each of these situations are seen within the Nakdong Estuary, respectively with the West Nakdong River, E. and W. Eulsuk Channels. The rapid geomorphologic reclassification from tide-dominated to wave-dominated provides insight to the implications of anthropogenic alterations to estuarine systems. High sediment accumulation rates within the middle estuary are a result of seawall construction and land reclamation that caused a reduction in accommodation space. Tidal prism reduction, modification of sediment delivery, and a redistribution of facies are direct impacts of modifications to the Nakdong Estuary within the last century.

**5.2 Yeongsan Estuary**

The shoreline geometry, sediment accumulation rates, depositional environments, and distribution of organic matter have all dramatically changed due to anthropogenic alteration within the Yeongsan Estuary. Modifications to the system that have resulted in these changes include significant tidal flat reduction during massive land reclamation projects, and construction of an estuarine dam. The construction of seawalls has eliminated overbank deposition with the hardening of shorelines. The reduction of accommodation space associated with land reclamation has resulted in rapid accumulation rates and increased sediment trapping efficiency. Comparing the modern average accumulation rates derived from $^{210}$Pb geochronology to Holocene rates interpreted from seismic data suggests rates have increased over average by at least an order of magnitude within the last half-century. The timing and intensity of discharge have also been modified from a natural system reflecting a major change in the sediment delivery mechanisms due to impoundment. Scouring adjacent to the dam is a result of high flow velocities associated with discharge. Furthermore, the controlled discharge has resulted in episodic sedimentation. After the construction of the estuarine dam, the

distribution of organic matter and source signature throughout the system shifted. Reflecting the elimination of natural estuarine circulation and the influence of discharge, pre and post-dam lake and inner estuary sediments exhibit increased %TOM, respectively.

Additionally, the sedimentary record reveals a significant increase in anthropogenic Hg input to the Yeongsan Estuary, with the transition from background values to enriched sediment occurring during the late 1970-80's. The primary sources of atmospheric anthropogenic Hg (i.e. coal, oil, and cement production) in S. Korea dramatically increased during this time period, reflecting the rapid economic and industrial growth of S. Korea. The concomitant enrichment of T-Hg in sediments suggests increased emissions have been recorded within the sediments of the Yeongsan Estuary. However, the relatively low concentrations observed in this study are likely the result of the location of the primary S. Korean Hg sources being located near Seoul (NW) and Busan (SE), outside of the Yeongsan watershed (SW). The highest surficial T-Hg concentration values are observed in the upper lake, transitioning to lower values within the inner estuary. Evidence of regional source being the primary contributor of Hg input to the Yeongsan Estuary, rather than long range transport is suggested by the contemporaneous timing of sediment enrichment and increased emissions. Review of literature indicates that locally influenced Hg increases are common, implying that with sufficient regional historic emission data, T-Hg may be applied as a geochronologic tool.

The Yeongsan Estuary is represents many environmental changes that have occurred globally throughout the Anthropocene. Over the next century, it is predicted that coastal engineering will continue to rapidly increase and anthropogenic Hg input will rise, primarily due to fossil fuel consumption, cement production, and mining practices. Impacts such as those observed within the Nakdong and Yeongsan Estuaries are likely to be magnified with coastal population increases, industrialization, and rising eustatic sea level. Determination and elucidation of the multiple feedback mechanisms driving natural responses to anthropogenic alterations through continued observation is

necessary. Regional investigation of anthropogenic Hg accumulation in sediments is imperative for ecosystem impact evaluation and inventorying historical Hg production. These results provide advancement in the knowledge of how estuarine sedimentation processes respond to anthropogenic alteration within estuaries, and may be used to develop future estuarine management strategies throughout the world.

# REFERENCES


Ackermann, F., Bergmann, H. and Schleichert, U. (1983) 'Monitoring of Heavy Metals in Coastal and Estuarine Sediments - A Question of Grain Size: <20 μm Versus <60 μm', *Environmental Technology Letters,* 4(7), 317-328.

Al Mukaimi, M. E. (2013) *Enhanced Land Subsidence and Seidment Dynamics in Galveston Bay- Implications for Geochemical Processes and Fate and Transport of Contaminants*, unpublished thesis Texas A & M University.

Alonso-Hernández, C. M., Martin-Perez, J., Gasco, C., Díaz-Asencio, M., Bolanos-Álvarez, Y. and Gómez-Batista, M. (2012) 'Vertical Distribution and Inventories of $^{239,240}$Pu and Mercury in Sagua La Grande Estuary, Cuba', *Journal of Environmental Radioactivity,* 112, 23-28.

Álvarez-Iglesias, P., Quintana, B., Rubio, B. and Pérez-Arlucea, M. (2007) 'Sedimentation Rates and Trace Metal Input History in Intertidal Sediments from San Simón Bay (Ría De Vigo, Nw Spain) Derived from $^{210}$Pb and $^{137}$Cs Chronology', *Journal of Environmental Radioactivity,* 98(3), 229-250.

AMAP/UNEP (2008) *Technical Background Report to the Global Atmospheric Mercury Assessment*, Arctic Monitoring and Assessment Programme / UNEP Chemicals Branch.

Appleby, P. G. (2001) 'Chronostratigraphic Techniques in Recent Sediments' in Last, W. M. and Smol, J. P., eds., *Tracking Environmental Change Using Lake Sediments*, Springer Netherlands, 171-203.

Appleby, P. G. and Oldfield, F. (1978) 'The Calculation of Lead-210 Dates Assuming a Constant Rate of Supply of Unsupported $^{210}$Pb to the Sediment', *CATENA,* 5(1), 1-8.

Ban, Y. B. (1984) 'The Tidal Flat around the Nakdong River Mouth', *Korea Journal of Geography,* 9, 537-559.

Barghigiani, C., Ristori, T. and Lopez Arenas, J. (1996) 'Mercury in Marine Sediment from a Contaminated Area of the Northern Tyrrhenian Sea: <20 μm Grain-Size Fraction and Total Sample Analysis', *Science of The Total Environment,* 192(1), 63-73.

Barusseau, P. J., B, M., Descamps, C., Salif Diop, E., Diouf, B., Kane, A., Saos, J. L. and Soumar, A. (1998) 'Morphological and Sedimentological Changes in the Senegal River Estuary after the Constuction of the Diama Dam', *Journal of African Earth Sciences,* 26(2), 317-326.

Bianchi, T. S. (2007) *Biogeochemistry of Estuaries,* Oxford; New York: Oxford University Press.

Bianchi, T. S. and Canuel, E. A. (2011) *Chemical Biomarkers in Aquatic Ecosystems,* Princeton: Princeton University Press.

Biggs, R. B. and Howell, B., A. (1984) 'The Estuary as a Sediment Trap: Alternate Approaches to Estimating Its Filtering Efficiency' in Kennedy, D. P., ed. *The Estuary as a Filter*, New York: Academic Press, 107-129.

Bloom, A. L. and Park, Y. A. (1985) 'Holocene Sea-Level History and Tectonic Movements, Republic of Korea.', *Quaternary Research,* 24, 77-84.

Bokuniewicz, H. (1995) 'Chapter 3 Sedimentary Systems of Coastal-Plain Estuaries' in Perillo, G. M. E., ed. *Developments in Sedimentology*, Elsevier, 49-67.

BP (2014) 'British Petroleum Statistical Review of World Energy', London, UK.

Brandenberger, J. M., Louchouarn, P. and Crecelius, E. A. (2011) 'Natural and Post-Urbanization Signatures of Hypoxia in Two Basins of Puget Sound: Historical

Reconstruction of Redox Sensitive Metals and Organic Matter Inputs', *Aquatic Geochemistry,* 17, 645-670.

Bratton, J. F., Colman, S. M. and Seal Ii, R. R. (2003) 'Eutrophication and Carbon Sources in Chesapeake Bay over the Last 2700 Yr: Human Impacts in Context', *Geochimica et Cosmochimica Acta,* 67(18), 3385-3402.

BuTayban, N. A.-M. and Preston, M. R. (2004) 'The Distribution and Inventory of Total and Methyl Mercury in Kuwait Bay', *Marine Pollution Bulletin,* 49(11–12), 930-937.

Byun, D. S., Wang, X. H., Zavatarelli, M. and Cho, Y.-K. (2007) 'Effects of Resuspended Sediments and Vertical Mixing on Phytoplankton Spring Bloom Dynamics in a Tidal Estuarine Embayment', *Journal of Marine Systems,* 67(1-2), 102-118.

Byun, D. S., Wang, X. H. and Holloway, P. E. (2004) 'Tidal Characteristic Adjustment Due to Dyke and Seawall Construction in the Mokpo Coastal Zone, Korea', *Estuarine, Coastal and Shelf Science,* 59(2), 185-196.

Carlin, J. A. and Dellapenna, T. M. (2014) 'Event-Driven Deltaic Sedimentation on a Low-Gradient, Low-Energy Shelf: The Brazos River Subaqueous Delta, Northwestern Gulf of Mexico', *Marine Geology,* 353(0), 21-30.

Chakraborty, P., Sharma, B., Raghunath Babu, P. V., Yao, K. M. and Jaychandran, S. (2014) 'Impact of Total Organic Carbon (in Sediments) and Dissolved Organic Carbon (in Overlying Water Column) on Hg Sequestration by Coastal Sediments from the Central East Coast of India', *Marine Pollution Bulletin,* 79(1–2), 342-347.

Chang, C. P. (2004) *East Asian Monsoon, World Scientific Series on Meteorology of East Asia,* Toh Tuck Link, Singapore: World Scientific Publishing Co. Ptd. Lte.

Chang, J. H. and Choi, J. Y. (2001) 'Tidal-Flat Sequence Controlled by Holocene Sea-Level Rise in Gomso Bay, West Coast of Korea', *Estuarine, Coastal and Shelf Science,* 52(3), 391-399.

Choi, D. L., Hyun, S. M. and Lee, T. H. (2002) 'Recent Geomorphological Changes and Late Quaternary Depositional Sequence of Gwangyang Bay, Southern Coast of Korea', *Journal of the Korean Society of Oceanography,* 8(1), 35-43.

Choi, E.-M., Kim, S.-H., Holsen, T. M. and Yi, S.-M. (2009) 'Total Gaseous Concentrations in Mercury in Seoul, Korea: Local Sources Compared to Long-Range Transport from China and Japan', *Environmental Pollution,* 157(3), 816-822.

Choi, J. Y., Kwon, Y. K. and Chung, G. S. (2012a) 'Late Quaternary Stratigraphy and Depositional Environment of Tidal Sand Ridge Deposits in Gyeonggi Bay, West Coast of Korea', *Journal of Korean Earth Science Society,* 33(1), 1-10.

Choi, K., Kim, S., Hong, G. and Chon, H. (2012b) 'Distributions of Heavy Metals in the Sediments of South Korean Harbors', *Environmental Geochemistry and Health,* 34(1), 71-82.

Choi, S.-U. K., Yoon, B. and Woo, H. (2005) 'Effects of Dam-Induced Flow Regime Change on Downstream River Morphology and Vegetation Cover in the Hwang River, Korea', *River Research and Applications,* 21(2-3), 315-325.

Church, J. A., Clark, P. U., Cazenave, A., Gregory, J. M., Jevrejeva, S., Levermann, A., Merrifield, M. A., Milne, G. A., Nerem, R. S., Nunn, P. D., Payne, A. J., Pfeffer, W. T., Stammer, D. and Unnikrishnan, A. S. (2014) 'Sea Level Change' in Stocker, T. F., Qin, D., Plattner, G.-K., Tignor, M., Allen, S. K., Boschung, J., Nauels, A., Xia, Y., Bex, V. and Midgley, P. M., eds., *Climate Change 2013: The Physical Science Basis. Contribution of Working Group I to the Fifth Assessment Report of the Intergovernmental Panel on Climate Change*,

Cambridge, United Kingdom and New York, NY, USA.: Cambridge University Press.

Cohen, J. E., Small, C., Mellinger, A., Gallup, J. and Sachs, J. (1997) 'Estimates of Coastal Populations', *Science,* 278(5341), 1209-1213.

Connan, O., Maro, D., Hébert, D., Roupsard, P., Goujon, R., Letellier, B. and Le Cavelier, S. (2013) 'Wet and Dry Deposition of Particles Associated Metals (Cd, Pb, Zn, Ni, Hg) in a Rural Wetland Site, Marais Vernier, France', *Atmospheric Environment,* 67, 394-403.

Cooper, J. A. G. (2002) 'The Role of Extreme Floods in Estuary-Coastal Behaviour: Contrasts between River- and Tide-Dominated Microtidal Estuaries', *Sedimentary Geology,* 150(12), 123-137.

Cooper, J. A. G. (2009) 'Anthropogenic Impacts on Estuaries' in Ignacio, F. and Iribarne, O., eds., *Coastal Zones and Estuaries*, Eolss Publishers Co Ltd, 523.

Crawford, G. W. and Lee, G.-A. (2003) 'Agricultural Origins in the Korean Peninsula', *Antiquity,* 77(295), 87.

Crossland, C. J., Kremer, H. H., Lindeboom, H. J., Marshall Crossland, J. I. and Tissier, M. D. A. (2005) *Coastal Fluxes in the Anthropocene : The Land-Ocean Interactions in the Coastal Zone Project of the International Geosphere-Biosphere Programme, Global Change, the IGBP Series,* Berlin, Heidelberg: Springer-Verlag Berlin Heidelberg.

Cuvilliez, A., Deloffre, J., Lafite, R. and Bessineton, C. (2009) 'Morphological Responses of an Estuarine Intertidal Mudflat to Constructions since 1978 to 2005: The Seine Estuary (France)', *Geomorphology,* 104(3–4), 165-174.

Dalrymple, R. W. and Choi, K. (2007) 'Morphologic and Facies Trends through the Fluvialmarine Transition in Tide-Dominated Depositional Systems: A Schematic

Framework for Environmental and Sequence-Stratigraphic Interpretation', *Earth-Science Reviews,* 81(34), 135-174.

Dalrymple, R. W., Zaitlin, B. A. and Boyd, R. (1992) 'Estuarine Facies Models: Conceptual Basis and Statigraphic Implications', *Journal of Sedimentary Petrology,* 62(6), 1130-1146.

Davis Jr, R. A., Cuffe, C. K., Kowalski, K. A. and Shock, E. J. (2003) 'Stratigraphic Models for Microtidal Tidal Deltas; Examples from the Florida Gulf Coast', *Marine Geology,* 200(14), 49-60.

Davis Jr, R. A. and Hayes, M. O. (1984) 'What Is a Wave-Dominated Coast?' in Greenwood, B. and Davis, R. A., eds., *Developments in Sedimentology*, Elsevier, 313-329.

Dellapenna, T. M., Kuehl, S. A. and Schaffner, L. C. (2003) 'Ephemeral Deposition, Seabed Mixing and Fine-Scale Strata Formation in the York River Estuary, Chesapeake Bay', *Estuarine, Coastal and Shelf Science,* 58(3), 621-643.

Donovan, P. M., Blum, J. D., Yee, D., Gehrke, G. E. and Singer, M. B. (2013) 'An Isotopic Record of Mercury in San Francisco Bay Sediment', *Chemical Geology,* 349–350, 87-98.

Driscoll, C. T., Chen, C. Y., Hammerschmidt, C. R., Mason, R. P., Gilmour, C. C., Sunderland, E. M., Greenfield, B. K., Buckman, K. L. and Lamborg, C. H. (2012) 'Nutrient Supply and Mercury Dynamics in Marine Ecosystems: A Conceptual Model', *Environmental Research,* 119, 118-131.

EIA (2014) *South Korea Analysis Brief: U.S. Energy Information Administration*.

EPA (1998) 'Method 7473: Mercury in Solids and Solutions by Thermal Decomposition Amalgamation and Atomic Absorption Spectrophotometry', *EPA SW-846*

*Cincinnati: USEPA Office of Research and Development Environmental Monitoring Systems Laboratory,*

Ethier, A. L. M., Scheuhammer, A. M., Blais, J. M., Paterson, A. M., Mierle, G., Ingram, R. and Lean, D. R. S. (2010) 'Mercury Empirical Relationships in Sediments from Three Ontario Lakes', *Science of The Total Environment,* 408(9), 2087-2095.

Eun, G. Y. N., Chung, C. H. and Klm, D. J. (1998) 'A Comparative Study of Depositional Environments through Coring Analysis in Yeongsan and Nakdong Estuaries', *Journal of Korean Environmental Sciences Society,* 7, 889-893.

Fang, G. C., S., W. Y. and Chang, T. H. (2008) 'Comparison of Atmospheric Mercury (Hg) among Korea, Japan, China and Taiwan During 2000-2008', *Journal of Hazardous Materials,* 162, 607-615.

Frouin, M., Sebag, D., Durand, A., Laignel, B., Saliege, J.-F., Mahler, B. J. and Fauchard, C. (2007) 'Influence of Paleotopography, Base Level and Sedimentation Rate on Estuarine System Response to the Holocene Sea-Level Rise: The Example of the Marais Vernier, Seine Estuary, France', *Sedimentary Geology,* 200(1–2), 15-29.

Gao, J.-h., Li, J., Wang, H., Bai, F.-l., Cheng, Y. and Wang, Y.-p. (2012) 'Rapid Changes of Sediment Dynamic Processes in Yalu River Estuary under Anthropogenic Impacts', *International Journal of Sediment Research,* 27(1), 37-49.

Gobeil, C., Tessier, A. and Couture, R.-M. (2013) 'Upper Mississippi Pb as a Mid-1800s Chronostratigraphic Marker in Sediments from Seasonally Anoxic Lakes in Eastern Canada', *Geochimica et Cosmochimica Acta,* 113, 125-135.

Gordon, E. S. and Goñi, M. A. (2003) 'Sources and Distribution of Terrigenous Organic Matter Delivered by the Atchafalaya River to Sediments in the Northern Gulf of Mexico', *Geochimica et Cosmochimica Acta,* 67(13), 2359-2375.

Gupta, H., Kao, S.-J. and Dai, M. (2012) 'The Role of Mega Dams in Reducing Sediment Fluxes: A Case Study of Large Asian Rivers', *Journal of Hydrology,* 464–465, 447-458.

Han, S., Gill, G. A., Lehman, R. D. and Choe, K.-Y. (2006) 'Complexation of Mercury by Dissolved Organic Matter in Surface Waters of Galveston Bay, Texas', *Marine Chemistry,* 98(2–4), 156-166.

Han, Y.-J., Kim, J.-E., Kim, P.-R., Kim, W.-J., Yi, S.-M., Seo, Y.-S. and Kim, S.-H. (2014) 'General Trends of Atmospheric Mercury Concentrations in Urban and Rural Areas in Korea and Characteristics of High-Concentration Events', *Atmospheric Environment,* 94, 754-764.

Hao, Y., Guo, Z., Yang, Z., Fan, D., Fang, M. and Li, X. (2008) 'Tracking Historical Lead Pollution in the Coastal Area Adjacent to the Yangtze River Estuary Using Lead Isotopic Compositions', *Environmental Pollution,* 156(3), 1325-1331.

Harris, D., Horwáth, W. R. and van Kessel, C. (2001) 'Acid Fumigation of Soils to Remove Carbonates Prior to Total Organic Carbon or Carbon-13 Isotopic Analysis', *Soil Sci. Soc. Am. J.,* 65(6), 1853-1856.

Heaton, T. H. E. (1986) 'Isotopic Studies of Nitrogen Pollution in the Hydrosphere and Atmosphere: A Review', *Chemical Geology: Isotope Geoscience section,* 59, 87-102.

Hung, J. J., Lu, C. C., Huh, C. A. and Liu, J. T. (2009) 'Geochemical Controls on Distributions and Speciation of as and Hg in Sediments Along the Gaoping

(Kaoping) Estuary–Canyon System Off Southwestern Taiwan', *Journal of Marine Systems,* 76(4), 479-495.

Hwang, C. S., Kim, K. T., Oh, C. Y., Jin, C. G. and Choi, C. U. (2010) 'A Study on Correlation between Rusle and Estuary in Nakdong River Watershed', *Journal of the Korean Society for Geospatial Information System,* 18(3), 3-10.

Jackson, N. L. (2013) '10.12 Estuaries' in Shroder, J. F., ed. *Treatise on Geomorphology*, San Diego: Academic Press, 308-327.

Jeong, K.-S., Kim, D.-K. and Joo, G.-J. (2007) 'Delayed Influence of Dam Storage and Discharge on the Determination of Seasonal Proliferations of Microcystis Aeruginosa and Stephanodiscus Hantzschii in a Regulated River System of the Lower Nakdong River (South Korea)', *Water Research,* 41(6), 1269-1279.

Jha, S. K., Chavan, S. B., Pandit, G. G. and Sadasivan, S. (2003) 'Geochronology of Pb and Hg Pollution in a Coastal Marine Environment Using Global Fallout $^{137}$Cs', *Journal of Environmental Radioactivity,* 69(1–2), 145-157.

Ji, U. (2006) *Numerical Model for Sediment Flushing at the Nakdong River Estuary Barrage*, unpublished thesis Colorado State University.

Joo, H. S., Park, J. C., Kim, J., Lee, W. B. and Lee, S. W. (2000) 'Physicochemical Composition and Heavy Metal Contents on the Sediment of Kwangyang Bay', *Korean Journal of Limnology,* 33(1), 31-37.

Kading, T. J., Mason, R. P. and Leaner, J. J. (2009) 'Mercury Contamination History of an Estuarine Floodplain Reconstructed from a 210pb-Dated Sediment Core (Berg River, South Africa)', *Marine Pollution Bulletin,* 59(4–7), 116-122.

Kang, J.-H., Lee, Y. S., Ki, S. J., Lee, Y. G., Cha, S. M., Cho, K. H. and Kim, J. H. (2009) 'Characteristics of Wet and Dry Weather Heavy Metal Discharges in the

Yeongsan Watershed, Korea', *Science of The Total Environment,* 407(11), 3482-3493.

Kang, J. W. (1999) 'Changes in Tidal Characteristics as a Result of the Construction of Sea-Dike/Sea-Walls in the Mokpo Coastal Zone in Korea', *Estuarine, Coastal and Shelf Science,* 48(4), 429-438.

Karagas, M. R., Choi, A. L., Oken, E., Horvat, M., Schoeny, R., Kamai, E., Cowell, W., Grandjean, P. and Korrick, S. (2012) 'Evidence on the Human Health Effects of Low-Level Methylmercury Exposure', *Environmental Health Perspectives,* 120(6), 799-806.

KCA (2013) 'Korea Cement Association Statistical Review'.

KCoal (2014) 'Korean Coal Association 2013 Demand and Supply Statistics Report'.

KEEI (2013) 'Korea Energy Economics Institute 2013 Yearbook of Energy Statistics'.

Kemp, A. C., Sommerfield, C. K., Vane, C. H., Horton, B. P., Chenery, S., Anisfeld, S. and Nikitina, D. (2012) 'Use of Lead Isotopes for Developing Chronologies in Recent Salt-Marsh Sediments', *Quaternary Geochronology,* 12, 40-49.

Kench, P. S. (1999) 'Geomorphology of Australian Estuaries: Review and Prospect', *Australian Journal of Ecology,* 24(4), 367-380.

Khim, B. K., Choi, K. S. and Park, Y. A. (2000) 'Elemental Composition of Siderite Grains in Early-Holocene Deposits of Youngjong Island (West Coast of Korea), and Its Palaeoenvironmental Implications' in B.W. Flemming, M. T. D. and Liebezeit, G., eds., *Proceedings in Marine Science*, Elsevier, 205-217.

Khim, B. K., Kim, B. O. and Lee, S. R. (2009) 'Variation of the Textural Parameters of Surface Sediments between Spring and Fall Season on the Jinu-Do Beach,

Nakdong River Estuary', *Korean Society of Coastal and Ocean Engineers,* 21(6), 444-452.

Kim, B. O., Khim, B. K. and Lee, S. R. (2005) 'Development of Mosaic Aerial Photographs for Shoreline Change Study in Nakdong Estuary', *Ocean and Polar Research,* 27(4), 497-507.

Kim, B. O., Khim, B. K. and Lee, S. R. (2007) 'Rate of Shoreline Changes for Barrier Islands in Nakdong Estuary', *Korean Society of Coastal and Ocean Engineers,* 19(4), 361-374.

Kim, D. C., Sung, J. Y., Park, S. C., Lee, G. H., Choi, J. H., Kim, G. Y., Seo, Y. K. and Kim, J. C. (2001) 'Physical and Acoustic Properties of Shelf Sediments, the South Sea of Korea', *Marine Geology,* 179(1-2), 39-50.

Kim, E., Noh, S., Lee, Y.-g., Kundu, S. R., Lee, B.-G., Park, K. and Han, S. (2014) 'Mercury and Methylmercury Flux Estimation and Sediment Distribution in an Industrialized Urban Bay', *Marine Chemistry,* 158, 59-68.

Kim, J.-H., Park, J.-M., Lee, S.-B., Pudasainee, D. and Seo, Y.-C. (2010) 'Anthropogenic Mercury Emission Inventory with Emission Factors and Total Emission in Korea', *Atmospheric Environment,* 44(23), 2714-2721.

Kim, K.-H. and Kim, M.-Y. (2000) 'The Effects of Anthropogenic Sources on Temporal Distribution Characteristics of Total Gaseous Mercury in Korea', *Atmospheric Environment,* 34(20), 3337-3347.

Kim, K.-H. and Kim, M.-Y. (2002) 'A Decadal Shift in Total Gaseous Mercury Concentration Levels in Seoul, Korea: Changes between the Late 1980s and the Late 1990s', *Atmospheric Environment,* 36(4), 663-675.

Kim, K.-H., Yoon, H.-O., Brown, R. J. C., Jeon, E.-C., Sohn, J.-R., Jung, K., Park, C.-G. and Kim, I.-S. (2013) 'Simultaneous Monitoring of Total Gaseous Mercury at

Four Urban Monitoring Stations in Seoul, Korea', *Atmospheric Research,* 132–133, 199-208.

Kim, K. T., Ra, K., Kim, E. S., Yim, U. H. and Kim, J. K. (2011) 'Distribution of Heavy Metals in the Surface Sediments of the Han River and Its Estuary, Korea', *Journal of Coastal Research,* SI 64, 903-907.

Kim, S. H. (2005) 'The Morphological Changes of Deltaic Barrier Islands in the Nakdong River Estuary after the Construction of River Barrage', *Journal of Geographical Society of Korea,* 40(4), 373-478.

Kim, S. H. (2009) 'The Sedimentological Environment of Deltaic Barrier Islands in the Nakdong River Estuary', *Journal of the Korean Geomorphological Association,* 16(4), 119-129.

Kim, S. H. and Rhew, H. S. (2007) 'Exploring the Applicability of Grain Size Trend Analysis to Understanding the Morphological Responses of the Deltaic Barrier Islands in the Nakdong River', *Korea Journal of Geography,* 13(2), 119-128.

Kim, S. Y. and Ha, J. S. (2001) 'Sedimentary Facies and Environmental Changes of the Nakdong River Estuary and Adjacent Coastal Area', *Journal of Korean Fisheries Society,* 34(3), 268-278.

Kim, T. I., Choi, B. H. and Lee, S. W. (2006) 'Hydrodynamics and Sedimentation Induced by Large-Scale Coastal Developments in the Keum River Estuary, Korea', *Estuarine, Coastal and Shelf Science,* 68(3-4), 515-528.

Kim, W. H. and Lee, H. H. (1980) 'Sediment Transport and Deposition in the Nakdong Estuary, Korea', *Journal of the Geological Society of Korea,* 16(3), 180-188.

Klingbeil, A. D. and Sommerfield, C. K. (2005) 'Latest Holocene Evolution and Human Disturbance of a Channel Segment in the Hudson River Estuary', *Marine Geology,* 218(1–4), 135-153.

Kummu, M., Lu, X. X., Wang, J. J. and Varis, O. (2010) 'Basin-Wide Sediment Trapping Efficiency of Emerging Reservoirs Along the Mekong', *Geomorphology,* 119(3–4), 181-197.

Kwon, H. J. (1973) 'A Geomorphic Study of the Naktong Delta', *Korean Journal of Geology*, 40, 8-23.

Kwon, Y. K. (2012) 'Late Quaternary Sequence Stratigraphy in Kyeonggi Bay, Mid-Eastern Yellow Sea', *Journal of Korean Earth Science Society,* 33(3), 242-258.

Lambertsson, L. and Nilsson, M. (2006) 'Organic Material: The Primary Control on Mercury Methylation and Ambient Methyl Mercury Concentrations in Estuarine Sediments', *Environmental Science & Technology,* 40(6), 1822-1829.

Lario, J., Zazo, C., Goy, J. L., Dabrio, C. J., Borja, F., Silva, P. G., Sierro, F., González, A., Soler, V. and Yll, E. (2002) 'Changes in Sedimentation Trends in Sw Iberia Holocene Estuaries (Spain)', *Quaternary International,* 93–94, 171-176.

Lasorsa, B. K., Gill, G. A. and Horvat, M. (2012) 'Analytical Methods for Measuring Mercury in Water, Sediment, and Biota' in Bank, M. S., ed. *Mercury in the Environment, Pattern and Process*, 1 ed., Berkely and Los Angeles, California: University of California Press, 27-54.

Lee, G. H., Kim, D. C., Park, M. K., Park, S. C., Kim, H. J., Jou, H. T. and Khim, B. K. (2010) 'Internal Reflection Pattern of Korea Strait Shelf Mud (Nakdong River Subaqueous Delta) Off Southeast Korea and Implications for Holocene Relative Base-Level Change', *Island Arc,* 19(1), 71-85.

Lee, H.-Y., Park, K.-P., Koo, N.-H., Yoo, D.-G., Kang, D.-H., Kim, Y.-G., Hwang, K.-D. and Kim, J.-C. (2004) 'High-Resolution Shallow Marine Seismic Surveys Off Busan and Pohang, Korea, Using a Small-Scale Multichannel System', *Journal of Applied Geophysics,* 56(1), 1-15.

Lee, H. J., Wang, Y. P., Chu, Y. S. and Jo, H. R. (2006) 'Suspended Sediment Transport in the Coastal Area of Jinhae Bay - Nakdong Estuary, Korea Strait', *Journal of Coastal Research,* 22(5), 1062-1069.

Lee, J. S., Yoon, E. C., Baek, S. W. and Lee, J. C. (2003) 'Three-Dimensional Behavior of Nakdong River Plume During the Flood Period of Summer', *Journal of Korean Fisheries Society,* 36(5), 549-561.

Lee, K.-H., Rho, B.-H., Cho, H.-J. and Lee, C.-H. (2011) 'Estuary Classification Based on the Characteristics of Geomorphological Features, Natural Habitat Distributions and Land Uses', *Journal of the Korean Society for Oceanography,* 16(2), 53-69.

Lee, K. E., Chon, H. T. and Jung, M. C. (2008) 'Contamination Level and Distribution Patterns of Hg in Soil, Sediment, Dust and Sludge from Various Anthropogenic Sources in Korea', *Mineralogical Magazine,* 72(1), 445-449.

Lee, Y. D. (1993) 'A Study on the Characteristics of Submarine Geology in Pusan Bay: Sedimentation Processes in the Nakdong River Estuary, Korea', *Journal of Korean Earth Science Society,* 14(1), 67-74.

Lee, Y. G., An, K.-G., Ha, P. T., Lee, K.-Y., Kang, J.-H., Cha, S. M., Cho, K. H., Lee, Y. S., Chang, I. S., Kim, K.-W. and Kimj, J. H. (2009) 'Decadal and Seasonal Scale Changes of an Artificial Lake Environment after Blocking Tidal Flows in the Yeongsan Estuary Region, Korea', *Science of The Total Environment,* 407(23), 6063-6072.

Leonardo, R. D., Tranchida, G., Bellanca, A., Neri, R., Angelone, M. and Mazzola, S. (2006) 'Mercury Levels in Sediments of Central Mediterranean Sea: A 150+ Year Record from Box-Cores Recovered in the Strait of Sicily', *Chemosphere,* 65(11), 2366-2376.

Li, H.-B., Yu, S., Li, G.-L., Deng, H., Xu, B., Ding, J., Gao, J.-B., Hong, Y.-W. and Wong, M.-H. (2013) 'Spatial Distribution and Historical Records of Mercury Sedimentation in Urban Lakes under Urbanization Impacts', *Science of The Total Environment,* 445–446, 117-125.

Lim, D.-i., Choi, J.-W., Shin, H. H., Jeong, D. H. and Jung, H. S. (2013) 'Toxicological Impact Assessment of Heavy Metal Contamination on Macrobenthic Communities in Southern Coastal Sediments of Korea', *Marine Pollution Bulletin,* 73(1), 362-368.

Lim, D.-i., Jung, H. S., Kim, K. T., Shin, H. H. and Jung, S. W. (2012) 'Sedimentary Records of Metal Contamination and Eutrophication in Jinhae-Masan Bay, Korea', *Marine Pollution Bulletin,* 64(11), 2542-2548.

Lim, D. I., Jung, H. S., Kim, B. O., Choi, J. Y. and Kim, H. N. (2004) 'A Buried Palaeosol and Late Pleistocene Unconformity in Coastal Deposits of the Eastern Yellow Sea, East Asia', *Quaternary International,* 121(1), 109-118.

Lim, D. I. and Park, Y. A. (2003) 'Late Quaternary Stratigraphy and Evolution of a Korean Tidal Flat, Haenam Bay, Southeastern Yellow Sea, Korea', *Marine Geology,* 193(3–4), 177-194.

Lima, A. L., Bergquist, B. A., Boyle, E. A., Reuer, M. K., Dudas, F. O., Reddy, C. M. and Eglinton, T. I. (2005) 'High-Resolution Historical Records from Pettaquamscutt River Basin Sediments: 2. Pb Isotopes Reveal a Potential New Stratigraphic Marker', *Geochimica et Cosmochimica Acta,* 69(7), 1813-1824.

Liu, G.-f., Wu, J.-x. and Wang, Y.-y. (2014) 'Near-Bed Sediment Transport in a Heavily Modified Coastal Plain Estuary', *International Journal of Sediment Research,* 29(2), 232-245.

Long, A. J., Innes, J. B., Kirby, J. R., Lloyd, J. M., Rutherford, M. M., Shennan, I. and Tooley, M. J. (1998) 'Holocene Sea-Level Change and Coastal Evolution in the Humber Estuary, Eastern England: An Assessment of Rapid Coastal Change', *The Holocene,* 8(2), 229-247.

Long, E., Macdonald, D., Smith, S. and Calder, F. (1995) 'Incidence of Adverse Biological Effects within Ranges of Chemical Concentrations in Marine and Estuarine Sediments', *Environmental Management,* 19(1), 81-97.

Lotze, H. K., Lenihan, H. S., Bourque, B. J., Bradbury, R. H., Cooke, R. G., Kay, M. C., Kidwell, S. M., Kirby, M. X., Peterson, C. H. and Jackson, J. B. C. (2006) 'Depletion, Degradation, and Recovery Potential of Estuaries and Coastal Seas', *Science,* 312(5781), 1806-1809.

Louchouarn, P. and Lucotte, M. (1998) 'A Historical Reconstruction of Organic and Inorganic Contamination Events in the Saguenay Fjord/St. Lawrence System from Preindustrial Times to the Present', *Science of The Total Environment,* 213(1–3), 139-150.

Louchouarn, P., Lucotte, M. and Farella, N. (1999) 'Historical and Geographical Variations of Sources and Transport of Terrigenous Organic Matter within a Large-Scale Coastal Environment', *Organic Geochemistry,* 30, 675-699.

Lu, X. and Matsumoto, E. (2005) 'Recent Sedimentation Rates Derived from 210pb and 137cs Methods in Ise Bay, Japan', *Estuarine, Coastal and Shelf Science,* 65(1–2), 83-93.

Macko, S. A. and Ostrom, N. E. (1994) 'Pollution Studies Using Stable Isotopes' in Lajtha, K. and Michener, R. H., eds., *Stable Isotopes in Ecology and Environmental Science*, London: Blackwell Publishing.

McGranahan, G., Balk, D. and Anderson, B. (2007) 'The Rising Tide: Assessing the Risks of Climate Change and Human Settlements in Low Elevation Coastal Zones', *Environment and Urbanization,* 19(1), 17-37.

Mergler, D., Anderson, H. A., Chan, L. H., Mahaffey, K. R., Murray, M., Sakamoto, M. and Stern, A. H. (2007) 'Methylmercury Exposure and Health Effects in Humans: A Worldwide Concern', *AMBIO: A Journal of the Human Environment,* 36(1), 3-11.

Mil-Homens, M., Blum, J., Canário, J., Caetano, M., Costa, A. M., Lebreiro, S. M., Trancoso, M., Richter, T., de Stigter, H., Johnson, M., Branco, V., Cesário, R., Mouro, F., Mateus, M., Boer, W. and Melo, Z. (2013) 'Tracing Anthropogenic Hg and Pb Input Using Stable Hg and Pb Isotope Ratios in Sediments of the Central Portuguese Margin', *Chemical Geology,* 336, 62-71.

Mitchell, S. B. and Uncles, R. J. (2013) 'Estuarine Sediments in Macrotidal Estuaries: Future Research Requirements and Management Challenges', *Ocean & Coastal Management,* 79, 97-100.

Mullenbach, B. L. and Nittrouer, C. A. (2000) 'Rapid Deposition of Fluvial Sediment in the Eel Canyon, Northern California', *Continental Shelf Research,* 20(16), 2191-2212.

Mullenbach, B. L. and Nittrouer, C. A. (2006) 'Decadal Record of Sediment Export to the Deep Sea Via Eel Canyon', *Continental Shelf Research,* 26(17–18), 2157-2177.

Muntean, M., Janssens-Maenhout, G., Song, S., Selin, N. E., Olivier, J. G. J., Guizzardi, D., Maas, R. and Dentener, F. (2014) 'Trend Analysis from 1970 to 2008 and Model Evaluation of Edgarv4 Global Gridded Anthropogenic Mercury Emissions', *Science of The Total Environment,* 494–495, 337-350.

Nahm, W.-H., Kim, J. C., Bong, P.-Y., Kim, J.-Y., Yang, D.-Y. and Yu, K.-M. (2008) 'Late Quaternary Stratigraphy of the Yeongsan Estuary, Southwestern Korea', *Quaternary International,* 176-177, 13-24.

Nguyen, H. T., Kim, M.-Y. and Kim, K.-H. (2010) 'The Influence of Long-Range Transport on Atmospheric Mercury on Jeju Island, Korea', *Science of The Total Environment,* 408(6), 1295-1307.

Nittrouer, C. A., Sternberg, R. W., Carpenter, R. and Bennett, J. T. (1979) 'The Use of Pb-210 Geochronology as a Sedimentological Tool: Application to the Washington Continental Shelf', *Marine Geology,* 31(3-4), 297-316.

Oh, G. H. (1994) 'The Paleoenvironment of the Northern Part of the Nakdong River Delta', *The Korean Journal of Quaternary Research,* 8(1), 33-42.

Oh, G. H. (1999) 'Landform Changes of Terminal Area of the Nagdong River Delta, Korea', *The Korean Journal of Quaternary Research,* 13(1), 67-78.

Oh, S., Kim, M.-K., Yi, S.-M. and Zoh, K.-D. (2010) 'Distributions of Total Mercury and Methylmercury in Surface Sediments and Fishes in Lake Shihwa, Korea', *Science of The Total Environment,* 408(5), 1059-1068.

Osterman, L. E. and Smith, C. G. (2012) 'Over 100 Years of Environmental Change Recorded by Foraminifers and Sediments in Mobile Bay, Alabama, Gulf of Mexico, USA', *Estuarine, Coastal and Shelf Science,* 115, 345-358.

Pacyna, E. G., Pacyna, J. M., Sundseth, K., Munthe, J., Kindbom, K., Wilson, S., Steenhuisen, F. and Maxson, P. (2010) 'Global Emission of Mercury to the Atmosphere from Anthropogenic Sources in 2005 and Projections to 2020', *Atmospheric Environment,* 44(20), 2487-2499.

Pacyna, J. M. and Pacyna, E. G. (2001) 'An Assessment of Global and Regional Emissions of Trace Metals to the Atmosphere from Anthropogenic Sources Worldwide', *Environmental Reviews,* 9(4), 269-298.

Park, H. B., Kang, K., Lee, G. H. and Shin, H. J. (2012a) 'Distribution of Salinity and Temperature Due to the Freshwater Discharge in the Yeongsan Estuary in the Summer of 2011', *Journal of Korean Society of Oceanography,* 17(3), 139-148.

Park, J. J., Kim, K. J., Yoo, S. M., Kim, E. H., Seok, K. S., Huh, I. A. and Kim, Y. H. (2012b) 'Distribution of Heavy Metals and Mercury in Sediment from the Lake an-Dong', *Journal of Korean Analytical Science and Technology,* 25(6), 441-446.

Park, S. C., Kim, Y. S. and Hong, S. K. (1991) 'Shallow Seismic Stratigraphy and Distribution Pattern of Late Quaternary Sediments in a Macrotidal Bay: Gunhung Bay, West Coast of Korea', *Marine Geology,* 98(1), 135-144.

Park, S. C. and Lee, K. W. (1996) 'Modern Sedimentary Environment of Jinhae Bay, Se Korea', *The Journal of the Korean Society of Oceanography,* 31(2), 43-54.

Park, S. C., Lee, K. W. and Song, Y. I. (1995) 'Acoustic Characters and Distribution Pattern of Modern Fine-Grained Deposits in a Tide-Dominated Coastal Bay - Jinhae-Bay, Southeast Korea', *Geo-Marine Letters,* 15(2), 77-84.

Park, S. C. and Yoo, D. G. (1988) 'Depositional History of Quaternary Sediments on the Continental Shelf Off the Southeastern Coast of Korea (Korea Strait)', *Marine Geology,* 79(1-2), 65-75.

Park, S. C., Yoo, D. G., Lee, K. W. and Lee, H. H. (1999) 'Accumulation of Recent Muds Associated with Coastal Circulations, Southeastern Korea Sea (Korea Strait)', *Continental Shelf Research,* 19(5), 589-608.

Park, Y., Cho, K. and Cho, C. (2008) 'Seasonal Variation of Water Temperature and Dissolved Oxygen in the Youngsan Reservoir', *Journal of Korean Society on Water Quality,* 24(1), 44-53.

Park, Y. A. (1983) ' The Nature of Holocene Sedimentation and Sedimentary Facies on the Continental Shelves of Korea.', *Summer Conference for Domestic and Foreign Scholar of Science and Technology,* 72-80.

Park, Y. A. and Yi, H., II (1995) 'Late Quaternary Climatic Changes and Sea-Level History Along the Korean Coasts', *Journal of Coastal Research,* 17, 163-168.

Pekar, S. F., McHugh, C. M. G., Christie-Blick, N., Jones, M., Carbotte, S. M., Bell, R. E. and Lynch-Stieglitz, J. (2004) 'Estuarine Processes and Their Stratigraphic Record: Paleosalinity and Sedimentation Changes in the Hudson Estuary (North America)', *Marine Geology,* 209(1–4), 113-129.

Pirrone, N. and Mason, R. (2009) *Mercury Fate and Transport in the Global Atmosphere: Emissions, Measurements and Models,* New York: Springer.

Poppe, L. J., Eliason, A. H., Fredericks, J. J., Rendigs, R. R., D., B. and Polloni, C. F. (2003) *U.S. Geological Survey Open-File Report 00-358: Grain-Size Analysis of Marine Sediments: Methodology and Data Processing*.

Pudasainee, D., Lee, S. J., Lee, S.-H., Kim, J.-H., Jang, H.-N., Cho, S.-J. and Seo, Y.-C. (2010) 'Effect of Selective Catalytic Reactor on Oxidation and Enhanced Removal of Mercury in Coal-Fired Power Plants', *Fuel,* 89(4), 804-809.

Pye, K. and Blott, S. J. (2014) 'The Geomorphology of Uk Estuaries: The Role of Geological Controls, Antecedent Conditions and Human Activities', *Estuarine, Coastal and Shelf Science*, 40, 1-19.

Rafaj, P., Bertok, I., Cofala, J. and Schöpp, W. (2013) 'Scenarios of Global Mercury Emissions from Anthropogenic Sources', *Atmospheric Environment,* 79, 472-479.

Ram, A., Rokade, M. A., Borole, D. V. and Zingde, M. D. (2003) 'Mercury in Sediments of Ulhas Estuary', *Marine Pollution Bulletin,* 46(7), 846-857.

Ran, L., Lu, X. X., Xin, Z. and Yang, X. (2013) 'Cumulative Sediment Trapping by Reservoirs in Large River Basins: A Case Study of the Yellow River Basin', *Global and Planetary Change,* 100, 308-319.

Rhew, H. S. and Lee, G. H. (2011) 'Magnitude-Frequency Relationships between Rainfall and Extreme Freshwater Discharge in the Altered Yeongsan Estuary, Korea', *Journal of Korean Society of Oceanography,* 16(4), 223-237.

Rodriguez, A. B., Anderson, J. B. and Simms, A. R. (2005) 'Terrace Inundation as an Autocyclic Mechanism for Parasequence Formation: Galveston Estuary, Texas, U.S.A', *Journal of Sedimentary Research,* 75(4), 608-620.

Rothenberg, S. E., McKee, L., Gilbreath, A., Yee, D., Connor, M. and Fu, X. (2010) 'Evidence for Short-Range Transport of Atmospheric Mercury to a Rural, Inland Site', *Atmospheric Environment,* 44(10), 1263-1273.

Ryu, C. R. and Chang, S. D. (1979) 'Tide and Tidal Current in the Estuary of the Nakdong River', *The Journal of the Oceanological Society of Korea,* 13(2), 71-77.

Sanders, C. J., Santos, I. R., Silva-Filho, E. V. and Patchineelam, S. R. (2006) 'Mercury Flux to Estuarine Sediments, Derived from Pb-210 and Cs-137 Geochronologies (Guaratuba Bay, Brazil)', *Marine Pollution Bulletin,* 52(9), 1085-1089.

Sanei, H. and Goodarzi, F. (2006) 'Relationship between Organic Matter and Mercury in Recent Lake Sediment: The Physical–Geochemical Aspects', *Applied Geochemistry,* 21(11), 1900-1912.

Sanei, H., Outridge, P. M., Stern, G. A. and Macdonald, R. W. (2014) 'Classification of Mercury–Labile Organic Matter Relationships in Lake Sediments', *Chemical Geology,* 373(0), 87-92.

Santschi, P. H., Allison, M. A., Asbill, S., Perlet, A. B., Cappellino, S., Dobbs, C. and McShea, L. (1999) 'Sediment Transport and Hg Recovery in Lavaca Bay, as Evaluated from Radionuclide and Hg Distributions', *Environmental Science & Technology,* 33(3), 378-391.

Santschi, P. H., Guo, L., Asbill, S., Allison, M., Britt Kepple, A. and Wen, L.-S. (2001) 'Accumulation Rates and Sources of Sediments and Organic Carbon on the Palos Verdes Shelf Based on Radioisotopic Tracers ($^{137}$Cs, $^{239,240}$Pu, $^{210}$Pb, $^{234}$Th, $^{238}$U and $^{14}$C)', *Marine Chemistry,* 73(2), 125-152.

Santschi, P. H. and Honeyman, B. D. (1989) 'Radionuclides in Aquatic Environments', *Radiation and Physical Chemistry,* 34(2), 213-240.

Schelske, C. L. and Hodell, D. A. (1995) 'Using Carbon Isotopes of Bulk Sedimentary Organic Matter to Reconstruct the History of Nutrient Loading and Eutrophication in Lake Erie', *Limnology and Oceanography,* 40(5), 918-929.

Schneider, H., Höfer, D., Trog, C., Busch, S., Schneider, M., Baade, J., Daut, G. and Mäusbacher, R. (2010) 'Holocene Estuary Development in the Algarve Region (Southern Portugal) – a Reconstruction of Sedimentological and Ecological Evolution', *Quaternary International,* 221(1–2), 141-158.

Schroeder, W. H. and Munthe, J. (1998) 'Atmospheric Mercury—An Overview', *Atmospheric Environment,* 32(5), 809-822.

Schubel, J. R. and Carter, H. H. (1984) 'The Estuary as a Filter for Fine-Grained Suspended Sediment ' in Kennedy, V. S., ed. *The Estuary as a Filter*, New York: Academic Press, 81-105.

Schuster, P. F., Krabbenhoft, D. P., Naftz, D. L., Cecil, L. D., Olson, M. L., Dewild, J. F., Susong, D. D., Green, J. R. and Abbott, M. L. (2002) 'Atmospheric Mercury Deposition During the Last 270 Years: A Glacial Ice Core Record of Natural and Anthropogenic Sources', *Environmental Science & Technology,* 36(11), 2303-2310.

Selin, N. E. (2012) 'Atmospheric Chemistry, Modeling, and Biogeochemistry of Mercury' in Bank, M. S., ed. *Mercury in the Environment: Patterns and Process*, 1 ed., Berkely and Los Angeles, California: University of California Press, 73-79.

Shi, J.-b., Ip, C. C. M., Zhang, G., Jiang, G.-b. and Li, X.-d. (2010) 'Mercury Profiles in Sediments of the Pearl River Estuary and the Surrounding Coastal Area of South China', *Environmental Pollution,* 158(5), 1974-1979.

Shin, H. J. and Lee, G. (2014) 'Flow Velocities from the Yeongsan Estuarine Dam ', *Journal of Korean Society of Oceanography,* 19, 180-190.

Shotyk, W., Goodsite, M. E., Roos-Barraclough, F., Frei, R., Heinemeier, J., Asmund, G., Lohse, C. and Hansen, T. S. (2003) 'Anthropogenic Contributions to Atmospheric Hg, Pb and as Accumulation Recorded by Peat Cores from Southern Greenland and Denmark Dated Using the 14c “Bomb Pulse Curve”', *Geochimica et Cosmochimica Acta,* 67(21), 3991-4011.

Smith, V. H., Joye, S. B. and Howarth, R. W. (2006) 'Eutrophication of Freshwater and Marine Ecosystems', *Limnology and Oceanography,* 51(1), 351-355.

Sommerfield, C. K., Nittrouer, C. A. and Alexander, C. R. (1999) '$^{7}$Be as a Tracer of Flood Sedimentation on the Northern California Continental Margin', *Continental Shelf Research,* 19(3), 335-361.

Streets, D. G., Zhang, Q. and Wu, Y. (2009) 'Projections of Global Mercury Emissions in 2050', *Environmental Science & Technology,* 43(8), 2983-2988.

Struck, U., Emeis, K. C., Voss, M., Christiansen, C. and Kunzendorf, H. (2000) 'Records of Southern and Central Baltic Sea Eutrophication in $\Delta^{13}$C and $\Delta^{15}$N of Sedimentary Organic Matter', *Marine Geology,* 164(3–4), 157-171.

Stupar, Y. V., Schäfer, J., García, M. G., Schmidt, S., Piovano, E., Blanc, G., Huneau, F. and Le Coustumer, P. (2014) 'Historical Mercury Trends Recorded in Sediments from the Laguna Del Plata, Córdoba, Argentina', *Chemie der Erde - Geochemistry,* 74(3), 353-363.

Sunderland, E. M. and Mason, R. P. (2007) 'Human Impacts on Open Ocean Mercury Concentrations', *Global Biogeochemical Cycles,* 21(GB4022), 1-15.

Swartzendruber, P. and Jaffe, D. (2012) 'Sources and Transport: A Global Issue' in Bank, M. S., ed. *Mercury in the Environment: Patterns and Process*, 1 ed., Berkeley and Los Angeles, California: University of California Press, 3-18.

Syvitski, J. P. M., Vrsmarty, C. J., Kettner, A. J. and Green, P. (2005) 'Impact of Humans on the Flux of Terrestrial Sediment to the Global Coastal Ocean', *Science,* 308(5720), 376-380.

Taylor, D. L., Linehan, J. C., Murray, D. W. and Prell, W. L. (2012) 'Indicators of Sediment and Biotic Mercury Contamination in a Southern New England Estuary', *Marine Pollution Bulletin,* 64(4), 807-819.

Tönis, I. E., Stam, J. M. T. and van de Graaf, J. (2002) 'Morphological Changes of the Haringvliet Estuary after Closure in 1970', *Coastal Engineering,* 44(3), 191-203.

UNEP (2013) *Global Mercury Assessment 2013: Sources, Emissions, Releases and Environmental Transport*, Geneva, Switzerland.

Vukovic, D., Vukovic, Z. and Stankovic, S. (2014) 'The Impact of the Danube Iron Gate Dam on Heavy Metal Storage and Sediment Flux within the Reservoir', *CATENA,* 113, 18-23.

Walling, D. E. (2006) 'Human Impact on Land-Ocean Sediment Transfer by the World's Rivers', *Geomorphology,* 79(3-4), 192-216.

Walraven, N., van Os, B. J. H., Klaver, G. T., Middelburg, J. J. and Davies, G. R. (2014) 'Reconstruction of Historical Atmospheric Pb Using Dutch Urban Lake Sediments: A Pb Isotope Study', *Science of The Total Environment,* 484, 185-195.

Wang, Y., Dong, P., Oguchi, T., Chen, S. and Shen, H. (2013) 'Long-Term (1842–2006) Morphological Change and Equilibrium State of the Changjiang (Yangtze) Estuary, China', *Continental Shelf Research,* 56, 71-81.

Wang, Y. P., Chu, Y. S., Lee, H. J., Han, C. K. and Oh, B. C. (2005) 'Estimation of Suspended Sediment Flux from Acoustic Doppler Current Profiling Along the Jinhae Bay Entrance', *Acta Oceanologica Sinica,* 24(2), 16-25.

Weiss-Penzias, P. S., Gustin, M. S. and Lyman, S. N. (2011) 'Sources of Gaseous Oxidized Mercury and Mercury Dry Deposition at Two Southeastern U.S. Sites', *Atmospheric Environment,* 45(27), 4569-4579.

Williams, J., Dellapenna, T., Lee, G. and Louchouarn, P. (2014) 'Sedimentary Impacts of Anthropogenic Alterations on the Yeongsan Estuary, South Korea', *Marine Geology,* 357, 256-271.

Williams, J. R., Dellapenna, T. M. and Lee, G. (2013) 'Shifts in Depositional Environments as a Natural Response to Anthropogenic Alterations: Nakdong Estuary, South Korea', *Marine Geology,* 343, 47-61.

Wolanski, E. and Chappell, J. (1996) 'The Response of Tropical Australian Estuaries to a Sea Level Rise', *Journal of Marine Systems,* 7(2-4), 267-279.

Won, J. S., Kim, H. Y. and Ryu, J. H. (1999) 'Coastal Geomorphologic Change Detection Using Sar and Optical Remote Sensing Data at the Nakdong River Estuary, Korea', *Geoscience and Remote Sensing Symposium, 1999. IGARSS '99 Proceedings. IEEE 1999 International,* 5, 2733-2735.

Wong, P. P., Losada, I. J., Gattuso, J.-P., Hinkel, J., Khattabi, A., McInnes, K. L., Saito, Y. and Sallenger, A. (2014) 'Coastal Systems and Low-Lying Areas' in Field, C. B., Barros, V. R., Dokken, D. J., Mach, K. J., Mastrandrea, M. D., Bilir, T. E., Chatterjee, M., Ebi, K. L., Estrada, Y. O., Genova, R. C., Girma, B., Kissel, E. S., Levy, A. N., MacCracken, S., Mastrandrea, P. R. and White, L. L., eds., *Climate Change 2014: Impacts, Adaptation, and Vulnerability. Part A: Global and Sectoral Aspects. Contribution of Working Group Ii to the Fifth Assessment Report of the Intergovernmental Panel of Climate Change*, Cambridge, United Kingdom and New York, NY, USA: Cambridge University Press.

Worrell, E., Price, L., Martin, N., Hendriks, C. and Meida, L. O. (2001) 'Carbon Dioxide Emissions from the Global Cement Industry', *Annual Review of Energy and the Environment,* 26(1), 303-329.

Xu, Y., Sun, Q., Yi, L., Yin, X., Wang, A., Li, Y. and Chen, J. (2014) 'The Source of Natural and Anthropogenic Heavy Metals in the Sediments of the Minjiang River Estuary (Se China): Implications for Historical Pollution', *Science of The Total Environment,* 493, 729-736.

Yang, H. and Rose, N. L. (2003) 'Distribution of Mercury in Six Lake Sediment Cores across the UK', *Science of The Total Environment,* 304(1–3), 391-404.

Yoo, C. I., Ryu, C. R. and Yoon, H. S. (2011) 'Formation and Evolution of the Shoal at Jinudo in Nakdong River Estuary, Korea: Field Observation and Numerical Modeling', *Journal of Coastal Research,* (64), 2084-2088.

Yoo, D.-G. and Park, S.-C. (2000) 'High-Resolution Seismic Study as a Tool for Sequence Stratigraphic Evidence of High-Frequency Sea-Level Changes: Latest Pleistocene-Holocene Example from the Korea Strait', *Journal of Sedimentary Research,* 70(2), 296-309.

Yoon, B. and Woo, H. (2000) 'Sediment Problems in Korea', *Journal of Hydraulic Engineering,* 126(7), 486.

Yoon, E. C. and Lee, J. S. (2008) 'Characteristics of Seasonal Variation to Sedimentary Environment at the Estuary Are of the Nakdong', *Korean Society of Coastal and Ocean Engineers,* 20(4), 372-389.

Yoon, H. S., Yoo, C. I., Na, W. B., Lee, I. C. and Ryu, C. R. (2007) 'Geomorphologic Evolution and Mobility of Sand Barriers in the Nakdong Estuary, South Korea', *Journal of Coastal Research*, 40, 358-363.

Zamora, H. A., Nelson, S. M., Flessa, K. W. and Nomura, R. (2013) 'Post-Dam Sediment Dynamics and Processes in the Colorado River Estuary: Implications for Habitat Restoration', *Ecological Engineering,* 59, 134-143.

Zhang, X., Siddiqi, Z., Song, X., Mandiwana, K. L., Yousaf, M. and Lu, J. (2012) 'Atmospheric Dry and Wet Deposition of Mercury in Toronto', *Atmospheric Environment,* 50, 60-65.

Zimmerman, A. R. and Canuel, E. A. (2002) 'Sediment Geochemical Records of Eutrophication in the Mesohaline Chesapeake Bay', *Limnology and Oceanography,* 47(4), 1084-1093.